2020

Inorganic Carbon Chemistry In East Antarctic Coastal Polynyas

Mar C. Arroyo
William & Mary - Virginia Institute of Marine Science, mcarroyo94@gmail.com

Inorganic Carbon Chemistry in East Antarctic Coastal Polynyas

A Thesis

Presented to

The Faculty of the School of Marine Science

The College of William and Mary in Virginia

In Partial Fulfillment

of the Requirements for the Degree of

Master of Science

by

Mar C. Arroyo

January 2020

APPROVAL PAGE

This thesis is submitted in partial fulfillment of

the requirements for the degree of

Master of Science

Mar C. Arroyo

Approved by the Committee,

Elizabeth H. Shadwick, Ph.D.
Committee Chair / Advisor

Marjorie A. M. Friedrichs, Ph.D.

Donglai Gong, Ph.D.

Walker O. Smith, Jr., Ph.D.

Peter Sedwick, Ph.D.
Old Dominion University
Norfolk, VA, USA

TABLE OF CONTENTS

ACKNOWLEDGEMENTS

I firstly give my greatest thanks to my advisor, Dr. Elizabeth Shadwick, for her guidance and support throughout my graduate degree. Thank you for providing me the opportunity to work, learn, and conduct research in exciting and truly life changing places. Thank you for your continuous mentorship, despite the distance in time and in space, and for challenging me to think more critically.

Thank you to my committee members for their insight and time on my thesis research: Dr. Walker Smith for his constructive input and for providing me with new research opportunities; Dr. Marjy Friedrichs for her encouragement and positivity; Dr. Donglai Gong for reminding me to focus on the fundamentals, and Dr. Peter Sedwick for providing thoughtful perspective on Antarctic biogeochemistry.

I am grateful to the many colleagues and friends made on research cruises during the last three years. Thanks to Dr. Bronte Tilbrook and Dr. Steve Rintoul for my first Antarctic research experience and to Kate Berry for her technical training and support at sea. Thanks to Dr. Hugh Ducklow for productive talks on the Palmer LTER cruise. Thanks to Dr. Dennis McGillicuddy and Dr. Gordon Zhang for sharing their enthusiasm for adaptive sampling on SPIROPA. Thanks to Olivia De Meo for all the help with cruise preparation and technical support in the lab. I would especially like to thank Dr. Dennis Hansell and Dr. Sarah Bercovici for first encouraging me to explore the ocean as an undergraduate and for continuing to mentor me as I grow as a scientist. My research and field experiences at VIMS were made possible by the funding and educational support from the Office of Academic Studies at VIMS, the Rebecca M. Dickhut family, and the National Science Foundation's Graduate Research Fellowship Program.

I am extremely grateful to my family and friends who have supported me throughout my graduate journey. Thanks to my VIMS family, and in particular thanks to the world's best labmate, Jackie, for the fun and friendship. Lastly, I am forever thankful for my parents, Fran and José, and brother, Nick, for their endless love and constant support in all aspects of life.

LIST OF TABLES

LIST OF FIGURES

ABSTRACT

Polynyas are large areas of open water or reduced sea ice coverage that persistently form in polar environments and often experience enhanced rates of physical, chemical, and biological processes that impact ocean dynamics on local to global scales. Polynyas that form adjacent to the coast, known as coastal polynyas, play an important role in the global carbon cycle by regulating the exchange of CO_2 between the ocean and atmosphere in the high latitudes. Because of their importance to the global carbon cycle, there is a particular interest to better characterize CO_2 system processes in Antarctic coastal polynyas. In this study, the inorganic carbon chemistry in three East Antarctic coastal polynyas – the Dalton Polynya, the Mertz Polynya, and the Ninnis Polynya – is investigated using a combination of ship-board water column and underway observations, remote sensing products, and model outputs.

The first biogeochemical observations in the Dalton Polynya are presented, and the physical and biological controls on total dissolved inorganic carbon (TCO_2) are examined. Despite the evidence of TCO_2 depletion due to biological production, the surface waters of the Dalton Polynya were a weak net source of CO_2 to the atmosphere during the summer survey. Satellite estimates of sea surface chlorophyll *a* concentration suggest that the shipboard observations were made prior to the peak of the productive season and are more likely representative of the transition between spring and summer. Compared to coastal polynyas, the rates of net community production and air-sea CO_2 exchange in the Dalton polynya were relatively small.

The Mertz and Ninnis Polynyas are regions that supply deep water from the continental shelf to meridional overturning circulation. The formation of Dense Shelf Water (DSW), the precursor to Antarctic Bottom Water, establishes a connection between the surface and deep layers of the ocean, permitting the exchange of CO_2, while transporting shelf-derived products offshore and to depth. The transport of inorganic carbon with DSW was quantified by combining summertime TCO_2 concentrations with volumetric model-derived DSW transport. The calculated transports indicate that substantial amount of inorganic carbon is exported from the Adélie Land coast with DSW annually. While the interannual variability in mixed-layer TCO_2 is large, the TCO_2 concentration in DSW at depth is invariant due to the dominance of physical processes including the inflow of modified Circumpolar Deep Water and brine released during sea ice formation. The lateral movement of DSW offshore acts as a continental shelf pump for CO_2 to the deep ocean.

AUTHOR'S NOTE

The chapters that comprise this thesis were written in manuscript format for scientific publication. Thus, the formatting of each chapter follows the guidelines of the journal to which the manuscript was or will be submitted. At the time of writing, citations for individual chapters are as follows:

Chapter 3:

Arroyo, M. C., Shadwick, E. H., & Tilbrook, B. (2019). Summer Carbonate Chemistry in the Dalton Polynya, East Antarctica. *Journal of Geophysical Research: Oceans*, *124*(8), 5634–5653. https://doi.org/10.1029/2018JC014882

Chapter 4:

Arroyo, M. C., Shadwick, E. H., Tilbrook, B., Rintoul, S. R., & Kusahara, K. A Continental Shelf Pump for CO_2 on the Adélie Land Coast, East Antarctica. *In Prep*.

Inorganic Carbon Chemistry in East Antarctic Coastal Polynyas

Chapter 1:

INTRODUCTION

1.1 Motivation

Within the global carbon cycle, the ocean serves as the largest exogenic reservoir of carbon, containing a massive pool of 38,000 Pg (1 Pg = 10^{15} g) of dissolved inorganic carbon, or approximately 45 times that of the atmosphere (Ciais et al., 2013). The ocean exchanges carbon dioxide gas (CO_2) with the atmosphere at the sea surface boundary and consequently exerts a fundamental control on the long-term concentrations of CO_2 in the atmosphere over glacial/interglacial cycles (Broecker, 1982; Sigman & Boyle, 2000). Since the beginning of the industrial era around 1750, the concentration of CO_2 in the atmosphere has increased from approximately 277 parts per million (ppm) to 407.38 ± 0.10 ppm in 2018 (Dlugokencky & Tans, 2019). This rise is primarily due to anthropogenic emissions from fossil fuel burning and land use change, and greatly exceeding atmospheric CO_2 concentrations over the last 800,000 years (Lüthi et al, 2008). Of the roughly 9.4 Pg C yr^{-1} released into the atmosphere between 2008 and 2017 by anthropogenic activities, approximately 25% was taken up by the global ocean (Gruber et al., 2019; Le Quéré et al., 2018). The oceanic uptake of anthropogenic CO_2 induces fundamental changes in seawater chemistry that impact the physical and biogeochemical cycling of ocean carbon (Caldeira & Wickett, 2003; Feely et al., 2004). Without the ocean sink, the atmospheric CO_2 concentration would be much higher, with significant implications for global climate. There is a need to better understand the cycling of carbon in the marine environment to

more accurately assess future changes in the climate and the consequences for marine ecosystems (e.g., Orr et al., 2005).

The Southern Ocean plays a critical role in the global carbon cycle by maintaining one of the largest oceanic sinks for anthropogenic CO_2, responsible for approximately 40% of the total ocean uptake in regions below 35°S (Khatiwala et al., 2009; Sabine et al., 2004). Despite this paramount importance of the Southern Ocean to the global and marine biogeochemical cycles and advances in observational and analytical techniques, the region remains poorly sampled with respect to the CO_2 system and biogeochemical parameters compared to other open ocean regions. In particular, far fewer observations exist outside of the open Southern Ocean in the seasonal sea ice zone on the continental shelves of Antarctica. Due to its remoteness and inaccessibility for much of the year, the limited number of direct observations that do exist are highly localized on both spatial and temporal scales (predominantly in the ice-free summer season), increasing our reliance on ocean models to characterize the CO_2 system. Many ocean biogeochemical models, however, are incompletely resolved in the coastal Antarctic, leading to differences between model and observational results and a high degree of uncertainty with respect to air-sea CO_2 exchange (e.g., Gruber et al., 2009; Lenton et al., 2013; Takahashi et al., 2009). An improved understanding of carbon cycle dynamics and the physical and biogeochemical processes that drive these dynamics in the coastal regions of the Antarctic will provide important insights into the role these understudied systems play in global carbon cycling.

1.2 The Southern Ocean Carbon Cycle

The inorganic carbon cycle in the Southern Ocean is strongly influenced by the dynamics of water mass circulation and biological activity. The open Southern Ocean is a major source of intermediate and deep water masses to meridional overturning circulation (Marshall & Speer, 2012). The exchange of CO_2 between surface waters and the atmosphere and the subsequent transport of these waters into the ocean interior makes this region an important regulator of the deep ocean storage of carbon over long time scales (Caldeira & Duffy, 2000; Frölicher et al., 2015; Khatiwala et al., 2013; McNeil, et al., 2001; Murata et al., 2019).

An intense sea surface divergence at approximately 60°S driven by the combined effect of strong westerly and opposing polar easterly winds upwells large volumes of deep water to the surface layer, introducing a source of dissolved inorganic carbon and nutrients at high concentrations to surface waters in the Antarctic Polar Front region. These upwelled deep waters, having been out of contact with the atmosphere since preindustrial times, contain extremely small concentrations of anthropogenic CO_2 (Figure 1.1, left) and instead are rich in natural dissolved inorganic carbon resulting from the accumulation of remineralized organic material and the dissolution of biogenic calcium carbonate (Figure 1.1, right). Surface waters diverge to the north and south and absorb natural and anthropogenic CO_2 from, and release natural CO_2 to, the atmosphere before they return to the subsurface (Figure 1.2). It is the spatial superposition of these fluxes that determine whether or not a region is a contemporary oceanic CO_2 source or sink with respect to the atmosphere.

Surface waters that are transported northward act as a substantial source of natural CO_2 to the atmosphere through outgassing. As the northward flowing surface water warms, the solubility of CO_2 gas decreases and thus CO_2 is released to the atmosphere. In addition, due to a lack of micronutrient (e.g., iron) availability, marine phytoplankton are unable to convert the high inorganic carbon and nutrient concentrations in the surface layer into organic material, maintaining an inefficient biological pump of carbon from the surface to depth. Concurrently, southward flowing surface waters derived from the subtropics, with lower inorganic carbon concentrations, begin to cool and increase their capacity to absorb CO_2 from the atmosphere, constituting a strong natural CO_2 sink. When these two sources of water converge at approximately 45°S, the subduction of the convergent surface water delivers a significant amount of both natural and anthropogenic CO_2, as well as nutrients, to the mid-layers of the interior ocean. The transport of intermediate water masses from the open Southern Ocean to low latitude environments is an effective process for moving anthropogenic CO_2 into the ocean interior and delivers an essential supply of nutrients to oligotrophic ecosystems that supports global ocean biological productivity (Sabine et al., 2004; Sarmiento et al., 2004).

Upwelled waters that travel southward to the high latitudes follow a similar trend in the release of natural CO_2 and uptake of anthropogenic CO_2 at the sea surface. In contrast to the northward moving surface waters, southward flowing surface waters spend a smaller amount of time in contact with the atmosphere, and the presence of seasonal sea ice zone extending from Antarctica can limit air-sea CO_2 gas exchange (Loose et al., 2011). Near the Antarctic continent, sources of dissolved iron supplied in part from sea ice and benthic inputs (e.g., Lannuzel et al., 2010; McGillicuddy et al., 2015; Sedwick & DiTullio, 1997)

promotes enhanced rates of seasonal primary productivity and CO_2 fixation. As surface waters move southbound, they cool and, in certain regions such as coastal polynyas, can ultimately contribute to Antarctic Bottom Water that fills the deep layers of the Atlantic, Pacific, and Indian Oceans (Orsi et al., 1999). Given its long residence time, Antarctic Bottom Water has the potential to sequester CO_2 and organic material in the abyssal ocean over centennial timescales and longer, highlighting the importance of this water mass to the global carbon cycle and Earth's climate system (Orsi et al., 1999; Shadwick et al., 2014; Takahashi & Chipman, 2012).

1.3Antarctic Coastal Polynyas

Coastal polynyas are persistent areas of open water within the sea ice zone that form in the lee of a glacial tongue, grounded iceberg, coastline, or other fixed boundary. In these regions, sea ice is consistently formed during winter months and mechanically advected away from the coastal boundary by a combination of offshore katabatic winds and ocean currents (Massom et al., 1998; Morales Maqueda et al., 2004). Most coastal polynyas in the Antarctic form on the continental shelf adjacent to the coastline, where they play important roles in atmospheric heat exchange (e.g., Nihashi & Ohshima, 2015) and in ocean-ice shelf interactions (e.g., Silvano et al., 2016).

The seasonal dynamics of inorganic carbon in polynyas is driven by a combination of physical and biogeochemical processes. During the growing season, surface waters in Antarctic coastal polynyas are often associated with enhanced rates of biological productivity relative to surrounding sea ice covered regions and the open Southern Ocean (Arrigo & van Dijken, 2003). As the timing and intensity of phytoplankton blooms are

influenced by light and micronutrient availability, vertical mixing, and the degree of open water (Mitchell & Holm-Hansen, 1991; Smith & Jones, 2015), the physical conditions in early spring and summer typically promote a favorable environment for a highly productive marine ecosystem. Because of their open or reduced sea ice coverage, surface waters in coastal polynyas are generally the first areas within the sea ice zone to receive incoming solar radiation with the return of sunlight in the spring. As surrounding sea ice melts with the increase in solar irradiance and sea surface warming, the onset of summer stratification enhances the potential for biological CO_2 drawdown and organic matter formation by extensive open-water and under-ice phytoplankton blooms. These processes characteristically induce large deficits total dissolved inorganic carbon concentrations in the surface mixed layer and an associated air-sea CO_2 disequilibrium that promotes the uptake of CO_2 from the atmosphere (e.g., Shadwick et al., 2014; Yager et al., 1995).

During the transition to autumn months, enhanced sea ice production and an increase in windspeed generates cold, deep mixed layers resulting from strong surface buoyancy loss. As sea ice forms, a significant amount of brine is rejected to the underlying polynya surface waters, increasing the salinity and density, that generates deep convective mixing. Subsurface waters are typically enriched in inorganic carbon as the product of organic matter remineralization, and their introduction to the surface layer increases the concentration of total dissolved inorganic carbon and the potential for CO_2 outgassing from the surface ocean to the atmosphere (if not impeded by the presence of sea ice). In certain polynyas, the brine release associated with high rates of sea ice formation leads to the formation of Dense Shelf Water, the cold, salty precursor to Antarctic Bottom Water. Dense Shelf Water and Antarctic Bottom Water formation occurs primarily in four

locations: the Weddell Sea (Foster & Carmack, 1976), the Ross Sea (Jacobs et al., 1970), Prydz Bay (Ohshima et al., 2013) and on the Adélie and George V Land coast in East Antarctica (Gordon & Tchernia, 1972; Rintoul, 1998).

Despite this growing understanding of carbon cycling in coastal polynyas, there are likely large degrees of variability with respect to CO_2-system properties both within and between coastal polynyas (e.g., Arroyo et al., 2019; McNeil et al., 2011). The physical and biogeochemical processes that influence the concentrations of inorganic carbon vary widely in magnitude and in their relative contributions. In some cases, the observed variability of carbonate measurements taken 10 years apart was much larger than the expected change due to equilibration with the increased CO_2 in the atmosphere alone over that same time period (Roden et al., 2013). In order to assess the importance of Antarctic coastal polynyas to the global carbon cycle, observational data from a diversity of polynyas is required. The work presented in this thesis seeks to advance the understanding of CO_2-system processes in East Antarctic coastal polynyas.

1.4Thesis Objectives and Structure

This study incorporates new observations and analyses from the Dalton Polynya on the Sabrina Coast (113°E – 121°E) and the Mertz Polynya and Ninnis Polynya in Adélie Land (140°E – 150°E), East Antarctica. The key research questions are:

1. What controls the biogeochemical variability in the Dalton Polynya in the summer season?
2. Does Dense Shelf Water export from the Mertz Polynya and Ninnis Polynya serve as a continental shelf pump for dissolved inorganic carbon?

This thesis is structured as follows:

Chapter 2 provides an overview of the carbonate system in seawater and details the field and laboratory methods used to obtain the CO_2-system measurements discussed in Chapters 3 and 4.

Chapter 3 characterizes the physical and biogeochemical processes that impact carbonate chemistry in the Dalton Polynya using newly available observations from the 2014/2015 austral summer. The drivers of total dissolved inorganic concentrations in the summer mixed layer were evaluated with respect to the relative impact of air-sea CO_2 exchange, sea ice melt and formation, and seasonal net community production. The variability of the summer biogeochemical conditions in the Dalton polynya was assessed temporally by using remotely sensed products and regionally by comparison to other coastal systems in East Antarctica.

Chapter 4 quantifies the export of total dissolved inorganic carbon with Dense Shelf Water transport from the Mertz and Ninnis Polynya, using CO_2-system observations from the austral summers of 2014/2015 and 2016/2017. The characteristic concentrations of total dissolved inorganic carbon in Dense Shelf Water were combined with model-derived volumetric Dense Shelf Water transport estimates to determine the transport of inorganic carbon from the continental shelf to the deep ocean. A framework for a continental shelf pump for CO_2 on the Adélie Land coast is discussed.

Chapter 5 presents a summary of the contributions from Chapters 3 and 4, and discusses the significance of this research.

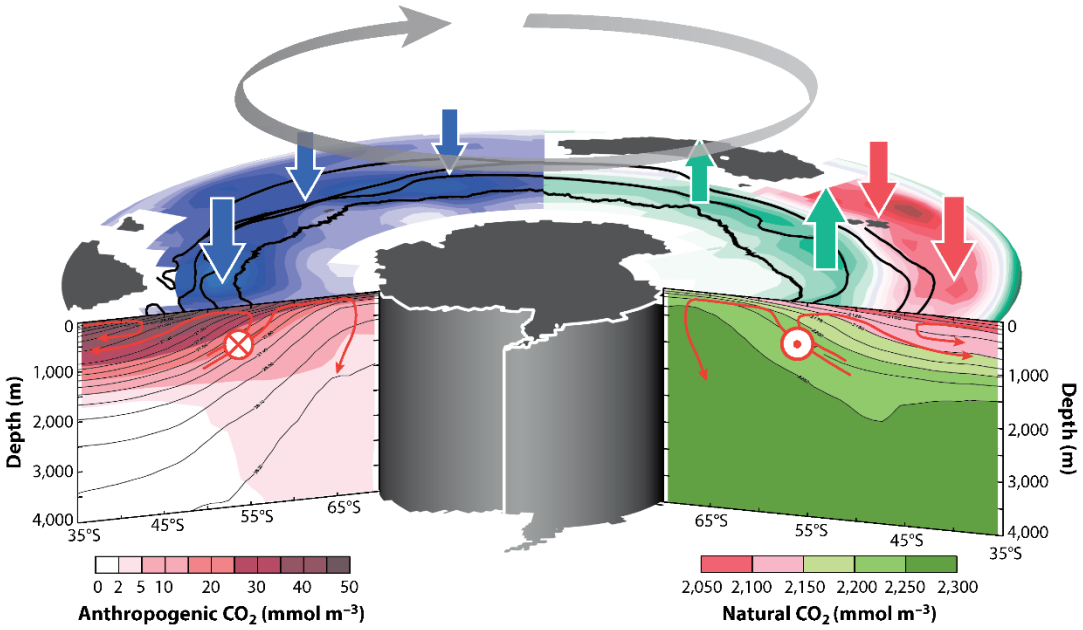

Figure 1.1. Schematic diagram of the zonal mean overturning circulation of total dissolved inorganic carbon and the associated fluxes of anthropogenic (left) and natural (right) CO_2 (mmol m^{-3}) in the Southern Ocean. The gray arrow and red circles indicate the flow of the Antarctic Circumpolar Current flowing into the figure (circle with x) and out of the figure (circle with dot) in the water column. Arrows out of or into the sea surface represent the air-sea fluxes of CO_2. Figure modified from Gruber et al. (2019) and based on the analysis by Gruber et al. (2009).

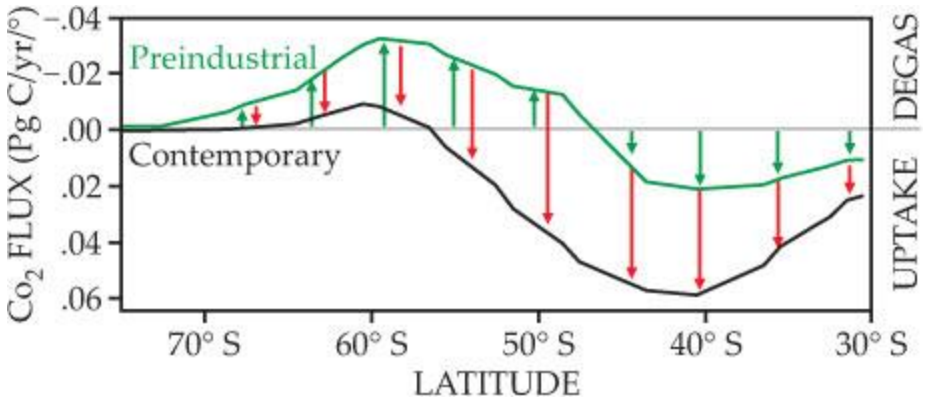

Figure 1.2. The air-sea flux of CO_2 (Pg C/yr/°) in the Southern Ocean as a function of latitude. The preindustrial CO_2 flux is indicated in green. Red arrows indicate the anthropogenic contribution to the preindustrial CO_2 flux whereby the contemporary flux (black) is the sum of preindustrial and anthropogenic CO_2 fluxes. Figure from Morrison et al. (2015).

Chapter 2:

THE CARBONATE SYSTEM IN SEAWATER

2.1 Carbonate Chemistry

More than 96% of carbon in the combined atmospheric and oceanic reservoirs is stored in the oceans as dissolved inorganic carbon (Ciais et al., 2013). Carbon dioxide in the atmosphere ($CO_{2\ (g)}$) can exchange across the air-sea interface and dissolve in the ocean surface waters as aqueous CO_2 ($CO_{2\ (aq)}$). $CO_{2\ (aq)}$ subsequently undergoes a series of chemical reactions to dissociate into three additional inorganic species in equilibrium: carbonic acid (H_2CO_3), bicarbonate ion (HCO_3^-), and carbonate ion (CO_3^{2-}; Figure 2.1). These equilibrium reactions are described by the following equations:

$$CO_{2\ (g)} \leftrightarrow CO_{2\ (aq)} \quad (2.1)$$

$$CO_{2\ (aq)} + H_2O \leftrightarrow H_2CO_3 \quad (2.2)$$

$$H_2CO_3 \leftrightarrow H^+ + HCO_3^- \quad (2.3)$$

$$HCO_3^- \leftrightarrow H^+ + CO_3^{2-} \quad (2.4)$$

Both $CO_{2\ (aq)}$ and H_2CO_3 are unstable in seawater and are not analytically separable. Often, these two species are expressed as the sum of their concentrations, denoted as the hypothetical species CO_2^* where

$$[CO_2^*] = [CO_{2\ (aq)}] + [H_2CO_3]. \quad (2.5)$$

In thermodynamic equilibrium, the concentrations of $CO_{2\ (g)}$ and CO_2^* in seawater are governed by Henry's law:

$$[CO_2^*] = K_0\, fCO_2 \quad (2.6)$$

where K_0 is the solubility coefficient of CO_2 in seawater as a function of temperature and salinity (Weiss, 1974) and fCO_2 is the fugacity of gaseous CO_2. The fCO_2 is equal to the partial pressure of CO_2 (pCO_2) corrected for CO_2 non-ideality with respect to molecular interactions between CO_2 and other dissolved gases. The pCO_2 is proportional to the CO_2 mole fraction dissolved in seawater, assuming solubility equilibrium. The fCO_2 and pCO_2 are related by

$$fCO_2 = \gamma\, pCO_2 \qquad (2.7)$$

where γ is the fugacity coefficient and is a function of temperature. Typically, the difference between fCO_2 and pCO_2 is approximately 1% (Zeebe & Wolf-Gladrow, 2001). Although the concentration of CO_2 in the gas phase in equilibrium with seawater is small (< 1%), it is not negligible and directly controls the rate of air-sea CO_2 exchange. The equilibration time between the ocean and atmosphere for CO_2 gas is relatively rapid with a time scale of days to months (Broecker & Peng, 1974; Feely et al., 2009).

The dissociation of CO_2^* into its acid-base components is extremely rapid, on the time scales of microseconds, and the partitioning of individual dissolved inorganic carbon species is assumed to be in equilibrium in most cases (Dickson et al., 2007; Feely et al., 2009; Zeebe & Wolf-Gladrow, 2001). The relative stoichiometry of carbonate species in seawater is dominated by approximately 87.1% HCO_3^-, followed by 12.4% CO_3^{2-} and 0.5% CO_2^* at a typical surface seawater pH (pH = -log($[H^+]$)) of 8.1, salinity of 35, and temperature of 25 °C, indicating that most dissolved inorganic carbon is in the form of HCO_3^-. The abundance of these species with respect to pH is illustrated in Figure 2.1.

The sum of the concentrations of the total pool of dissolved carbonate species is measured as the total dissolved inorganic carbon (hereafter TCO_2, also conventionally abbreviated as DIC):

$$TCO_2 \equiv \sum CO_2 = [CO_{2\,(aq)}] + [H_2CO_3] + [HCO_3^-] + [CO_3^{2-}]. \quad (2.8)$$
$$= [CO_2^*] + [HCO_3^-] + [CO_3^{2-}]$$

As TCO_2 records the abundance of inorganic carbon, the total alkalinity (TA) records the charge balance of seawater. TA is a measure of the imbalance of electroneutrality of the major, conservative ions in natural seawater, given by:

$$TA = [Na^+] + [K^+] + 2\,[Mg^{2+}] + 2\,[Ca^{2+}] + \text{minor cations excluding } [H^+] \quad (2.9)$$
$$- [Cl^-] - 2\,[SO_4^{2-}] - [Br^-] - [NO_3^-] - \text{minor non-titratable anions}$$

By this definition, TA is expressed as a conservative quantity from the difference between conservative cations and non-titratable anions, unaffected by changes in temperature and pressure. The TA in seawater can thus be defined as the sum of the concentrations of weak bases that exist due to this charge imbalance, or more rigorously as "the number of moles of hydrogen ion equivalent to the excess of proton acceptors (bases formed from weak acids with a dissociation constant $K \leq 10^{-4.5}$, at 25 °C and zero ionic strength) over proton donors (acids with $K > 10^{-4.5}$) in one kilogram of sample", expressed as:

$$TA = [HCO_3^-] + 2\,[CO_3^{2-}] + [B(OH)_4^-] + [OH^-] + [HPO_4^{2-}] + 2\,[PO_4^{3-}] \quad (2.10)$$
$$+ [H_3(SiO_4)^-] + [NH_3] + [HS^-] - [H^+] - [HSO_4^-] - [HF] - [H_3PO_4]$$

following Dickson (1981). Equation 2.10 is often approximated to the sum of the concentrations of the carbonate species (HCO_3^- and CO_3^{2-}), borate ($B(OH)_4^-$), hydroxide

ion (OH^-), and free hydrogen ion (H^+) while the remaining minor components are neglected.

Of the carbonate species described above, only the fCO_2, pH, TCO_2, and TA can be analytically determined. Using the thermodynamic equilibrium relationships that describe CO_2 dissolution in seawater, the determination of any two of these four parameters can be used to resolve the entire seawater CO_2 system including all species ($[CO_2^*]$, $[HCO_3^-]$, $[CO_3^{2-}]$, and $[H^+]$) if the physical environmental conditions are known (salinity, temperature, and pressure). Of these parameters, the two that are most frequently measured to resolve the carbonate system in seawater by recommendation are TCO_2 and TA, due in part to the global use of the Certified Reference Material (CRM) program for ocean CO_2 measurements that ensures seawater sample precision and accuracy for TCO_2 and TA (Dickson et al., 2003).

2.2 Field and Laboratory Methods

In the studies relating to the coastal polynyas in East Antarctica discussed in this thesis, the concentrations of TCO_2 and TA were discretely measured in seawater samples. The pH and the saturation state of the aragonite form calcium carbonate (Ω_{Ar}) were calculated from TCO_2 and TA using the system of equations described above along with temperature, salinity, and measured concentrations of silicate and phosphate using the CO2SYS MATLAB program (van Heuvan et al., 2011). Additionally, the fCO_2 was measured at the sea surface throughout each study by an underway seawater flow-through system. This section describes the methods used to analytically determine the

concentrations of TCO_2 and TA and the fCO_2 in seawater that are only briefly described in the method sections of Chapters 3 and 4.

In each study, TCO_2 and TA were collected inline from Niskin bottles and immediately poisoned with a solution of saturated mercuric chloride ($HgCl_2$) to halt biological activity. Samples were stored in the dark until analysis either at sea or on land at CSIRO in Hobart, Australia. The analytical techniques described below follow standard protocols outlined in Dickson et al. (2007). Seawater samples collected for both TCO_2 and TA were routinely calibrated with CRMs provided by A. G. Dickson to verify the analytical uncertainties (precision and accuracy). High-resolution underway measurements of fCO_2 were determined along the cruise tracks through a continuous flow equilibration method using a non-dispersive infrared gas spectrometer (Pierrot et al., 2009). The analytical determination methods are detailed below.

2.2.1 Determination of TCO_2 by Coulometric Titration

Concentrations of TCO_2 in seawater were determined using a Single Operator Multi-parameter Metabolic Analyzer (SOMMA) system (Dickson et al., 2007; Johnson et al., 1987; 1993). This system pairs a CO_2 gas extraction method with coulometric titration detection to quantify TCO_2 dissolved in seawater.

A calibrated pipette is used to deliver a known volume of seawater (~30 mL) from collection bottes maintained at a constant temperature of 20 °C into a CO_2 gas extraction chamber. Temperature and salinity are measured upon delivery to compute sample density for subsequent concentration calculations. Within this gas extraction chamber, 1 mL of 10% (by volume) solution of phosphoric acid is added to the solution to convert all

dissolved inorganic carbon species into the gaseous CO_2 phase. The gas sample is subsequently stripped from the seawater with a pure, inert carrier gas (in this case, high purity nitrogen N_2 at > 99.995%) bubbled through a submerged ceramic frit at the base of the chamber. The CO_2 and carrier gas are then guided through a scrubber and a condenser to remove any residual acidic and water vapors. The dried gas sample is carried to the temperature-controlled coulometer system and is dispensed into the cathode chamber cell. The cathode cell contains a platinum (Pt) cathode electrode and is filled with an absorbent ethanolamine solution and a pH-sensitive dye indicator (thymolphthalein) in dimethylsulfoxide (DMSO) solute (Johnson et al., 1985). CO_2 reacts with the ethanolamine in cathode solution to generate hydroxyethylcarbamic acid that dissociates into its conjugate base and hydrogen ions (H^+) through the following chemical reaction:

$$CO_2 + HO(CH_2)_2NH_2 \rightarrow HO(CH_2)_2NHCOO^- + H^+ \qquad (2.11)$$

The production of H^+ acidifies the cathode solution and results in a corresponding color change of the thymolpthalein indicator. During this process, the pH of the solution is measured by the transmittance of the thymolphthalein indicator at a 610 nm wavelength. A UIC model 5011 coulometer was used in all TCO_2 analyses.

Determination of CO_2 absorbed in ethanolamine is accomplished by the coulometric titration of the cathode solution to its equivalence point. Electrons sourced from a dissolving (oxidizing) silver (Ag) anode electrode in the adjacent anode cell, filled with a solution of saturated potassium iodide in water and DMSO.

$$Ag_{(s)} \rightarrow Ag^+ + e^- \qquad (2.12)$$

Hydroxide ions (OH^-) are then generated at the Pt cathode via the electrolysis (reduction) of water.

$$H_2O + e^- \rightarrow \frac{1}{2} H_{2\,(g)} + OH^- \quad (2.13)$$

The resulting OH^- produced reacts with H^+ generated by the CO_2-ethanolamine reaction (Eq. 2.11) to restore the pH of the solution to its initial value at the equivalence point.

$$H^+ + OH^- \rightarrow H_2O \quad (2.14)$$

The coulometer determines the amount of charge (i.e., the number of electrons) required to produce hydroxide ions to restore the pH and the color of thymolphthalein indicator dye to its initial state. The overall coulometric technique aims to maintain a constant current throughout the system. The molality concentration of TCO_2 is then calculated using Faraday's second law of electrolysis.

The coulometer cells used for TCO_2 analysis were replaced periodically, when about 25 mg of carbon has been titrated by each cell. Upon cell replacement, the cells were thoroughly cleaned with acetone and milli-Q water before calibration with pure CO_2 gas (> 99.95%) standards of known volumes that bracket the amount of CO_2 expected in ocean seawater samples. The accuracy and precision of the measurements are tested with duplicate samples and CRMs.

2.2.2 Determination of TA by Potentiometric Titration

The concentration of TA in seawater samples can be determined by potentiometric titration using either a closed- or open-cell titration vessel. This titration procedure uses a glass pH electrode to continuously measure the potential across reference and indicator Ag/AgCl electrodes as aliquots of 0.1 N hydrochloric acid (HCl) are automatically delivered to the sample; the TA concentration is then computed from the potential measurements and added titrant volume.

A known volume of seawater sample (~100 mL) is delivered by a dosing device to the titration cell assembly containing the pH glass electrode, thermistor, and a capillary tube by which HCl is delivered. In an open-cell method, an initial single dose of HCl is added to the seawater sample to reduce its pH to about 3.5 and release CO_2 gas to the surroundings before the potentiometric titration. The sample is mixed with a magnetic over a period of time (10 minutes) to allow CO_2 gas to escape. A 0.1 mol/kg HCl solution is prepared in a 0.6 mol/kg sodium chloride matrix to approximate the ionic strength of seawater. The temperature of the cell assembly is maintained at 20 °C by a recirculating water bath through an outer water jacket. The sample is continuously mixed with a magnetic stirrer during the titration process. A burette delivers the acid in small doses (~0.15 mL) to the titration cell while pH and potential are measured until the solution reaches a final pH of 3.0. A non-linear least-squares fitting routine is used to calculate TA, similar to the computations described in Johansson and Wedborg (1982) and Dickson et al. (2007).

2.2.3 Determination of Underway fCO_2 by a Non-Dispersive Infrared Laser (NDIR) CO_2 Analyzer

The fugacity of CO_2 is determined in air that is equilibrated with a continuous flow of underway seawater (Pierrot et al., 2009). Seawater is pumped from ~4 m below the surface through the ship's intake as *in situ* water temperature and salinity are measured. The flow of seawater is pumped on board the ship to an equilibrator chamber at a known flow rate and temperature, where the stream is sprayed into a fixed volume of headspace air maintained at ambient atmospheric pressure. The equilibrated headspace air is dried and

then directed through a non-dispersive infrared (NDIR) CO_2 analyzer built by LICOR that measures the mole fraction of CO_2 (xCO_2) relative to a CO_2-free reference gas. The CO_2 content is corrected to 100% humidity and *in situ* underway water temperature at the ship's intake. Calibration of the fCO_2 measurements occurs at regular intervals (e.g., every four hours) with a series of CO_2 gas standards and a CO_2-free gas standard. The mole fraction of CO_2 in the atmosphere is periodically measured in parallel with underway seawater.

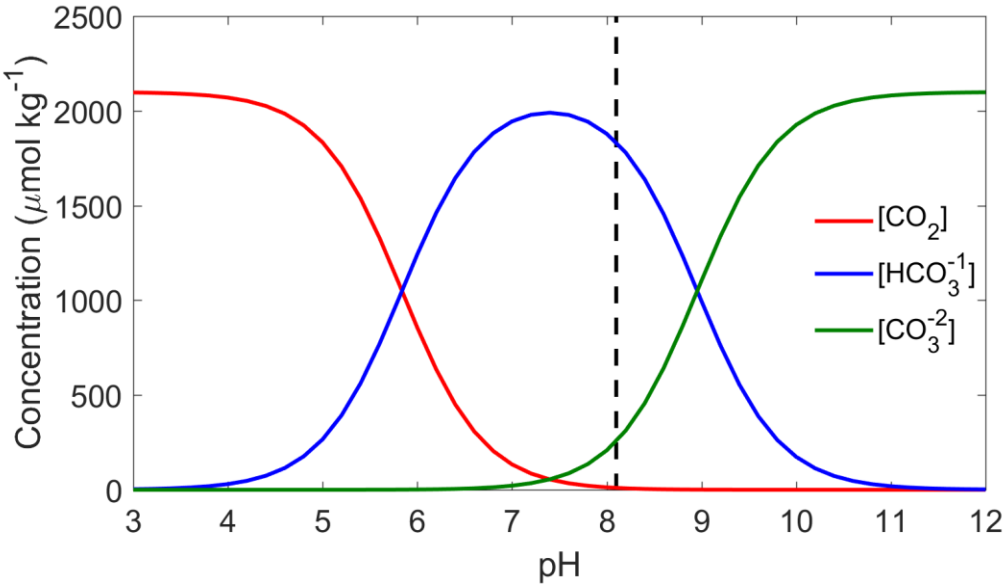

Figure 2.1. The relative abundance of ionic species of the carbonate system in seawater as a function of pH under conditions of T = 25 °C, S = 35, and TCO_2 = 2,100 µmol/kg using the thermodynamic equilibrium constants defined by Mehrbach et al. (1973) and refit by Dickson and Millero (1987). The dashed line denotes the present day mean surface open ocean pH of 8.1.

Chapter 3:

SUMMER CARBONATE CHEMISTRY IN THE DALTON POLYNYA, EAST ANTARCTICA

Mar C. Arroyo[1], Elizabeth H. Shadwick[1,2], and Bronte Tilbrook[2,3]

[1]Virginia Institute of Marine Science, William & Mary, Gloucester Point, Virginia, USA

[2]CSIRO Oceans & Atmosphere, Hobart, Tasmania, Australia

[3]Antarctic Climate & Ecosystems Cooperative Research Centre, Hobart, Tasmania, Australia

Published in *Journal of Geophysical Research: Oceans*

July 2019

Issue 124

doi: 10.1029/2018JC014882

Key Points

- The Dalton Polynya was a weak net source of CO_2 to the atmosphere during summer observations
- Net community production estimates were 5 – 20 mmol C m^{-2} day^{-1} in ice-free and -4 – 0 mmol C m^{-2} day^{-1} in ice-covered regions
- Remotely sensed products reveal below average surface chlorophyll *a* and above average sea ice cover in contrast to long-term summer means

Abstract

The carbonate chemistry in the Dalton Polynya in East Antarctica (115°–123°E) was investigated in summer 2014/2015 using high-frequency underway measurements of CO_2 fugacity (fCO_2) and discrete water column measurements of total dissolved inorganic carbon (TCO_2) and total alkalinity. Air-sea CO_2 fluxes indicate this region was a weak net source of CO_2 to the atmosphere (0.7 ± 0.9 mmol C m^{-2} day^{-1}) during the period of observation, with the largest degree of surface water supersaturation (ΔfCO_2 = +45 µatm) in ice-covered waters near the Totten Ice Shelf (TIS) as compared to the ice-free surface waters in the Dalton Polynya. The seasonal depletion of mixed-layer TCO_2 (6 to 51 µmol/kg) in ice-free regions was primarily driven by sea ice melt and biological CO_2 uptake. Estimates of net community production (NCP) reveal net autotrophy in the ice-free Dalton Polynya (NCP = 5 – 20 mmol C m^{-2} day^{-1}) and weakly heterotrophic waters near the ice-covered TIS (NCP = - 4 – 0 mmol C m^{-2} day^{-1}). Satellite-derived estimates of chlorophyll *a* (Chl *a*) and sea ice coverage suggest that the early summer season in 2014/2015 was anomalous relative to the long-term (1997-2017) record, with lower surface Chl *a* concentrations and a greater degree of sea ice cover during the period of observation; the implications for seasonal primary production and air-sea CO_2 exchange are discussed. This study highlights the importance of both physical and biological processes in controlling air-sea CO_2 fluxes and the significant interannual variability of the CO_2 system in Antarctic coastal regions.

Plain Language Summary

Coastal polynyas in Antarctica are dynamic regions that play important roles in the global cycling of carbon. Polynyas are reoccurring areas of open water within sea ice and are often associated with enhanced rates of photosynthesis and exchange of carbon dioxide between the atmosphere and ocean surface. In this study, we use shipboard observations from the first oceanographic cruise in the Dalton Polynya near the Totten and Moscow University Ice Shelves in East Antarctica to characterize the inorganic carbon chemistry in the summertime. We find that the surface concentrations of total dissolved inorganic carbon are reduced in areas of open water mainly as a result of seasonal sea ice melt and the uptake of inorganic carbon by photosynthesis and less so due to air-sea exchange of carbon dioxide. Compared to other coastal polynyas in East Antarctica, our results show that the Dalton Polynya may have smaller rates of net photosynthesis and carbon dioxide exchange.

3.1 Introduction

The Southern Ocean plays an integral part in the global biogeochemical cycling of carbon, mediating the exchange of both natural and anthropogenic CO_2 between the upper ocean and atmosphere (Arrigo et al., 2008a; Sabine et al., 2004; Takahashi et al., 2009). Although several global estimates of air-sea CO_2 exchange agree that the open Southern Ocean sustains one of the largest sinks of atmospheric CO_2 (Gruber et al., 2009; Khatiwala et al., 2009; Lenton et al., 2013), uncertainties remain regarding the magnitude of this CO_2 uptake along Antarctic continental shelves that are seasonally covered with sea ice (Lenton et al., 2013). Models are confounded in these regions by the limited number of direct observations and significant natural variability of the CO_2 system on both temporal and spatial scales (e.g., McNeil et al., 2011).

Polynyas are reoccurring areas of open water surrounded by sea ice that form along the coasts of the Antarctic icescape, typically in the lee of a fixed boundary, such as a grounded iceberg or a glacial tongue. In these regions, strong ocean currents and/or katabatic winds push newly formed sea ice away to sustain areas of open water or thin ice for much of the year (Massom et al., 1998; Morales Maqueda et al., 2004). There is a growing understanding of the interactive physical and biological processes impacting CO_2 system dynamics in seasonally sea ice-covered regions such as the East Antarctic (Roden et al., 2016; Shadwick et al., 2014), the West Antarctic Peninsula (Jones et al., 2017; Legge et al., 2017), and the Amundsen (Mu et al., 2014; Yager et al., 2016) and Ross Seas (DeJong et al., 2015; DeJong & Dunbar, 2017). In the spring and summer, coastal polynyas often support intense biological activity relative to their small surface areas as reduced sea ice coverage exposes surface waters to incoming solar radiation (Arrigo & van Dijken, 2003),

driving a dramatic undersaturation in CO_2 at the ocean surface. The timing and magnitude of surface biological CO_2 drawdown are strongly influenced by local sea ice dynamics that determine light and micronutrient (e.g., iron) availability, water column stratification, and the degree of open water. The organic matter that forms during the productive season can be recycled in the mixed layer or exported to depth where it will be subsequently remineralized back to CO_2. In winter, deep convective mixing driven by brine rejection during sea ice formation reinjects CO_2-rich waters to the surface layer where the presence of sea ice may act as a barrier for air-sea exchange and prevent the outgassing of CO_2 to the atmosphere (Loose et al. 2011; Yager et al., 1995). In some Antarctic polynyas, these CO_2-rich waters may additionally be transported off the continental shelf with the formation of dense water (Shadwick et al., 2014). Their disproportionate roles in the air-sea exchange of CO_2 (e.g., Sweeny, 2003), primary production (e.g., Shadwick et al., 2017), and in some cases Dense Shelf Water and Antarctic Bottom Water formation (Orsi et al., 1999; Rintoul, 1998; Williams et al., 2008) make these coastal polynya systems important players in the biogeochemical cycles of the Southern Ocean.

Despite the importance of the continental shelf regions in global carbon cycling, few observational CO_2 system studies have been conducted in the coastal East Antarctic. The Dalton Polynya is a coastal polynya located on the Sabrina Coast in East Antarctica, forming in the lee of the Dalton Iceberg Tongue (Figure 3.1). The surrounding Totten and Moscow University Ice Shelves (TIS and MUIS, respectively), which terminate at the sea boundary in the Dalton Polynya, are among the fastest thinning on the East Antarctic Ice Sheet, with high rates of mass loss (Mohajerani et al., 2018) and basal ice shelf melting near their grounding lines over the past 15 years (Rignot et al., 2013). Basal melting of

these ice shelves is driven by on shelf intrusions of relatively warm (>0 °C) modified Circumpolar Deep Water to ice-shelf cavities (Li et al., 2015; Rintoul et al., 2016; Silvano et al., 2017) and is modulated by surface winds stress (Greene et al., 2017). These high basal melt rates (> 4 m/year) are similar to those observed in the West Antarctic Ice Sheet near the Amundsen and Bellingshausen Seas, regions often thought of as more vulnerable to mass loss and glacial thinning (Rignot et al., 2013; Silvano et al., 2017). Meltwater input to the Dalton Polynya contributes to significant water column freshening, reducing the possibility for dense water formation in the region (Silvano et al., 2018). Previous studies in the coastal Antarctic suggest glacially derived meltwater may influence mixed-layer biogeochemistry and carbon cycling by stimulating high levels of primary production through the delivery of iron and other essential micronutrients to surface waters (e.g., Eveleth et al., 2017, Gerringa et al., 2012). The potential impacts of glacial mass loss and high rates of basal melting to the Dalton Polynya system may drive future changes in biological production and air-sea CO_2 flux that ultimately influence the carbonate chemistry.

Here we present CO_2 system measurements from the Dalton Polynya in early summer (Figure 3.1). A combination of high-frequency underway measurements of sea surface CO_2 fugacity (fCO_2) along the ship track and discrete samples of total dissolved inorganic carbon (TCO_2) and total alkalinity (TA) is used to characterize the biogeochemistry of the region. The physical and biological processes responsible for observed distributions of mixed-layer TCO_2 are examined, and net community production is computed via seasonal deficits in TCO_2 concentration. Additionally, the spatial variability of air-sea CO_2 fluxes is evaluated. These new observations are also examined

in comparison to the long-term (1997–2017) surface chlorophyll *a* concentration and sea ice coverage derived from remote sensing products to assess interannual variability. Results from the Dalton Polynya highlight the importance of both physical and biological processes in controlling the significant seasonality in the CO_2 system of Antarctic coastal waters.

3.2 Oceanographic Setting

We follow the water mass characterization of Silvano et al. (2017) to define the four major water masses in the Dalton Polynya (DP) during the summer season, constrained here by potential density anomaly surfaces referenced to surface pressure (σ_θ, kg/m^3) and potential temperature (θ, °C; Figure 3.2 and Table 3.1). Antarctic Surface Water (AASW) is the lightest (σ_θ < 27.55 kg/m^3) and is highly variable in surface temperature (between -1.86 and -0.23 °C) and salinity (between 33.6 and 34.2; Figure 3.2). AASW is relatively fresh, due to seasonal melting from both the surrounding sea ice and the ice shelves to the south. This water mass varies in thickness across the region: in the ice-free DP, AASW occupies the upper ~80 m (Figure 3.3); near the TIS, signals of AASW virtually disappear, as Winter Water (WW) reaches the surface (Figure 3.4). WW ranges between 27.55 < σ_θ < 27.70 kg/m^3 and -1.92 < θ < -1.75 °C and occupies most of the water column in summer as a product of vertical convection. The depth range of WW depends on its location within the polynya, as WW shoals nearly to the surface along the ice shelves.

Dense Shelf Water does not form in the DP. Instead, relatively warm, salty modified Circumpolar Deep Water (mCDW) floods the deep basin in summer (σ_θ > 27.70 kg/m^3), bringing heat, nutrient, CO_2-rich, and relatively O_2-poor water onto the shelf. The

inflow of mCDW through deep troughs in both the TIS and MUIS delivers a substantial amount of heat to drive rapid basal melt at the grounding line (Greenbaum et al., 2015; Rintoul et al., 2016; Silvano et al., 2017). At the MUIS ice front, the melting drives the formation of Ice Shelf Water (ISW), through the mixture of basal ice shelf meltwater and WW. ISW is supercooled due to pressure at $\theta < -1.92$ °C within the same σ_θ range as WW. The input of basal meltwater, particularly near the MUIS, also leads to a shoreward freshening of WW near the southern edge of the DP (Silvano et al., 2017).

3.3 Methods

Observations were made during a survey of the Dalton Polynya and surrounding ice shelves along the Sabrina Coast (116° - 122 °E) on board the *RV Aurora Australis* between 25 December 2014 and 8 January 2015 (Figure 3.1; Rosenberg & Rintoul, 2016). The ship occupied 68 stations in the DP and near the MUIS and 13 stations in a lead in front of the TIS. During each cast, continuous measurements of temperature (°C), salinity, pressure (dbar), and dissolved oxygen (μmol/kg) were made using SeaBird instruments (SBE9plus and SBE43 models). Instruments were mounted onto a rosette frame with 22 10-L General Oceanics Niskin bottles for discrete seawater sampling; hydrographic property analysis of conductivity, temperature, and depth CTD data is described further in Silvano et al. (2017).

The shelf can be separated into two broad regions: DP refers to the region east of 119°E and TIS refers to the region west of 119°E. These regions are further partitioned into subregions illustrated in Figure 3.1. The DP includes measurements made between 24 and 29 December (DP1, blue), between 2 and 5 January and three CTD stations on 7 January

(DP2, red), and between 6 and 8 January (DP3; yellow). The TIS region includes measurements between 30 December 30 and 1 January and is divided into West Totten (WT; magenta) and East Totten (ET; green).

3.3.1 Discrete CO_2 System and Biogeochemical Observations

Discrete samples of TCO_2 and TA were collected into 250-ml bottles at each station. Each sample was immediately fixed with a saturated solution of mercuric chloride to halt biological activity. TCO_2 and TA concentrations were measured on board by coulometric titration using a Single Operator Multiparameter Metabolic Analyzer (SOMMA) system and by automatic open-cell potentiometric titration with 0.1 M hydrochloric acid, respectively, following methods of Dickson et al. (2007). Routine analysis of Certified Reference Material (CRM Batch #137) from A. G. Dickson ensured that the analytical uncertainties (precision and accuracy) were better than ± 1.4 µmol/kg for TCO_2 and ± 1.5 µmol/kg for TA.

Samples of dissolved oxygen were collected in parallel to CO_2 system observations and analyzed on board by Winkler Titration following methods of Hood et al. (2010), with an uncertainty of <1%. Inorganic nutrient samples were collected for phosphate (PO_4^{-3}) and silicic acid ($Si(OH)_4$), and frozen until analysis at CSIRO in Hobart, Australia, following standard methods of Grasshoff et al. (2007). Uncertainties for PO_4^{-3} and $Si(OH)_4$ were <5%.

The saturation state of aragonite (Ω_{Ar}) and pH on the total scale were calculated from TCO_2 and TA using the CO_2SYS program by van Heuven et al. (2011), using the thermodynamic equilibrium constants by Mehrbach et al. (1973) refit by Dickson and

Millero (1987). Average values of PO_4^{-3} (2.06 ± 0.07 µmol/kg) and $Si(OH)_4$ (64 ± 7 µmol/kg) were used. Calcium ion concentration was assumed to be conservative with and calculated from salinity (Riley & Tongudai, 1967).

3.3.2 Underway *f*CO_2 Measurements and Air-Sea CO_2 Flux Calculations

Continuous high-resolution underway measurements of the *f*CO_2, sea surface salinity, and sea surface temperature were made from the seawater intake ~4 m below the ocean surface. The *f*CO_2 in seawater was measured via continuous flow equilibration using a nondispersive infrared spectrometer (LI-COR, LI7000; Pierrot et al., 2009). The underway *f*CO_2 system was calibrated every 4 hrs with four standards: a CO_2-free air and three CO_2 concentrations of 299.41, 354.00, and 402.15 µatm in dry air on the WMOX2007 mole fraction scale. Approximately 70 s were needed for the seawater to pass from the ship intake to the CO_2 system, warming by less than 0.6 °C. All *f*CO_2 measurements were corrected to *in situ* temperature and salinity and to 100% humidity. The atmospheric mole fraction of CO_2 was also measured at roughly 16 m above sea level to calculate the atmospheric *f*CO_2. The mean atmospheric *f*CO_2 was 379 ± 1.7 µatm throughout the voyage. The *f*CO_2 measurement uncertainties are 2 µatm in seawater and 0.2 µatm in air at 350 µatm.

The air-sea flux of CO_2 between the sea surface and the atmosphere was computed via the following equation:

$$F_{CO2} = k\ \alpha\ \Delta fCO_2 \qquad (3.1)$$

where F_{CO2} is the flux (mmol C m^{-2} day^{-1}), k is the gas transfer velocity, α is the solubility of CO_2 (Weiss, 1974), and Δ*f*CO_2 (µatm) is the gradient in *f*CO_2 between the atmosphere and sea surface (Δ*f*CO_2 = *f*CO_2^{sea} – *f*CO_2^{air}). A positive flux indicates a net transfer from

the ocean to the atmosphere (i.e., outgassing). The parametrization of Wanninkhof (2014) was used to compute *k* using daily averaged short-term winds, consistent with methodology from other Antarctic polynya regions (e.g., Gibson & Trull, 1999; Shadwick et al., 2014, 2017), from the National Centers for Environmental Prediction/National Center for Atmospheric Research (NCEP/NCAR) Reanalysis product recorded at 10-m height above the sea surface (Kalnay et al., 1996). The exchange time of CO_2 between the surface ocean and the atmosphere is on the order of months (Broecker & Peng 1974), and air-sea CO_2 fluxes were similarly computed using a long-term gas transfer velocity term to provide a broader context for instantaneous (short-term) fluxes. A long-term *k* was calculated from the average of daily second moment of the wind speed ($<\text{wind speed}>^2$) across eight NCEP/NCAR grid cells (within the spatial range of 65 - 68 °S and 116 - 122 ºE) between December 2014 and January 2015 (Evans et al., 2015; Wanninkhof et al., 2004). We estimate an uncertainty associated with the air-sea CO_2 flux of 0.3 mmol C m^{-2} day^{-1} by comparing results obtained with several different gas transfer parameterizations (Edson et al., 2011; Ho et al., 2006; Sweeney et al., 2007; Wanninkhof, 1992).

3.3.3 Seasonal Partitioning of TCO_2 and Net Community Production Computations

Seasonal changes of TCO_2 in the summer mixed layer are influenced both by physical (e.g., air-sea CO_2 exchange, mixing, and calcium carbonate dissolution) and biological (e.g., photosynthesis, respiration, and calcium carbonate formation) processes. The summer mixed layer depth (MLD) at each station is defined here as the depth at which the potential density exceeds that of a reference measurement at 10 m by a threshold 0.01 kg/m^3 (e.g., Shadwick et al., 2014) and was comparable to MLD expressed as the maximum

of the buoyancy frequency (Carvalho et al., 2017). Although observed summer MLDs in the DP were typically <100 m, deeper vertical mixing earlier in the productive season (i.e., late winter, early spring) extends well below 100 m (Williams et al., 2011). Late-winter measurements in 2007 found the deepest winter mixed layer on the Sabrina Coast in the northern DP, reaching depths >350 m (Williams et al., 2011). Summer MLDs in front of the western TIS, however, were significantly deeper (MLDs > 180 m) than in the open waters of the DP.

Wintertime TCO_2 concentration in surface waters is often estimated using the value at the temperature minimum (e.g., Bates et al., 1998; Roden et al., 2016). However, on the Antarctic shelf, the temperature minimum is not well defined, for example in the areas in front of the MUIS where ISW is present (Silvano et al., 2017). Profiles of TCO_2 indicate a consistent concentration at depths in the WW water mass ($27.55 < \sigma_\theta < 27.70$ kg/m^3 and $-1.92 < \theta < -1.75$ °C), roughly between 150 and 350 m. Thus, we estimate the surface wintertime TCO_2 concentration as the average concentration at 150 m depth (TCO_2^{winter} = 2,216 ± 2 µmol/kg, n = 26). Measurements of TCO_2 and TA are normalized to the average regional salinity (S = 34.3) to account for the seasonal variations in concentration due to changes in salinity from sea ice formation and melting, as well as mixing (e.g., Shadwick et al., 2014).

The seasonal change in TCO_2 due to biological processes is expressed as the net community production (NCP), the difference between net primary production and heterotrophic respiration. NCP (mmol C m^{-2} day^{-1}) was computed at each station by the depth integrated seasonal deficit of salinity normalized TCO_2 ($nTCO_2$) via

$$NCP = \int_{z=0}^{z=100} [\mathrm{nTCO_2}]^{\mathrm{winter}} - [\mathrm{nTCO_2}]^{\mathrm{observations}} \, dz \qquad (3.2)$$

where *z* is depth in meters. Although MLDs at each station were above 100 m within the open waters of the Dalton Polynya, we integrated to 100 m to account for deeper vertical mixing earlier in the productive season (Bates et al., 1998; Shadwick et al., 2014; Williams et al., 2011). The length of the productive season was defined as time since 1 November 2014 based on the increase in surface chlorophyll *a* (Chl *a*) concentration relative to winter months (June, July, and August) inferred from Moderate Resolution Imaging Spectroradiometer (MODIS)-Aqua satellite imagery during the 2014/2015 summer season (see section 3.5.2). This estimation of NCP does not account for the contribution of seasonal air-sea CO_2 exchange, although the contribution is small based on summer F_{CO2} computations (see sections 3.4.2 and 3.5.1 for further discussion).

3.3.4 Satellite Remote Sensing Products

Satellite-derived sea surface Chl *a* concentrations were obtained from Level 3 processed, 9 km resolution measurements from SeaWiFS (Sea-viewing Wide Field-of-view Sensor) between July 1997 and June 2002 and from MODIS-Aqua between July 2002 and June 2017. Similarly, sea ice coverage estimates were obtained from the Special Sensor Microwave/Imager (SMM/I) and the Special Sensor Microwave Imager/Sounder (SMMIS) on the Defense Meteorological Satellite Program (DMSP) satellite from the National Snow and Ice Data Center (NSIDC) between July 1997 to June 2017 at 25-km resolution and Level 3 processing. All data presented here are monthly-averaged values in the Dalton Polynya, within the region between 65.8 and 67.0 °S and 119 and 121 °E (see Figure 3.1).

3.4 Results

3.4.1 Hydrographic and Biogeochemical Properties

AASW (σ_θ < 27.55 kg/m^3) in the DP was relatively warm and fresh, reflecting the summer conditions of surface warming and local sea ice melt (Figures 3.2 and 3.5 and Table 3.2). Sea surface salinity was about between 33.9 and 34.3 within the DP (east of 119°E). In the northern DP, minimum surface salinity (S <33.9) was observed toward the end of the voyage, likely driven by melting sea near the Dalton Iceberg Tongue. Sea surface temperatures were warmer in the central DP with values ranging from –1.2 to +0.4 °C, and colder near the outer edges of the polynya and near the TIS with a minimum of -1.8 °C (Figure 3.5 b). In front of the TIS, WW outcropped to the surface, and salinities of ~34.25 were observed.

The mean concentration of dissolved oxygen (~341 µmol/kg) in AASW was greater than values found elsewhere in East Antarctica (Roden et al., 2016; Shadwick et al., 2014), with concentrations more comparable to saturated conditions (~350 – 360 µmol/kg) though similar surface temperature and salinity was observed (Table 3.2). The percent saturation of dissolved oxygen at the sea surface was greatest (>99%) in the central, open waters of the Dalton Polynya (Figure 3.3 d) and decreased toward and along the outer edges of the polynya and near the TIS (Figure 3.4 d). In front of the TIS, surface dissolved oxygen reached a minimum concentration (305 µmol/kg, 85% saturation), coincident with the WW outcrop and entrainment of oxygen-poor subsurface waters. Dissolved oxygen concentration further decreased with depth below the surface mixed layer in WW (Figures 3.3 d and 3.4 d) to values ranging between 300 and 330 µmol/kg, signaling the biological imprint of dissolved oxygen consumption. The cumulative influence of the

remineralization of organic matter over longer time scales (i.e., years) is seen more dramatically in mCDW, where dissolved oxygen reaches as low as 220 µmol/kg due to its isolation from the atmosphere.

3.4.2 Underway fCO_2 and Air-Sea CO_2 Exchange

The surface and mixed layer distribution of dissolved oxygen spatially mirrors the trends in underway fCO_2 (Figures 3.3 d, 3.4 d, and 3.5 c), where the lowest concentrations of dissolved oxygen are found in areas of high fCO_2. The sea surface fCO_2 indicates that the region was mostly supersaturated or near equilibrium with respect to the average atmospheric value (379 µatm; Figures 3.5 c and 3.6 a) in both the DP and near the TIS. There was a distinct difference in surface fCO_2 in areas with the absence (within DP) or presence (near TIS) of sea ice. In areas of open water in the DP, fCO_2 ranged from 370 to 405 µatm, extending to a maximum of 410 µatm near the eastern MUIS. The largest fCO_2 values were recorded near the TIS, with a maximum of 424 µatm at the western edge, exhibiting the correspondingly greatest degree of supersaturation relative to the atmosphere (ΔfCO_2 = +45 µatm). In contrast, the northern DP showed the greatest degree of undersaturation with respect to the atmosphere (ΔfCO_2 = –20 µatm).

The Dalton Polynya was a net source of CO_2 to the atmosphere during the sampling period as determined by both the long-term and instantaneous air-sea CO_2 fluxes with means and standard deviations of 0.5 ± 0.6 mmol C m^{-2} day^{-1} and 0.7 ± 0.9 mmol C m^{-2} day^{-1}, respectively. F_{CO2} values evaluated with the long-term *k* reached a maximum of 2.3 mmol C m^{-2} day^{-1} in the most supersaturated waters near the TIS and a minimum of -1.1 mmol C m^{-2} day^{-1} in the northern DP (DP3). Using short-term winds, values of

instantaneous F_{CO2} had a larger range, between a maximum surface uptake of 1.0 mmol C m^{-2} day^{-1} to a maximum surface outgassing of 5.1 mmol C m^{-2} day^{-1} from within the center of the DP (DP2) during the study period. Short-term wind speeds were locally variable throughout, ranging between near 0 to 10 m/s (Figure 3.6 b); these fluctuations imposed a correspondingly large variation in flux. In particular, during periods of enhanced wind, defined here as wind speed > 8 m/s, and conditions with large ΔfCO_2, there were correspondingly large fluxes of CO_2 (Figure 3.6, shaded). We observed three high wind events: one at the beginning and two near the end of the study. In the first high wind event, the relatively large ΔfCO_2 resulted in an outgassing of roughly 4.3 mmol C m^{-2} day^{-1}. During the second high wind event in the DP, a maximum F_{CO2} of 5.1 mmol C m^{-2} day^{-1} was observed. Although both minimum and maximum ΔfCO_2 values were recorded near the northern DP and TIS, respectively, these gradients were observed during periods of much lower wind speeds (~1 to 3 m/s) and were associated with correspondingly weaker CO_2 fluxes on the order of ~0.02 mmol C m^{-2} day^{-1}.

3.4.3 CO_2 System Properties in the Dalton Polynya

Vertical profiles of TCO_2 and TA from stations in the DP during each sampling period (DP1, DP2, and DP3) were similar with depth, reflecting the different properties within each water mass (Figure 3.7). Surface TCO_2 concentrations ranged between 2,190 and 2,211 µmol/kg in the central DP. Minimum surface TCO_2 concentrations (~2,170 µmol/kg) were found in the northern polynya (yellow; DP3), corresponding with the surface salinity minimum. Similarly, surface TA values ranged between 2,303 and 2,314 µmol/kg in the central DP, with a similar feature of minimum values of ~2,276 µmol/kg

found in the northern DP. Subsurface parameters converge at a depth of approximately 150 m to an average TCO_2 concentration of 2,214 ± 3 µmol/kg and TA concentration of 2,315 ± 2 µmol/kg in WW (Figures 3.7 a and 3.7 b), similar to other observations made in shelf waters in the East Antarctic (Table 3.2; Roden et al., 2016; Shadwick et al., 2014).

Profiles of pH and Ω_{Ar} exhibit similar patterns with depth, reflecting the changes in TCO_2 and TA concentrations. The surface pH and Ω_{Ar} were elevated relative to subsurface values, enhanced by the biological drawdown of TCO_2 by photosynthesis. We observed pH values ranging from 8.01 to 8.07 at the surface. Surface Ω_{Ar} ranged from 1.22 and 1.38, with lower values near the western ice edge in the DP (not shown) coincident with regions of elevated surface TCO_2. Ω_{Ar} was supersaturated throughout most of the water column, although undersaturated values of Ω_{Ar} (i.e., $\Omega_{Ar} < 1$) were found at depth in the TCO_2-rich mCDW layer. Below ~400 m, TCO_2 and TA continued to increase while pH and Ω_{Ar} decrease with depth in the mCDW water mass.

The precipitation of calcium carbonate (ikaite) during sea ice formation in the previous autumn and winter season may influence the TCO_2 to TA ratio in both the newly formed sea ice and the underlying seawater (Dieckmann et al., 2008; Jones et al., 2010; Rysgaard et al., 2012; Shadwick et al., 2017). However, from our observations, the conservative behaviors of the TA-salinity and the nTA-$nTCO_2$ relationships (Figure 3.7 d inset) suggests that ikaite formation is not a dominant process in the Dalton Polynya.

Salinity-normalizing TCO_2 and TA values accounts for the freshwater dilution of sea ice melt in the Dalton Polynya on surface concentrations; surface to subsurface gradients in $nTCO_2$ and nTA are thus much weaker than in the in-situ observations (Figures 3.7 c and 3.7 d). Surface $nTCO_2$ values ranged between 2,200 and 2,216 µmol/kg and

surface nTA to between 2,315 and 2,323 µmol/kg. Higher surface $nTCO_2$ values were found along the western sea ice edges in the DP as compared to the center of the DP (not shown). At 150 m depth, mean $nTCO_2$ concentration was 2,216 ± 2 µmol/kg, which is assumed to represent the winter concentration of $nTCO_2$ at the surface (see section 3.3.3).

3.4.4 CO_2 System Properties near the Totten Ice Shelf

Profiles of CO_2 system parameters show somewhat different properties near the TIS than those described above (Figure 3.8). Here, WW outcrops to the surface near the TIS, particularly in the western edge (see Figure 3.4) where MLDs extended over 360 m. The stations occupied in the east TIS (magenta) show a similar pattern with depth as those in the DP, where AASW is present at the surface and MLDs ranged between 12 and 46 m. Surface TCO_2 in the eastern TIS stations show a mean value of 2,205 µmol/kg, similar to the DP, whereas surface TCO_2 in the western TIS show higher values with an average of 2,213 µmol/kg (Figure 3.8 a). Surface $nTCO_2$ was more depleted in the east (~2,212 µmol/kg) than in the west (~2,218 µmol/kg). In WW, the $nTCO_2$ in stations near the TIS converged to 2,217 ± 2 µmol/kg. In stations in the western TIS, $nTCO_2$ at the surface was modestly elevated (between 0 and 4 µmol/kg) relative to the subsurface winter value.

Mean surface pH (~8.02) and Ω_{Ar} (~1.24) near the TIS were lower as compared to the DP. Surface pH and Ω_{Ar} values also increased from west to east spatially in front of the TIS, corresponding to higher concentration of TCO_2 in the west. Ω_{Ar} reached undersaturation ($\Omega_{Ar} < 1$) at depths > 750 m.

3.5 Discussion

3.5.1 Net Community Production

Seasonal depletions of TCO_2 in the upper 100 m were determined and attributed to a combination of physical and biological processes in both waters in the ice-free DP and ice-covered TIS (Figure 3.9 and Table 3.3). Processes such as sea ice melt (formation), CO_2 outgassing (ingassing), and photosynthesis (respiration) decrease (increase) the concentration of TCO_2. Total integrated deficits of TCO_2 (ΔTCO_2^{total}; Table 3.3) were larger in ice-free regions as compared to areas with greater sea ice coverage. In the DP, the contribution from the seasonal melting of sea ice accounted for less than half of the total change in TCO_2 in DP1 and DP2 but was more significant in DP3. Observations of surface salinity and temperature in DP3 suggest that sea ice melt was ongoing near the Dalton Iceberg Tongue (section 3.4.1). At all stations in the Dalton Polynya, NCP was positive, ranging between 1 and 21 mmol C m^{-2} day^{-1} (Figure 3.10 a; see section 3.3.3), indicating net autotrophy or the dominance of primary production over respiration (Table 3.3). Both the $nTCO_2$ deficits and the resulting NCP values were greatest in the center of the DP and lower near the western boundary and the sea ice edge. Estimates of NCP are on the order of 10 to 20 mmol C m^{-2} day^{-1} within the ice-free regions in the polynya and increase over the duration of the of the cruise, from DP1 to DP3, in parallel with decreasing mixed layer $nTCO_2$ concentrations (Figure 3.10). In the northernmost stations of the polynya (DP3), sea ice melt locally enhanced stratification and stabilized the mixed layer (MLDs = ~12 m), increasing light availability and contributing to enhanced biological activity and greater NCP. This is consistent with observations of decreased fCO_2 in the region (Figure 3.4 a). By contrast, the $nTCO_2$ deficits and NCP are lower in front of the TIS (Table 3.3), ranging

from -3.8 to a maximum of 6.6 mmol C m^{-2} day^{-1}, increasing spatially from west to east in parallel to decreasing MLDs and the increasing dominance of AASW at the surface (Figure 3.4). In the eastern edge of the TIS (ET), deficits of TCO_2 are dominated by changes in salinity with smaller contributions from biological CO_2 uptake resulting in weakly autotrophic conditions. At stations of the western TIS (WT), NCP was negative ranging from -3.8 to 0 mmol C m^{-2} day^{-1}, suggesting the region may be weakly heterotrophic in the summer season, consistent with highly supersaturated fCO_2 in the surface waters of the region (Figure 3.5 c).

These estimates of NCP include uncertainties associated with the analytical determination of TCO_2 concentrations as well as the assumptions regarding winter TCO_2 concentrations. Vertical transport processes that may influence mixed-layer TCO_2 have not been explicitly accounted for, although it is assumed the integration to 100 m accounts for deeper mixing (e.g., Sweeney et al., 2000). In addition, both $CaCO_3$ precipitation/dissolution and the air-sea exchange of CO_2 are not explicitly included in the seasonal deficit approach, although the former has been shown to be a negligible process during the period of observation (section 3.4.3). The mean instantaneous F_{CO2} computed from our shipboard observations was 0.7 ± 0.9 mmol C m^{-2} day^{-1}. If this mean flux were to persist since 1 November (defined as the beginning of the productive season), then this would lead to an additional $nTCO_2$ concentration of 0.4 µmol/kg in the upper 100 m from the air-sea exchange of CO_2, which is small (< 2%), relative to the integrated deficits.

The onset of biological activity in the coastal Antarctic is generally thought to occur when MLDs < 40 m (Smith et al., 2000). As most MLD in the open waters of the DP are < 40 m, photosynthesis dominates respiration, associated with positive values of NCP. It

is likely that we observed the beginning of the productive season when NCP rates were relatively low capturing conditions consistent with the transition from winter to summer. In this period, the biological driver of fCO_2 drawdown has not yet fully compensated for the increased winter fCO_2 due to remineralization (and small seasonal warming of surface waters); thus, surface waters remain supersaturated in fCO_2 despite the positive NCP (i.e., autotrophic conditions). Similarly, dissolved oxygen concentration in AASW within the open waters of the DP was still slightly undersaturated (~1-12%) during the period of observation, suggesting the autotrophic community has not yet fully compensated for loss of dissolved oxygen during the predominating winter heterotrophy. The continuation of summer surface productivity beyond the period of shipboard observation is supported by satellite Chl *a* and discussed in more detail below.

The negative NCP that was observed near the TIS may be fueled by the remineralization of allochthonous organic material, which can include production remaining from previous years, assuming the particulate and dissolved organic carbon is labile, or semilabile. Upwelling and mixing of TCO_2-rich waters could also be associated with accumulated signals of biological remineralization (rather than the accumulation of organic matter) from distant sources. The MLDs near the western end of the TIS were relatively deep, reaching over 300 m in certain areas, extending well below the depth of our definition for winter TCO_2 concentration and seasonal integration (100 m). This deep mixing could entrain TCO_2-rich subsurface water into the summer mixed layer; if these deeper waters have sufficiently high TCO_2 concentrations (from the remineralization of organic matter over timescales that exceed a season), the resulting deficit would indicate net heterotrophic conditions. Finally, since the ice-covered waters near the TIS appear to

be significantly less productive than those in the ice-free Dalton Polynya (inferred from the degree of fCO_2 undersaturation), these early summer observations may represent pre-bloom conditions in the TIS perhaps due in part to light limitation associated with sea ice coverage. If the observations had been made later in the season, it is possible that greater surface TCO_2 depletions in a more open TIS region would result in positive NCP (i.e., net autotrophy), similar to conditions observed in the ice-free regions of the adjacent Dalton Polynya. This potential bias due to the timing of observations with respect to ice melt and the onset of open water biological production will be discussed in more detail in the next section.

3.5.2. Interannual Variability

Coastal shelf waters are known to exhibit significant variability that is difficult to diagnose with shipboard observations (Kaufman et al., 2014; Roden et al., 2013) Fortunately, satellite remote sensing products allow this variability to be assessed over seasonal and interannual timescales in regions where direct biogeochemical observations do not exist. Surface Chl *a* concentrations and sea ice coverage can serve as proxies to assess the variability in biological productivity and the physical environment, respectively, allowing long-term trends in regions with sparse in-situ observations to be evaluated.

Climatological estimates of Chl *a* (mg/m^3) and percent sea ice coverage (%) between 1997 and 2017 (Figure 3.11) reveal significant interannual variability in the Dalton Polynya. The average seasonal cycle of Chl *a* indicates that the onset of productive season can begin as early as October, when light returns in the austral spring, and suggests that the productive season was underway at the time of observations in early summer.

Maximum concentrations of Chl *a* typically peak in January, with an average maximum concentration of 2 mg/m^3 when sea ice coverage is below 50%. In winter (between May and October), there is little and/or non-detectable surface Chl *a* and sea ice coverage is on the order of 70%. Sea ice retreat typically begins in November.

In contrast to the long-term average Chl *a* concentration, the 2014/2015 surface Chl *a* concentrations remained relatively low until February, roughly 1 month after then end of the voyage (black line; Figure 3.11 a). Assuming that Chl *a* can be considered as reliable proxy for biomass, it is likely that increased fCO_2 undersaturation coincided with maximum surface Chl *a* concentrations due to biological drawdown by photosynthesis. During the period of observations in early January, areas of the Dalton Polynya exhibited fCO_2 supersaturation and low surface Chl *a* concentrations. Thus, during the 2014/2015 season, our sampling preceded the height of the open-water productive season, and we observed the early spring-to-summer transition when the surface waters were still supersaturated with respect to atmospheric CO_2. If the growing season persisted through March of the sampling year, as the satellite record suggests, it is likely that the open surface waters would have become undersaturated in the region as a whole and may have transitioned to a sink for atmospheric CO_2 in the late summer and early autumn seasons. This suggests that our seasonal estimates of NCP in the Dalton Polynya may be underestimated, and these values cannot be extrapolated over longer time scales. Similarly, as sea ice coverage near the TIS continued to decline in February, the region may also have transitioned to net autotrophic conditions.

In addition to the role of sea ice in light limitation, sea ice provides a source of dissolved iron to the surface waters during the seasonal melt (Lannuzel et al., 2007), which

may stimulate biological productivity (e.g., Sedwick & DiTullio, 1997). During the 2014/2015 season, the onset of sea ice melt in October is in line with the long-term mean (Figure 3.11 b). However, there was an increase in sea ice coverage in December and January, resulting in a greater degree of coverage than the long-term average. This late season sea ice growth would have impeded light penetration, limiting biological productivity and may have restricted the delivery of iron to the surface waters via sea ice melt in early summer.

3.5.3 Comparison of the Dalton Polynya with other coastal Antarctic systems

Coastal polynya systems range widely in their physical icescapes, formation mechanisms, seasonal sea ice dynamics, and wind and current regimes, which ultimately influence spring and summer biological production and CO_2 system properties (e.g., Arrigo et al., 2015). Of the 13 major Antarctic coastal polynyas identified by Nihashi and Ohshima (2015) and Ohshima et al. (2016), the Dalton Polynya ranks eleventh in terms of average wintertime polynya area ($3.7 \pm 2.0\ 10^3$ km^2/year with daily standard deviation) and twelfth in terms of its mean annual sea ice production (31 ± 3 km^3/year) between 2003 and 2011.

The Dalton Polynya has a substantially lower seasonal NCP and summer air-sea CO_2 flux than the majority of observed coastal polynyas and bays in the East Antarctic (Table 3.4). NCP from this study in the Dalton Polynya was similar to values reported in the Mertz Polynya (Adélie and George V Land region of East Antarctica, 143 – 148 °E) in January 2001 and January 2008, before the calving of the Mertz Glacier Tongue (MGT) in 2010 (Sambrotto et al., 2003; Shadwick et al., 2014). Pre-calving air-sea CO_2 fluxes in the Mertz Polynya were also slightly greater (-15 mmol C m^{-2} day^{-1}) than the instantaneous

fluxes in the Dalton Polynya reported here due to larger degrees of surface fCO_2 undersaturation (Shadwick et al., 2014). However, NCP and air-sea CO_2 exchange rates in the Dalton Polynya stand in contrast to rates from the post-calving configuration of the Mertz Polynya. The MGT calving event substantially reduced Mertz Polynya size and sea ice production in the subsequent years (Nihashi & Ohshima, 2015; Tamura et al., 2012), yet post-calving deficits in mixed-layer TCO_2 concentrations and the rates of NCP and air-to-sea flux of CO_2 in the Mertz Polynya dramatically increased in following summers (Shadwick et al., 2017). These corresponding impacts to the CO_2 system have been primarily attributed to an enhancement in biological production as a result of large increases in sea ice meltwater, potentially delivering a source of dissolved iron to the mixed layers (Shadwick et al., 2013). A recent analysis by Moreau et al. (2019) concluded that a larger volume of sea ice meltwater in the Mertz Polynya and neighboring Ninnis Polynya best explained their enhanced biological productivities relative to the Dalton Polynya. The calving of the MGT in the Mertz Polynya set up an interesting natural experiment to assess how changes to the Antarctic icescape impact polynya productivity. As the Dalton Polynya is sustained by the Dalton Iceberg Tongue to the east, a natural calving or shift in the sea ice regime near the Dalton Polynya could potentially lead to changes in the CO_2 system as similarly experienced in the Mertz Polynya system.

NCP and FCO_2 are significantly smaller in the Dalton Polynya than continental shelf waters of the Ross Sea, where annual rates of primary production can reach up to 180 g C m^{-2} $year^{-1}$, among the most productive in the Southern Ocean (Arrigo, et al., 2008b; Smith & Gordon, 1997). Rates of seasonal NCP exhibit a large range of variability in space and time (Peloquin & Smith, 2007; Smith et al., 2006;), though they are several times

greater than those observed in the Dalton Polynya (Table 3.4). In the Terra Nova Bay (TNB) polynya in the western Ross Sea (163 – 167 °E), late summer NCP is an order of magnitude larger than the Dalton polynya at roughly 425 mmol C m^{-2} day^{-1} (Table 3.4; DeJong et al., 2017). Biological production in TNB is typically dominated by diatoms in summer when stratification is stronger and mixed layers are shallower (Arrigo et al., 2000; Tortell et al., 2011), in contrast to the *Phaeocystis antarctica* communities in the Dalton Polynya (Moreau et al., 2019). Polynya formation in TNB is primarily driven by intense offshore katabatic winds (Bromwich & Kurtz, 1984) that prevent a consolidated sea ice pack from forming in the lee of the Drygalski Ice Tongue, with wind speeds often ranging between 10 and 30 m/s (Bromwich, 1989). DeJong et al. (2017) hypothesize these katabatic winds create ideal conditions for the formation of Langmuir circulation cells that encourage frazil ice formation, concentrate algal biomass in the surface, and potentially introduce micronutrient- (e.g., iron-) rich subsurface waters to boost productivity in late summer. The coupling between enhanced late season primary production and the corresponding undersaturation of surface fCO_2 and strong wind speeds results in extremely high CO_2 uptake rates in TNB surface waters (-75 ± 32 mmol C m^{-2} day^{-1}; Table 3.4). An analysis of environmental controls on coastal Antarctic productivity by Arrigo et al. (2015) revealed that continental shelf width plays an important role in controlling hot spots of productivity. Wider continental shelves, such as in TNB in the Ross Sea, increase the contact time of bottom waters with iron-rich sediments. Advection of iron-rich subsurface waters to the upper sun-lit layers could play a role in driving the late summer TNB productivity (DeJong et al., 2017). This mechanism of iron delivery is less likely on the narrower continental shelf waters in the Dalton Polynya.

In Prydz Bay, located in the Indian Ocean sector of the Antarctic (70 – 80 °E) , NCP rates on the order of 15 ± 3 mmol C m^{-2} day^{-1} (1.8 ± 0.4 mol C/m^2 over a 4-month period) have been reported (Roden et al., 2013). Seasonal deficits in mixed-layer TCO_2 were attributed to a combination of sea ice melt and biological production (Roden et al., 2013), similar to the drivers of TCO_2 depletion in the Dalton Polynya, resulting in low surface water fCO_2 and an air-to-sea flux of CO_2. Recent studies in Prydz Bay propose that glacial meltwater from the nearby Amery Ice Shelf may bring a large, bioavailable source of dissolved iron from marine-accredited ice beneath the ice shelf, locally enhancing primary productivity (Herraiz-Borreguero et al., 2016). In contrast to the glacial meltwaters introduced by the intrusions of mCDW beneath the TIS and MUIS (warm-regime) to Dalton Polynya, the glacial meltwaters introduced into Prydz Bay are the result of intrusions of cold Dense Shelf Water beneath the Amery Ice Shelf (cold-regime; Silvano et al., 2016). The resulting outflow of supercooled ISW can entrain subglacial dissolved iron into marine ice layer beneath the ice shelf and, upon basal melting, can deliver dissolved iron onto the continental shelf in concentrations up to 4 orders of magnitude higher than typical Southern Ocean waters (Herraiz-Borreguero et al., 2016). In the analysis by Arrigo et al. (2015), the input of basal meltwater by nearby ice shelves can explain almost 60% of the variance in mean chlorophyll concentrations in Antarctic polynyas. The ongoing input of glacial meltwater from the basal melting of the TIS and MUIS may drive future changes to the biological productivity and carbonate chemistry in the adjacent Dalton Polynya waters.

3.6. Conclusions

New shipboard observations from the Dalton Polynya were used to assess the biological and physical controls on the CO_2 system during the early summer season between December 2014 and January 2015. Profiles of TCO_2 concentration allowed the seasonal NCP to be estimated. The Dalton Polynya is found to be net autotrophic in ice-free areas, though the rates are lower than those observed elsewhere in the East Antarctic. The surface waters near the Totten Ice Shelf show relatively little TCO_2 drawdown, likely due to the ice coverage impeding light penetration to support photosynthesis. NCP near the TIS suggest weakly heterotrophic conditions, with a surplus of organic matter to fuel remineralization potentially coming from the TCO_2–rich winter water during deep mixing. Because polynyas are open or have reduced sea ice cover year-round, they are often thought of as areas of intense biological production leading to enhanced air-sea CO_2 exchange and uptake of atmospheric CO_2. The observations presented here provide an alternative view of Dalton Polynya, with midsummer outgassing of CO_2 to the atmosphere. However, satellite-derived Chl *a* concentrations suggest that late-summer productivity increased in parallel with declining sea ice coverage after the completion of the voyage. Long-term remote sensing data indicate interannual variability in surface productivity in the Dalton Polynya and neighboring areas is significant. Improved understanding of CO_2 system dynamics in the coastal Southern Ocean will require more observations to accurately assess the status of these systems as CO_2 sources or sinks.

Table 3.1. Water mass classification. Constraints of potential density anomaly (σ_θ; kg/m^3) and potential temperature (θ; °C) follow definitions by Silvano et al. (2017).

Water Mass	**σ_θ (kg/m^3)**	**θ (°C)**
Antarctic Surface Water (AASW)	$\sigma_\theta < 27.55$	
Winter Water (WW)	$27.55 < \sigma_\theta < 27.7$	$-1.92 < \theta < -1.75$
Ice Shelf Water (ISW)	$27.55 < \sigma_\theta < 27.7$	$\theta < -1.92$
Modified Circumpolar Deep Water (mCDW)	$27.7 < \sigma_\theta$	

Table 3.2. Characteristic mean values of potential density anomaly (σ_θ; kg/m^3), potential temperature (θ; °C), salinity (S), dissolved oxygen (O_2; µmol/kg), total dissolved inorganic carbon (TCO_2; µmol/kg), total alkalinity (TA; µmol/kg), pH, and aragonite saturation state (Ω_{Ar}) of each water mass in the Dalton Polynya region of East Antarctica.

Parameter	AASW	WW	ISW	mCDW
σ_θ	27.48	27.59	27.56	27.74
θ	-1.24	-1.84	-1.94	-0.36
S	34.17	34.27	34.24	34.53
O_2	341	316	311	251
TCO_2	2,200	2,215	2,214	2,242
TA	2,310	2,315	2,313	2,335
pH	8.04	8.01	8.01	7.94
Ω_{Ar}	1.30	1.17	1.17	1.03

Table 3.3. The total deficit in surface TCO_2 (ΔTCO_2^{total}; µmol/kg), with contributions from seasonal sea ice melt ($\Delta TCO_2^{salinity}$; µmol/kg) and biological processes and CO_2 gas exchange ($\Delta TCO_2^{bio+gas}$; µmol/kg) and estimates of net community production (NCP; mmol C m^{-2} day^{-1}) for each region during observations.

Variable	DP 1	DP 2	DP 3	WT	ET
ΔTCO_2^{total}	8.2	9.5	19.6	- 0.9	3.4
$\Delta TCO_2^{salinity}$	3.5	3.6	12.6	2.3	3.0
$\Delta TCO_2^{bio+gas}$	4.7	5.9	7.0	-3.2	0.4
NCP	12.7	12.9	14.1	-1.5	4.5

Table 3.4. Estimates of Net Community Production (NCP) and air-sea CO_2 exchange from coastal regions in East Antarctica. All units are mmol C m^{-2} day^{-1}.

Region	Location	NCP	Air-Sea CO_2 Exchange	Year	Reference
Dalton Polynya	66.5 °S 120 °E	10 – 20	-1 to 5	2015	This Study
Mertz Polynya	66.5 °S 145 °E	26 – 70	-30 to -5	2013	Shadwick et al., 2017
		35 – 76		2012	Shadwick et al., 2017
		25 – 78		2011	Shadwick et al., 2017
		13 – 27	-15	2008	Sambrotto et al., 2003
		11 – 19		2001	Shadwick et al., 2014
Terra Nova Bay, Ross Sea	75.0 °S 165 °E	425 ± 204		2013	DeJong et al., 2017
			-72 ± 32	2013	DeJong & Dunbar, 2017
Prydz Bay	68.5 °S 75 °E	15 ± 3	-15 to 2	2011	Roden et al., 2013
			-28.4	1995	Gibson & Trull, 1999
			-37.2	1994	Gibson & Trull, 1999

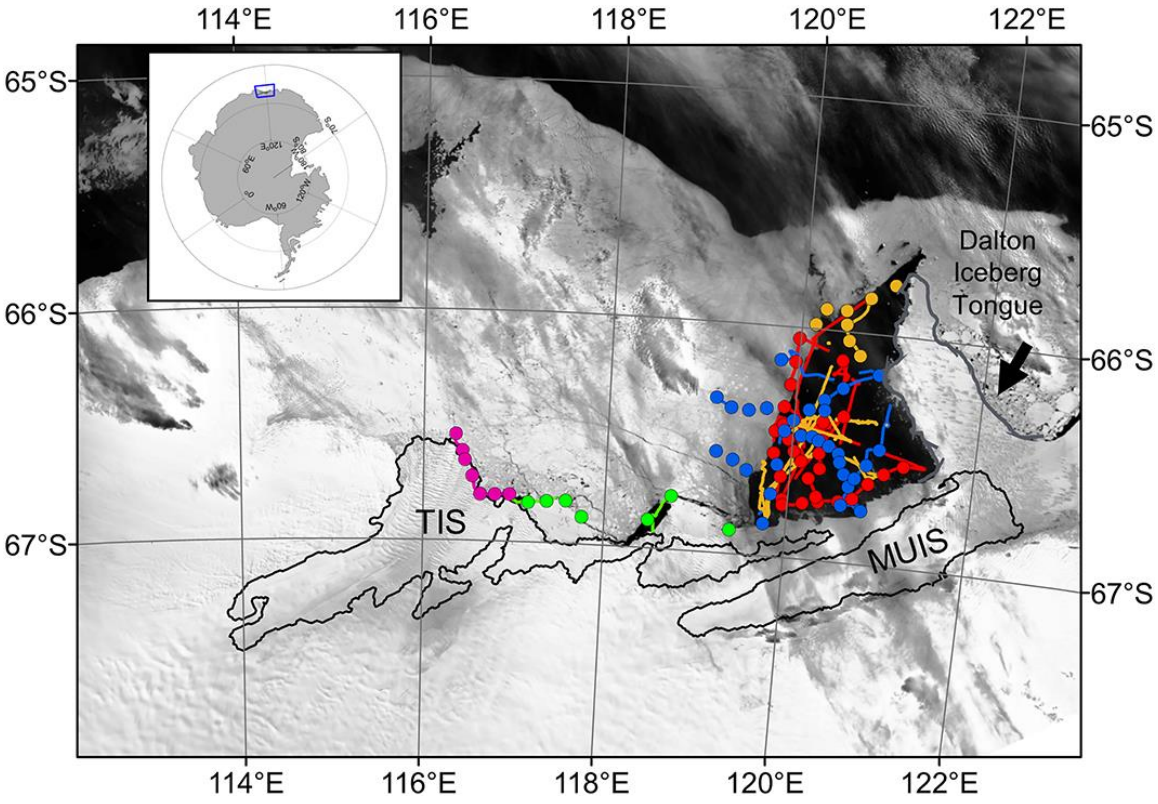

Figure 3.1. Map of the Dalton Polynya. Underway ship track (lines) and CTD stations (circles) on the *RV Aurora Australis* between 24 December 2014 and 8 January 2015 overlain on a MODIS-Terra satellite image from 10 January 2015. Observations were made within the polynya and near both the Moscow University Ice Shelf (MUIS) and the Totten Ice Shelf (TIS). Red indicates measurements between 24 and 29 December 2014 (DP1). Blue indicates measurements between 2 and 5 January 2015 and three CTD stations on 7 January (DP2). Yellow indicates measurements between 6 and 8 January 2015 (DP3). Measurements made near the TIS are indicated in magenta (West Totten; WT) and green (East Totten; ET) between 30 December 2014 and 1 January 2015.

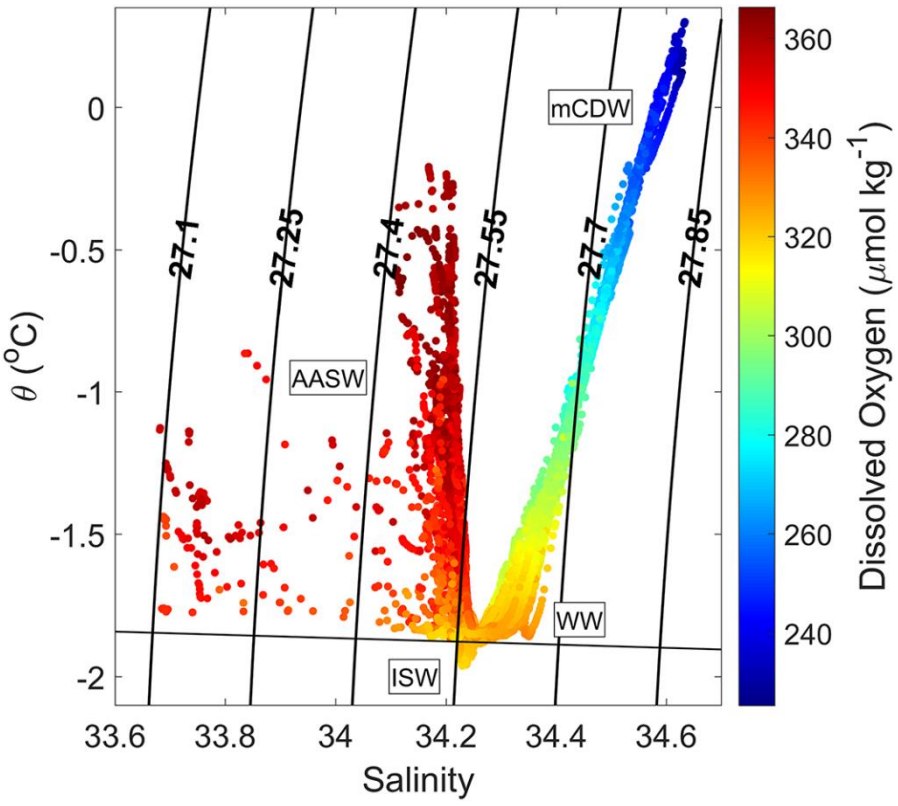

Figure 3.2. Potential temperature (θ; °C) and salinity diagram, with contours of potential density anomaly (σ_θ; kg/m^3), and colors for dissolved oxygen (μmol/kg). The thick solid black line marks the surface freezing point of seawater. Water masses are labeled as Antarctic Surface Water (AASW), modified Circumpolar Deep Water (mCDW), Winter Water (WW), and Ice Shelf Water (ISW). See text and Table 1 for definitions.

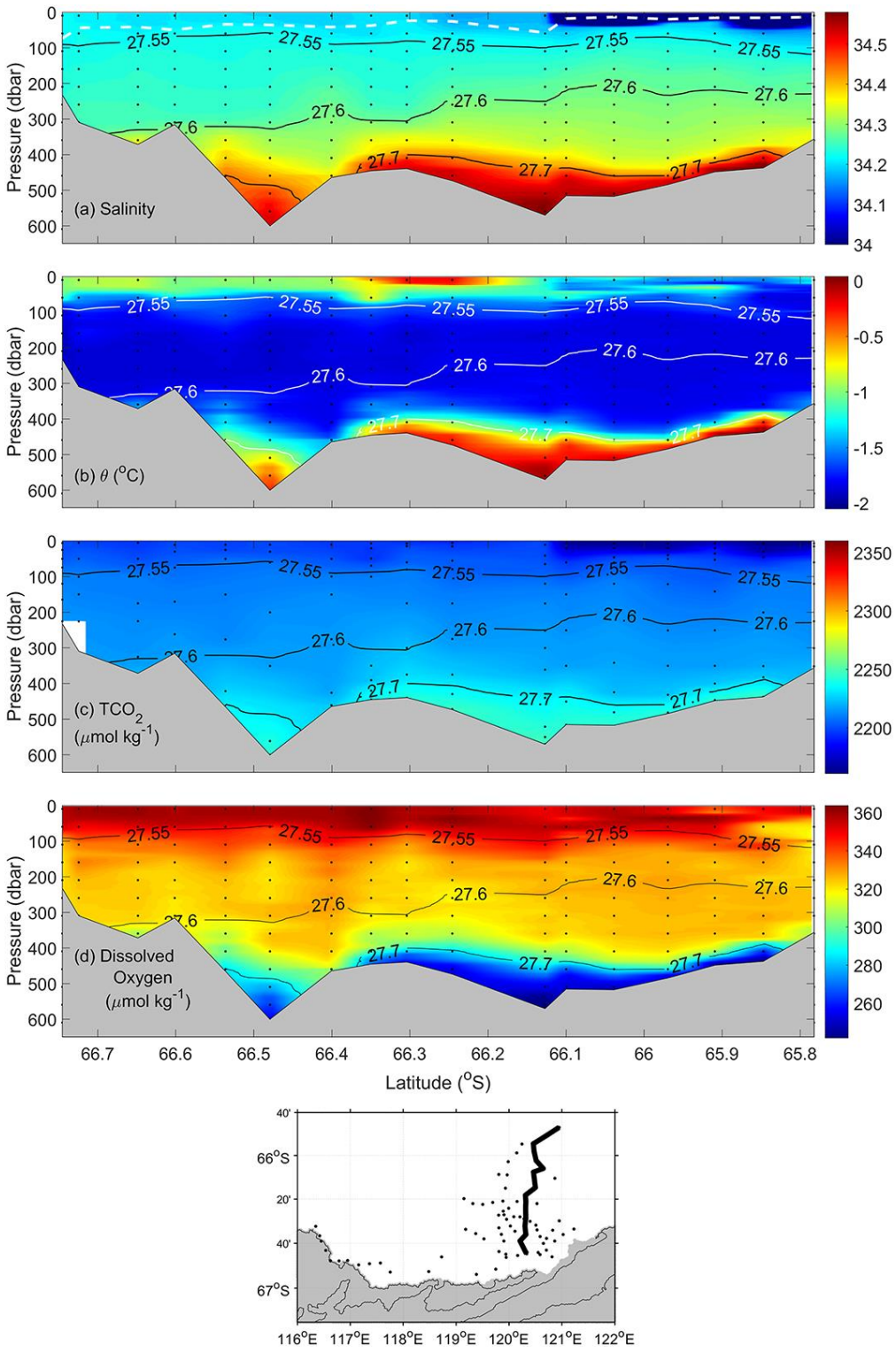

Figure 3.3. Offshore (north-south) section through the Dalton Polynya for (a) salinity, (b) potential temperature (θ; °C), (c) TCO_2 (μmol/kg), and (d) dissolved oxygen (μmol/kg) with contours of potential density anomaly (kg/m^3) and white dashed contour of calculated mixed layer depth in (a). The black dots indicate the station locations.

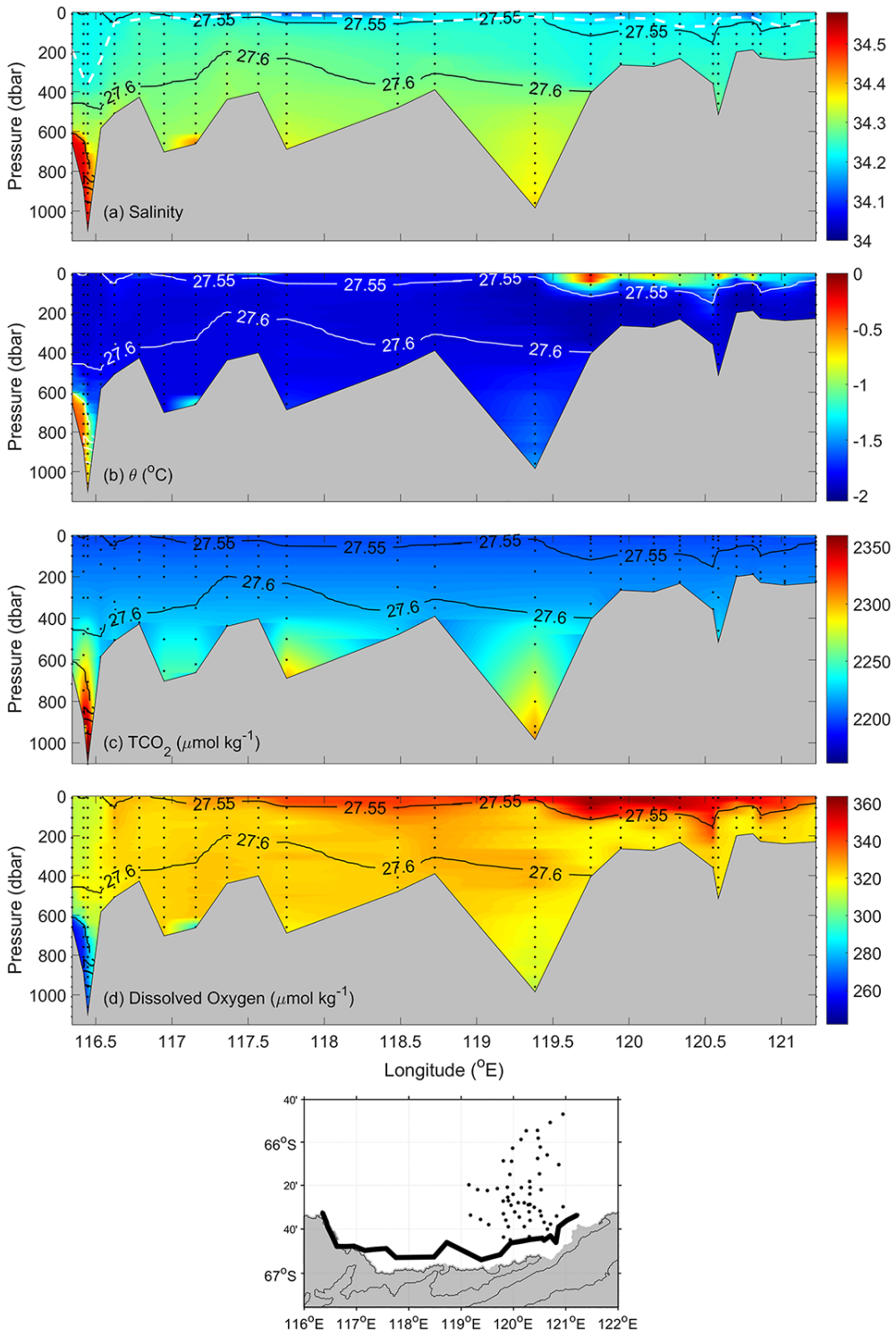

Figure 3.4. Along-shore (west-east) section in front of the Totten and Moscow University Ice Shelves for (a) salinity, (b) potential temperature (θ; °C), (c) TCO_2 (μmol/kg), and (d) dissolved oxygen (μmol/kg) with contours of potential density anomaly (kg/m^3) and white dashed contour of calculated mixed layer depth in (a). The black dots indicate the station locations.

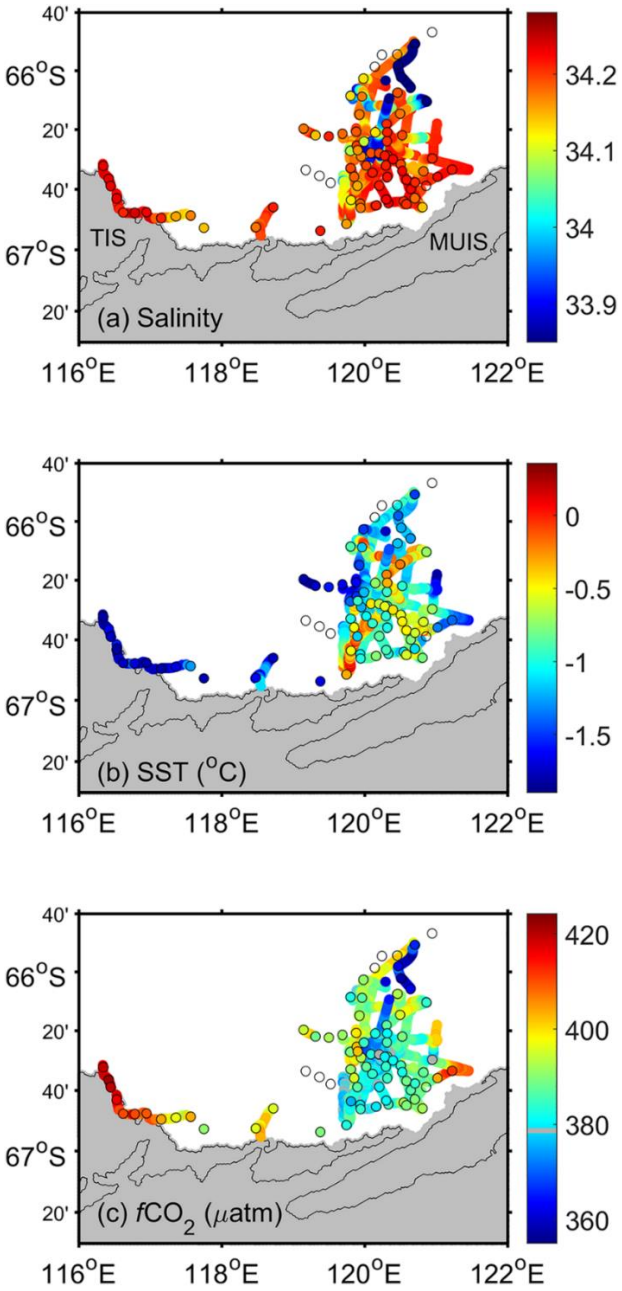

Figure 3.5. Underway surface measurements in the Dalton Polynya for (a) salinity, (b) sea surface temperature (SST; °C), and (c) fCO_2 (µatm). The mean atmospheric fCO_2 (379 µatm) is indicated by the gray line in the color bar of (c). Colored circles correspond to the underway measurements taken at the time of CTD sampling. TIS = Totten Ice Shelf; MUIS = Moscow University Ice Shelf.

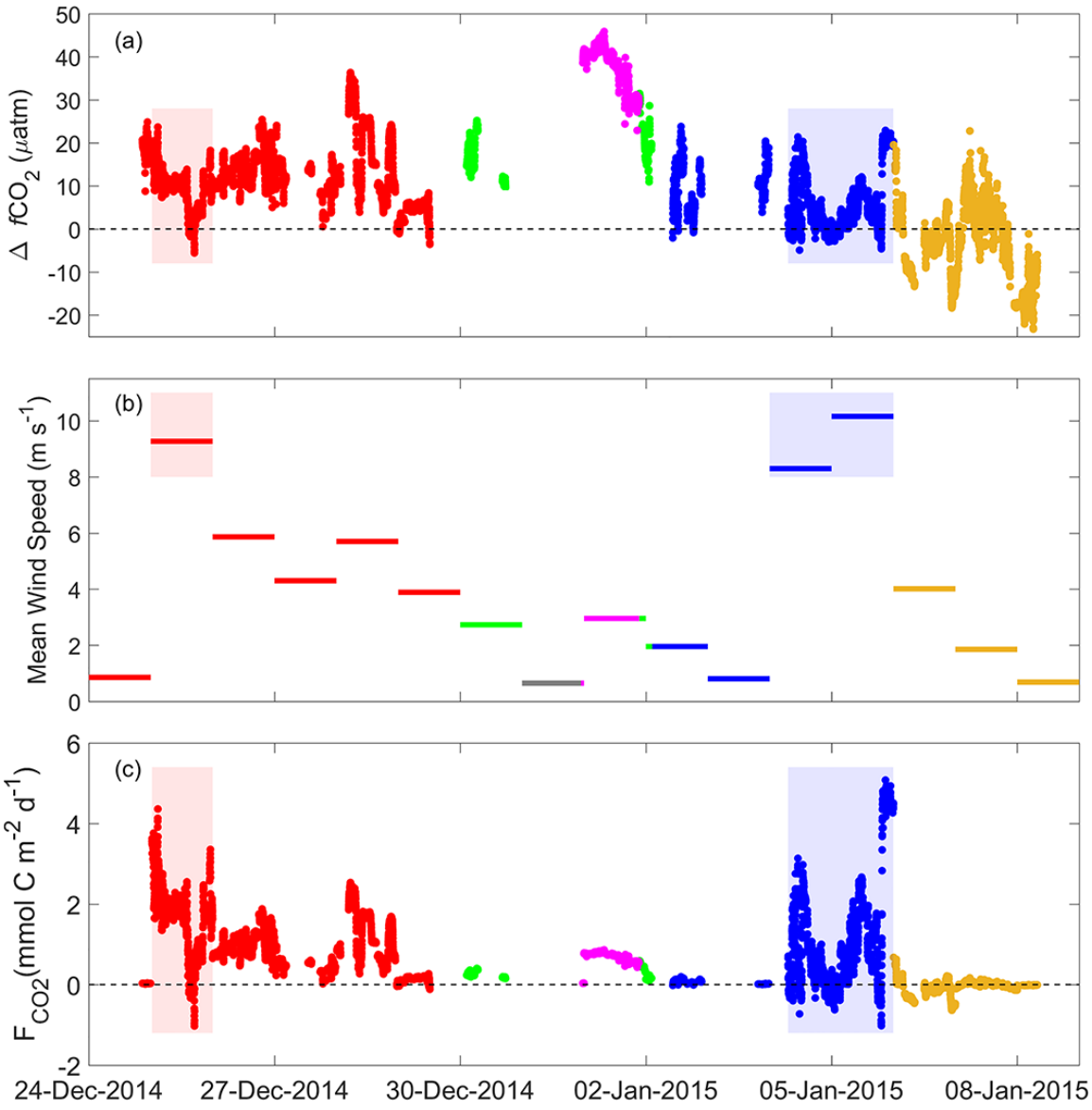

Figure 3.6. Underway measurements as a function of time between 24 December 2014 and 9 January 2015. (a) Δ fCO_2 (μatm), (b) daily mean wind speed (m/s). Wind speeds > 8 m/s are defined as high wind events and are indicated by the red shading in DP1 and blue shading in DP2. (c) Instantaneous F_{CO2} (mmol C m^{-2} day^{-1}) where a positive flux indicates a net ocean source of CO_2. See Figure 3.1 for color references.

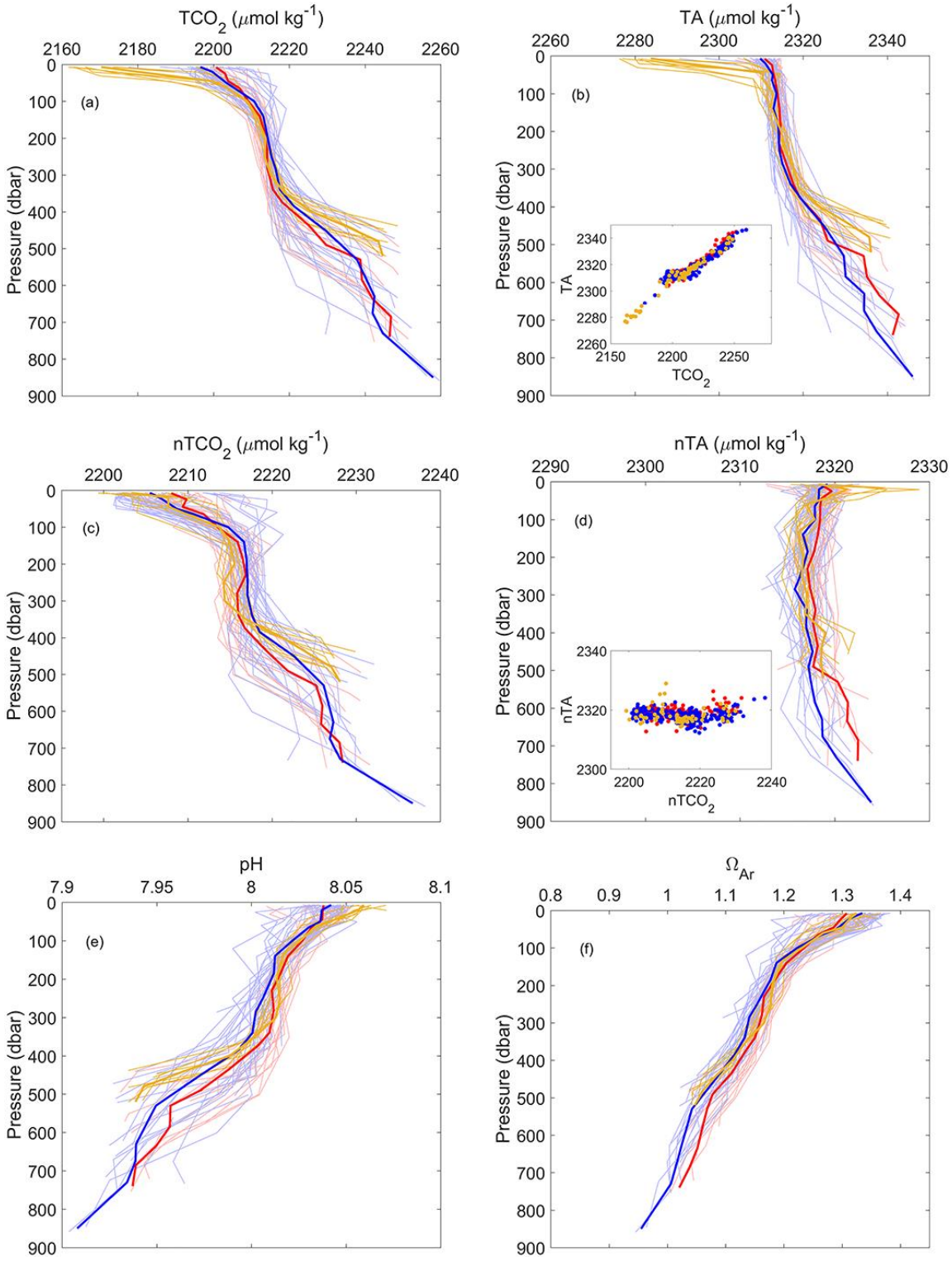

Figure 3.7. Profiles of CO_2 system properties in the Dalton Polynya. (a) TCO_2 (µmol/kg), (b) TA (µmol/kg) with TA versus TCO_2 inset, (c) $nTCO_2$ (µmol/kg), (d) nTA (µmol/kg) with nTA versus $nTCO_2$ inset, (e) pH, and (f) saturation state of aragonite (Ω_{Ar}). Bin-averaged profiles are indicated in each with a bold line.

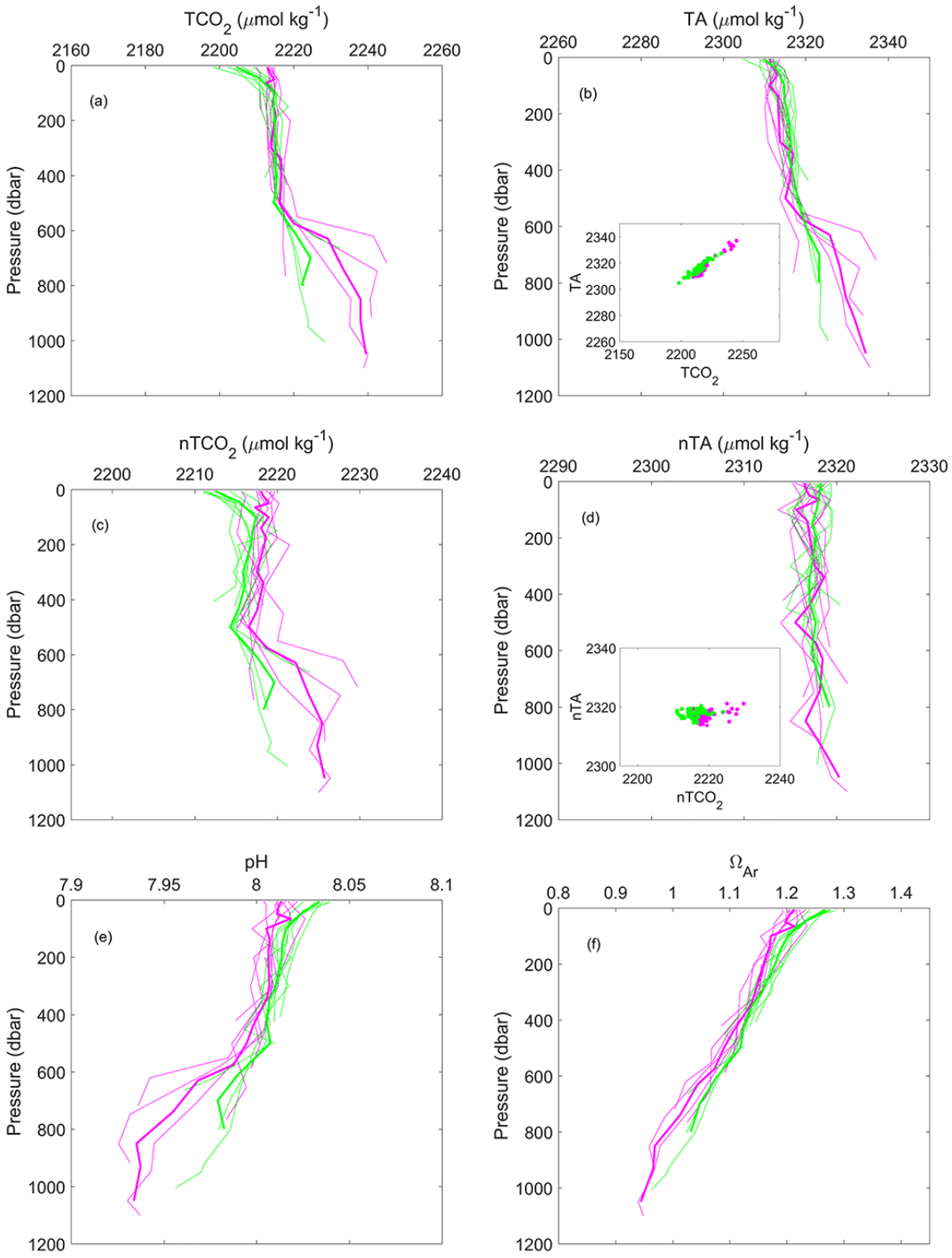

Figure 3.8. Profiles of CO_2 system properties in front of the Totten Ice Shelf. (a) TCO_2 (μmol/kg), (b) TA (μmol/kg) with TA versus TCO_2 inset, (c) nTCO (μmol/kg)$_2$, (d) nTA (μmol/kg) with nTA versus $nTCO_2$ inset, (e) pH, and (f) saturation state of aragonite (Ω_{Ar}). Binned-averaged values are indicated in each with a bold line.

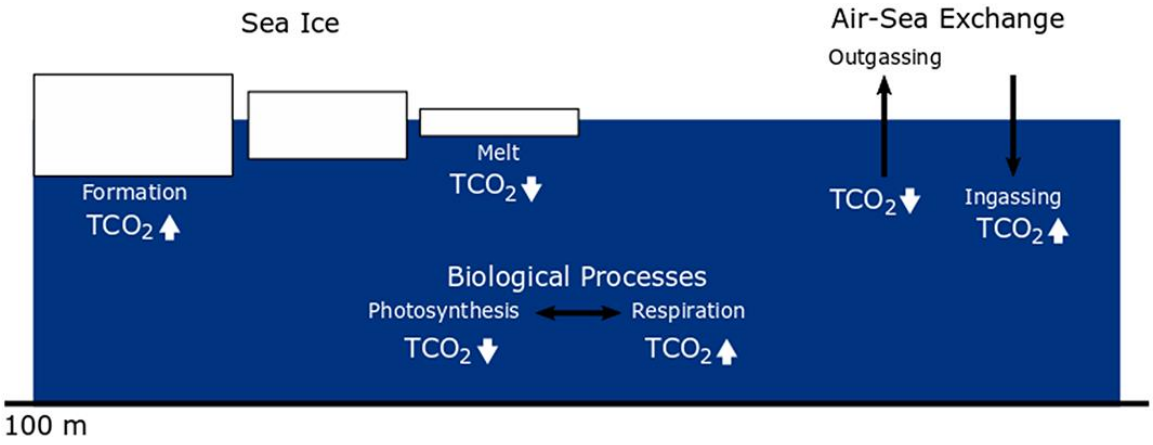

Figure 3.9. Schematic representing the physical and biological processes driving the changes in TCO_2 concentration in the upper 100 m from the transition from winter to summer in the Dalton Polynya. Physical processes such as sea ice formation and ingassing of atmospheric CO_2 increase TCO_2 concentrations while sea ice melt and outgassing of CO_2 decrease TCO_2 concentrations. Biological photosynthesis reduces TCO_2 concentration through the formation of organic matter, while respiration and the remineralization of this organic matter increases TCO_2 concentration.

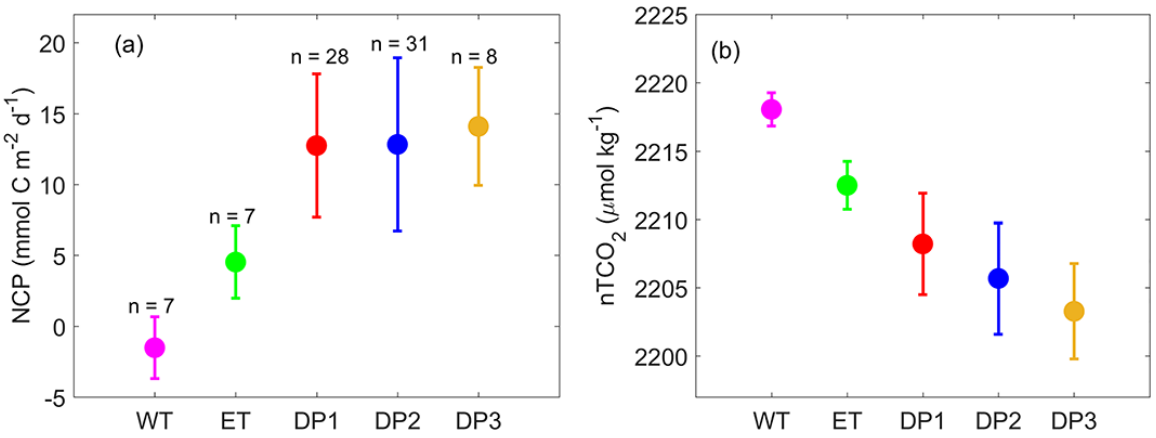

Figure 3.10. Mean (a) NCP (mmol C m^{-2} day^{-1}) and (b) $nTCO_2$ (μmol/kg) in the mixed layer for each region. Error bars represent the standard deviation.

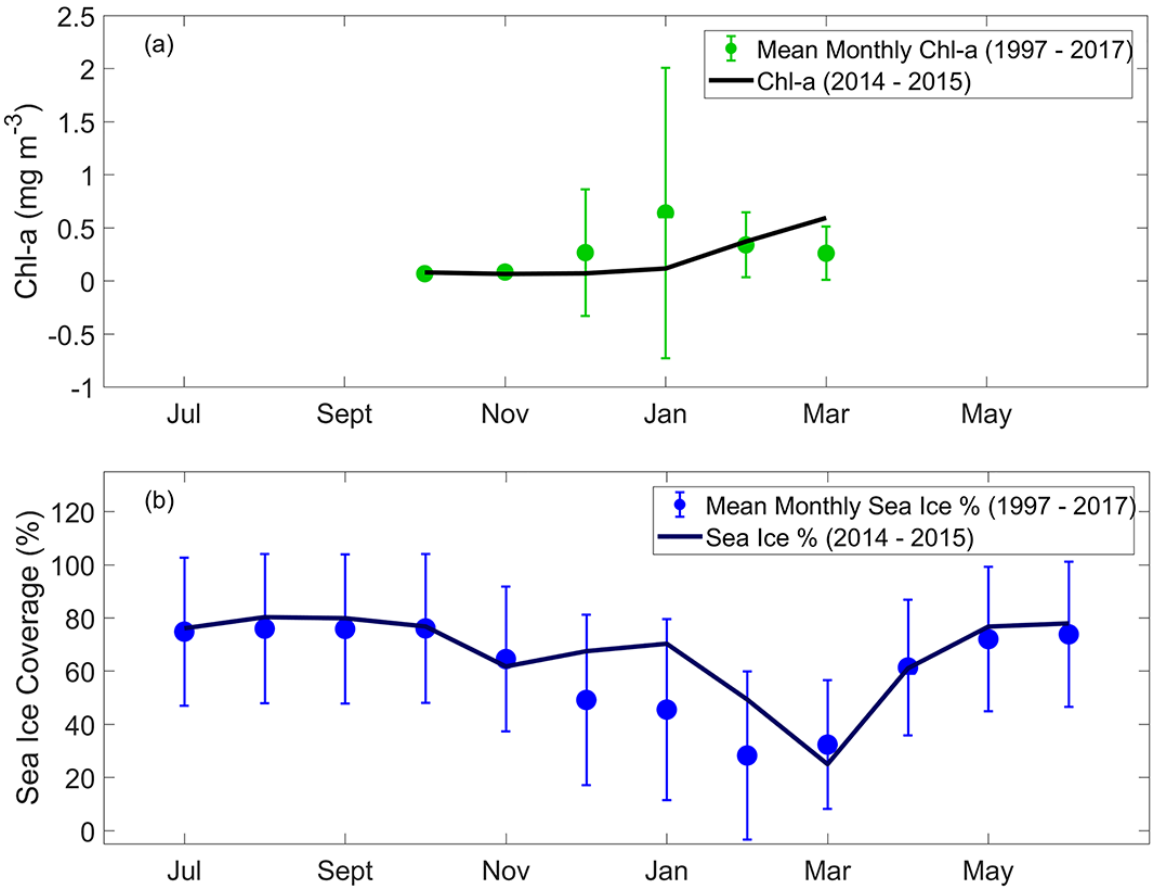

Figure 3.11. Satellite record of mean monthly (a) surface Chl *a* concentration (mg/m^3) from SeaWIFS (July 1997 – June 2002) and MODIS-Aqua (July 2002 – June 2017) and (b) percent sea ice coverage (%) from NSIDC (July 1997 – June 2017) in the Dalton Polynya. Error bars represent the monthly standard deviations. The black line in each represents the Chl *a* or percent sea ice coverage between July 2014 and June 2015. The absence of points and black line in (a) represents no data.

Chapter 4:

A CONTINENTAL SHELF PUMP FOR CO_2 ON THE ADÉLIE LAND COAST, EAST ANTARCTICA

Mar C. Arroyo[1], Elizabeth H. Shadwick[1,2], Bronte Tilbrook[2,3], Stephen R. Rintoul[2,3,4], and Kazuya Kusahara[3,5]

[1]Virginia Institute of Marine Science, William & Mary, Gloucester Point, Virginia, USA

[2]CSIRO Oceans & Atmosphere, Hobart, Tasmania, Australia

[3]Antarctic Climate & Ecosystems Cooperative Research Centre, Hobart, Tasmania, Australia

[4]Center for Southern Hemisphere Oceans Research, Hobart, Tasmania, Australia

[5]Japan Agency for Marine-Earth Science and Technology, Yokohama, Japan

Manuscript in Preparation

Key Points

- Dense Shelf Water annually exports 378 ± 130 Tg C from the Mertz Polynya and 180 ± 108 Tg C from the Ninnis Polynya in East Antarctica
- Inflowing modified Circumpolar Deep Water enriches the water column with inorganic carbon prior to winter sea ice formation and DSW export, with smaller local contributions from net community production and air-sea CO_2 exchange
- Continental shelf pumping through Dense Shelf Water export is an efficient mechanism to deliver CO_2 from shallow shelf seas to the deep open ocean

Abstract

Dense Shelf Water formation in Antarctic coastal polynyas is a critical component of the global carbon cycle through the direct connection between the atmosphere and surface ocean layer with the deep abyssal ocean through the formation of Antarctic Bottom Water. In this study, the export of inorganic carbon with Dense Shelf Water (DSW) from the shallow continental shelf is quantified near the Mertz Polynya and Ninnis Polynya on the Adélie Land coast in East Antarctica. Observations of total dissolved inorganic carbon (TCO_2) concentrations from two summer hydrographic surveys in 2015 and 2017 were paired with model-derived DSW transport estimates to quantify export of inorganic carbon in DSW. Transports indicate a net outflow of 378 ± 130 Tg C $year^{-1}$ from the Mertz Polynya and 180 ± 108 Tg C $year^{-1}$ from the Ninnis Polynya in DSW. The greatest net flux of inorganic carbon at 576 ± 86 Tg C $year^{-1}$ from the shelf region was exported through the northern boundary across the Adélie and Mertz Sills; an additional 262 ± 26 Tg C $year^{-1}$ was transported westward from the Mertz Polynya and is proposed to outflow through the D'Urville Trough Sill. Inorganic carbon exported in DSW is derived primarily from inflowing TCO_2-rich modified Circumpolar Deep Water; local processes (biological productivity, air-sea exchange of CO_2, and the addition of brine during sea ice formation) make much smaller contributions. This study proposes that Dense Shelf Water export serves as a continental shelf pump for CO_2 and is an important transport pathway to sequester inorganic carbon from the shallow Antarctic continental shelf into the abyssal ocean.

4.1 Introduction

The Southern Ocean is the central connecting feature of the world's ocean basins and plays an integral role regulating global marine biogeochemical cycles (Martinov et al., 2006; Sarmiento et al., 2004; Sigman & Boyle, 2000). Along the Antarctic continental margins, the production of cold, dense Antarctic Bottom Water (AABW) drives the lower limb of the meridional overturning circulation, delivering oxygen, carbon, and heat to the deep layers of the Atlantic, Indian and Pacific Oceans during its northward transit (Orsi et al., 1999, 2002). AABW is formed in four regions: the Weddell Sea (Carmack & Foster, 1975), the Ross Sea (Jacobs et al., 1970), Prydz Bay (Ohshima et al., 2013), and along the Adélie Land coast in East Antarctica (Gordon & Tchernia, 1972; Rintoul et al., 1998). Given its long residence time, AABW has the potential to sequester carbon in the abyssal ocean over centennial timescales and longer, highlighting the importance of this water mass to the global carbon cycle and Earth's climate system (England, 1995; Shadwick et al., 2014; Takahashi & Chipman, 2012).

Coastal polynyas are persistent areas of open water surrounded by sea ice that form in the lee of a coastline or otherwise fixed boundary (e.g., glacial tongue, grounded iceberg; Massom et al., 1998; Morales Mequeda et al., 2004). Polynyas are recognized for their high rates of seasonal primary productivity (Arrigo & van Dijken, 2003; Arrigo et al., 2008b), enhanced rates of sea ice formation and ocean-ice shelf interactions (Silvano et al., 2016), and their roles in the production of Dense Shelf Water (DSW), the precursor to AABW (Williams et al., 2008, 2010). Sources of AABW in the Australian-Antarctic Basin are supplied by the overflows of DSW formed on the continental shelves of the coastal polynyas on the Adélie Land coast in East Antarctica, collectively the Mertz and Ninnis

Polynya systems (Figure 4.1; Rintoul 1998; Williams & Bindoff, 2003; Williams et al., 2008, 2010).

Coastal polynyas where DSW forms are unique environments that serve as a direct pathway for the exchange of CO_2 from the atmosphere to the deep layers of the ocean, due to the deep mixing on the continental shelf and the movement of relatively shallow shelf waters to the abyssal layers of the open ocean. The export of carbon from these high latitude coastal polynya systems may be enhanced by a continental shelf pump for CO_2 (e.g., Tsunogai et al. 1999), facilitating the transport of carbon to depth. The continental shelf pump (CSP) describes the interaction of the solubility and biological pumps of carbon with physical mechanisms that move water from the shallow coastal sea to an adjacent deep ocean. Coastal polynyas are often thought of as a significant sink for atmospheric CO_2 due to their strong biological production and associated surface CO_2 undersaturation in the spring, as the return of solar radiation and the shallow surface mixed layers, which are macronutrient and often micronutrient rich, offer the phytoplankton community a relief from light limitation (e.g., Yager et al., 1995). The CSP has been shown to operate in the northern hemisphere and sea ice-free systems such as the East China Sea (Tsunogai et al., 1999), North Sea (Bozec et al., 2005; Thomas et al., 2004), and Chukchi Sea in the Arctic (Bates, 2006), but to our knowledge has yet to be explored in the coastal Antarctic (Takahashi & Chipman, 2012).

On the Adélie Land coast, the transport of DSW off the continental shelf may deliver a globally significant amount of dissolved inorganic carbon into the deep ocean as it cascades into the AABW water mass. This study investigates the potential for a CSP for CO_2 from the Mertz Polynya and Ninnis Polynya in East Antarctica. Using biogeochemical

observations from two austral summer surveys, the concentrations of total dissolved inorganic carbon (TCO_2) in DSW are characterized and are paired with model-derived volumetric DSW transport estimates to determine the lateral export of inorganic carbon from Adélie Land coastal waters. The local contributions of inorganic carbon to DSW derived from summer biological productivity are additionally characterized by the estimates of net community production using surface deficits in TCO_2 and by air-sea CO_2 gas exchange using underway measurements of CO_2 fugacity. The implications for Southern Ocean carbon export are discussed.

4.2 Oceanographic Setting

The Mertz Polynya and Ninnis Polynya are reoccurring coastal polynyas that form in the Adélie Coast region (142°E – 149°E) in East Antarctica, in the lee of the Mertz Glacier Tongue (MGT) and Ninnis Glacier, respectively (Figure 4.1). Both the Mertz and Ninnis Polynyas are regions of active DSW formation as a result of their high volumes of sea ice production. Offshore katabatic and synoptic scale winds force sea ice away from the coast and their neighboring glacial tongues, sustaining open water in these polynyas, and enhancing the intense sea ice growth (Massom et al., 1998). Brine rejection associated with sea ice production and surface cooling during the austral fall and winter increases density of the polynya surface waters, inducing a dramatic surface buoyancy loss to form DSW. Although shipboard oceanographic observations on the Adélie Land coast during winter are limited to one study in the Mertz Polynya (Bindoff et al., 2001; Williams & Bindoff, 2003), the seasonal cycle of water mass transformations recorded by a series of moorings revealed the Adélie Depression, a glacially scoured canyon reaching > 1300 m

deep located between 142°E and 146°E and west of the MGT (see Figure 4.1 b), is the primary source of DSW from the Adélie Land coast (Williams et al., 2008). The majority of DSW that forms predominantly in the Adélie Land coast is exported in the late winter and early spring (Williams et al., 2008) when it reaches a critical density and has sufficiently negative buoyancy to transit northward through the shallow Adélie Sill (142.5°E – 143°E; Williams et al., 2010). As DSW cascades down the continental slope, it entrains modified Circumpolar Deep Water (mCDW) to acquire its AABW properties (Williams et al., 2008, 2010).

Observational and modelling studies have reported a broad clockwise circulation flow in the Adélie Depression in winter, whereby southeasterly on-shelf intrusions of relatively warm and salty mCDW cross the northern flank of the shallow Adélie Sill and move southeastward into the Adélie Depression (See Figure 4.1 b). mCDW inflow partially compensate for the DSW outflow in the northwest direction along the southern flank of the Adélie Depression. In the early summer months (November and December), a reduction or cessation of sea ice production and the onset of seasonal sea ice melt (i.e., reduction in vertical surface salt flux) freshens and stratifies the water column, reducing or halting DSW formation. The restratification of the water column in summer allows for an increasing influence of mCDW intrusions to continue through the early autumn (March; Williams et al., 2008), bringing a substantial source of salinity and dissolved inorganic nutrients to the continental shelf that preconditions the mid-water column with saline water before the onset of DSW production in the following winter. Because the mCDW water mass primarily derives its biogeochemical properties from offshore (Whitworth et al., 1998), mCDW inflows are also highly enriched in nutrients and TCO_2, resulting from the

cumulative remineralization of organic matter from distant sources. Wintertime sea ice formation subsequently delivers brine to the underlying waters in the polynyas, further increasing its salinity, density, and TCO_2 concentration, and driving the formation of DSW. This water is then bathymetrically steered as an outflow along the coast and exported northwesterly across the Adélie Sill on the continental shelf break.

Williams et al. (2008) estimated an annual mean export of 0.1 – 0.5 Sv of DSW through the Adélie Sill for water masses with a potential density greater than 1027.88 kg/m^3. Later work identified a secondary source of DSW, characteristically fresher and lighter, within the Mertz Depression, east of the MGT and north of the Ninnis Polynya (Williams et al., 2010). Modelling and shipboard studies of the region have since supported the observations of a northward DSW export from the Mertz Depression though the Mertz Sill (147°E – 148°E) in addition DSW transport across the Adélie Sill (Cougnon et al., 2013; Kusahara et al., 2011a). Bathymetric studies have suggested that the Adélie Depression may extend beneath the floating MGT and connect to the deep bathymetry underlying the Ninnis Polynya, referred to here as the Ninnis Depression (e.g., Domack & Anderson, 1983; Williams et al., 2010). Dramatic changes to the local icescape and water mass transformations on the Adélie Land coast involving the calving of the MGT in 2010 and subsequent reduction in the activity and configuration of the Mertz Polynya (Kusahara et al., 2011b; Shadwick et al., 2013; Tamura et al., 2012) has led to an evolving definition of the DSW critical density criterion. Since the MGT calving, the DSW produced on the Adélie Land coast is lighter compared to the pre-calving conditions.

The major geomorphic features on continental shelf in the Adélie Land region including the series of large bathymetric depressions (Adélie Depression, Ninnis

Depression, and Mertz Depression) and shallow sills (Adélie Sill and Mertz Sill) along the shelf break, allowing for a small fraction of DSW formed during the previous winter season to accumulate annually on the continental shelf in summer (Lacarra et al., 2014; Williams et al., 2008, 2010). These depressions thereby act as reservoirs, where the signals of DSW from the previous formation season are preserved during the summer months (e.g., Lacarra et al., 2014). Accumulated DSW signatures are isolated from lateral exchange off the shelf break by the shallow sill barriers and by the presence of less dense mCDW in the intermediate water column. Accordingly, the bottom waters observed within the on-shelf depressions of the Mertz and Ninnis Polynyas during the summer surveys presented in this study that have signatures of potential density greater than or equal to the critical potential density of exported DSW were indicative of the DSW produced during the previous winter season.

4.3 Methods

This study uses hydrographic and CO_2-system data collected on the continental shelf of the Adélie Land coast (142°E – 149°E) during two summer cruises in 2015 (AU1402) and 2017 (AU1602) on board the *RSV Aurora Australis* (Figure 4.1). The AU1402 voyage includes 51 CTD stations occupied between 9-17 January 2015 overlying the Adélie Depression, along the western extent of the pre-calved of the MGT, and the at-present front of the MGT (Rosenberg & Rintoul, 2016). Observations from an additional 37 CTD stations from the AU1602 voyage were made between 14 – 21 January 2017 farther east on the Adélie Land coast (Rosenberg & Rintoul, 2017). This data set encompasses 15 CTD stations that were repeated from AU1402 along the (pre- and post-

calved) MGT (see Figure 4.1 a; open circles) as well as 14 CTD stations within the Ninnis Polynya and 8 CTD stations overlying the Mertz Depression.

On both voyages, CTD deployments obtained continuous measurements of 2-dbar averaged salinity, temperature (°C), and pressure (dbar) using a SeaBird SBE9plus CTD (serial 704) with dual temperature and conductivity sensors. The accuracies of temperature and salinity were ~0.001 °C and ~ 0.002, respectively. Similarly, continuous measurements of 2-dbar averaged dissolved oxygen (µmol/kg) were made with SBE 43 (serial 0178) in agreement to within 1% of discrete bottle data. The CTD was mounted on a rosette frame with 22 x 10 L General Oceanic Niskin bottles on the AU1402 voyage, and on AU1602, with up to 24 x 10 L Niskin bottles.

4.3.1 Underway fCO_2 Measurements and Air-Sea CO_2 Flux Calculations

High-frequency underway measurements for the fugacity of carbon dioxide (fCO_2), sea surface salinity, and sea surface temperature were taken from the seawater intake ~4 m below the ocean surface along the cruise tracks of both voyages. Measurements of fCO_2 were made using a non-dispersive infrared gas spectrometer (LI-COR, LI-7000) with continuous flow equilibration corrected to *in situ* underway temperature and salinity and to 100% humidity (Pierrot et al., 2009). Travel time between then the seawater intake and the CO_2 system on board was approximately 70 seconds, resulting in $\leq$ 0.6 °C warming. Underway fCO_2 measurements were calibrated every 3 – 4 hours with a set of four reference standards (0 µatm, 299.41 µatm, 353.00 µatm, and 402.15 µatm on AU1402; 0 µatm, 255.93 µatm, 380.52 µatm, and 451.12 µatm on AU1602) on the WMO-X2007 mole fraction scale for CO_2 in dry air (Zhao & Tans, 2006). The atmospheric mole fraction of

CO_2 was measured every four hours at ~16 m above sea level and used to calculate atmospheric fCO_2. Uncertainties were ±2 µatm for seawater fCO_2 and ±0.2 µatm for atmospheric fCO_2.

Air-sea fluxes of CO_2 were calculated using the equation

$$F_{CO_2} = k\ \alpha\ \Delta fCO_2 \quad (1)$$

where F_{CO_2} is the CO_2 flux (mmol C m^{-2} day^{-1}), k is the gas transfer velocity, and α is the solubility of CO_2 (Weiss, 1974). ΔfCO_2 (µatm) is the gradient of fCO_2 between the sea surface and the atmosphere ($fCO_2^{sea} - fCO_2^{air}$), where a negative flux indicates an ocean uptake of atmospheric CO_2. The gas transfer term (k; cm/hr) was parameterized with Wanninkhof (2014) given by

$$k = 0.251\ U_{10\,m}^2\ (Sc/660)^{-0.5} \quad (2)$$

using daily-averaged winds from 10 m above the sea surface ($U_{10\,m}^2$) obtained from the NCEP/NCAR Reanalysis product (Kalnay et al., 1996) and corrected to a Schmidt (Sc) number of 660.

4.3.2 Discrete CO_2 System and Biogeochemical Observations

Discrete measurements of total dissolved inorganic carbon (TCO_2) and total alkalinity (TA) were made at each station following analytical methods described in Dickson et al. (2007). Upon sampling, a saturated solution of mercuric chloride was added to each sample to halt biological activity. TCO_2 concentrations were either determined on board (AU1402) or stored in the dark at 4 °C and until analysis at CSIRO in Hobart (AU1602) by coulometric titration using a Single Operator Multiparameter Metabolic Analyzer (SOMMA) system (Johnson et al., 1993). TA concentrations were determined on

board both voyages by automatic open-cell potentiometric titration with 0.1 M hydrochloric acid using a Methrom Titrando system. All analyses were routinely checked with a Certified Reference Materials (CRMs Batch #137 on AU1402; #145 and #153 in AU1602) provided by A. G. Dickson at Scripps Institution of Oceanography (Dickson et al., 2003). Verified analytical uncertainties were better than ± 1.4 µmol/kg for TCO_2 and ± 1.5 µmol/kg for TA for AU1402 and better than ± 1.5 µmol/kg for TCO_2 and ± 1 µmol/kg for TA for AU1602.

The saturation state of aragonite (Ω_{Ar}) and pH on the seawater scale were calculated using CO_2SYS program by van Heuven et al. (2011) using the thermodynamic equilibrium constants defined by Mehrbach et al. (1973) as refit by Dickson and Millero (1987). These calculations use calcium ion concentrations, assumed to be conservative and calculated from salinity (Riley & Tongudai, 1967), and measured inorganic nutrient concentrations of phosphate (PO_4^{3-}) and silicate ($Si(OH)_4$). Discrete samples for PO_4^{3-} and $Si(OH)_4$, as well as for nitrate + nitrite (hereinafter nitrate, NO_3^-) and dissolved oxygen, were collected in parallel to CO_2-system measurements. PO_4^{3-} and NO_3^- samples were frozen and $Si(OH)_4$ samples were refrigerated until analysis at CSIRO following methods described in Grasshoff et al. (2007). Calculated CO_2-system parameters from AU1402 used voyage-averaged concentrations of PO_4^{-3} (2.06 ± 0.07 µmol/kg) and $Si(OH)_4$ (64 ± 7 µmol/kg). Nutrient uncertainties were < 5%. Discrete samples of dissolved oxygen were analyzed via the Winkler titration method following the protocol of Hood et al. (2010) with a reported uncertainty of < 1% on both voyages.

4.3.3 Seasonal Changes in TCO_2 and Net Community Production Computations

The summertime distribution of mixed-layer TCO_2 is influenced by a combination of physical and biological processes that can be partitioned. Biological processes were isolated by computing seasonal deficits in mixed-layer TCO_2. The mixed layer depth (MLD) was defined as the depth at which potential density anomaly exceeds a reference measurement at 10 m by 0.01 kg/m^3 (Shadwick et al., 2014). Deficits in TCO_2 were computed as the difference between the mixed-layer TCO_2 concentrations observed during summer and an inferred winter concentration defined as the average value at 150 m depth in combined AU1402 and AU1602 datasets (TCO_2^{winter} = 2,230 µmol/kg; s. d. = 4 µmol/kg; n=33) following Arroyo et al. (2019). TCO_2 and TA concentrations were normalized to an area-averaged salinity (S = 34.5) to account for the impact of seasonal sea ice dynamics and (horizontal and vertical) mixing on mixed-layer concentrations.

Net community production (NCP), defined as the difference between net primary production and heterotrophic respiration was computed at each station as the depth-integrated deficit in salinity-normalized TCO_2 between the observed summer and TCO_2^{winter} concentrations from the surface to 100 m over the duration of the productive season. The start of the productive season was defined as November 1 for each sampling year based on the onset of primary production inferred from monthly averaged chlorophyll *a* concentration derived from the MODIS-Aqua satellite product at 9 km resolution (Figure 4.2).

4.3.4 Inorganic Carbon Transport with Dense Shelf Water

Several numerical modelling studies have focused on the formation of DSW and circulation of water masses on the continental shelf of the Adélie Land coast (e.g., Cougnon et al., 2013, 2017; Kusahara et al., 2010, 2011a, 2017; Marsland et al., 2004, 2007; Snow et al., 2016). Global-scale coupled ocean-sea ice regimes have been used and agree well with observations in documenting the clockwise gyre circulation and dense water formation in the Adélie Depression (Marsland et al., 2004, 2007) and in the Mertz Depression (Kusahara et al. 2010, 2011a). More recently, a regional-scale ocean-ice shelf model implemented by Cougnon et al. (2013; 2017) addressed the impacts and sensitivity of the basal melt rate of the MGT and a changing icescape on DSW formation in Adélie and Mertz Depressions, highlighting the large interannual variability in DSW export linked to subglacial melting. An inverse box model approach was used to evaluate the mechanisms controlling cross-shelf and off-shelf circulation and emphasized the relationships between katabatic winds and summer circulation and between buoyancy loss induced by surface cooling, brine rejection, and winter circulation (Snow et al., 2016). Here the volumetric DSW transport estimates of Kusahara et al. (2017) are used. This global scale, coupled ocean-sea ice-ice shelf model has enhanced horizontal resolution (~5-6 km) in the Adélie Land region and uses bathymetry derived from the General Bathymetric Chart of the Oceans (GEBCO, IOC et al., 2003) and ice shelf draft derived from the 1-min refined topography (RTopo-1, Timmermann et al., 2010). The model uses the critical potential density for DSW greater than 1027.84 kg/m^3 and potential temperature less than -0.5 °C. Simulations quantify DSW formation over the continental shelf on the Adélie Land coast, as well and its export from the shelf break on seasonal and annual timescales from both the

Adélie Depression/Sill and the Mertz Depression/Sill regions, and the D'Urville Trough Sill (west of the Mertz Polynya) that are consistent with previous observational and modeling studies (Williams et al., 2010, Kusahara et al., 2011a).

Volume transports for the Mertz Polynya and Ninnis polynya represent both outflowing and inflowing DSW on the Adélie Land continental shelf through western, northern, and eastern boundaries as delineated by Kusahara et al. 2017 (Figure 4.1 b). The western boundary of the Mertz Polynya follows the latitudinal line of 142°E from the coastline to the shelf break at the 500-m depth contour (approximately 65.8°S). The eastern boundary of the Mertz Polynya and the western boundary of the Ninnis Polynya were separated at approximately between 146°E and 147°E southward to the pre-calved configuration of the MGT. The eastern boundary of the Ninnis Polynya extends from the coast to the shelf break along approximately 149°E. The Mertz Polynya northern boundary follows the shelf break (65.8°S to 66.2°S) across the Adélie Bank and Adélie Sill between 142°E and 147°E, and the Ninnis Polynya northern boundary extends from 147°E to 149°E across the Mertz Bank and Mertz Sill. The model was run under a scenario in which the MGT calved on 1 January 2000. Although the actual MGT calving event occurred in February 2010, the analysis by Kusahara et al. (2017) found that there are no pronounced differences in DSW formation and export during model simulations that assume a calving event on 1 January 2000 (C2000) or 1 January 2010 (C2010) during the period of overlap (2010 – 2013), demonstrating that the numerical results are independent of the timing of the MGT calving. Monthly seasonal DSW transport estimates (Sv; 10^6 m^3/s) at potential density intervals of 0.02 kg/m^3 binned increments were averaged from January 2011 to

December 2013, the time period after the MGT calving event, to better align with biogeochemical observations collected in January 2015 and 2017.

To determine the amount of inorganic carbon that is transported with dense shelf water from the Adélie Land coast, TCO_2 concentrations in DSW observed at depth in each summer study are combined with these model-derived volumetric DSW transport estimates. Because the deep depressions act as reservoirs for DSW formed during the previous winter, the summer observations of TCO_2 below $\sigma^\theta \geq 27.84$ kg/m^3 and $\theta \leq -0.5$ °C are assumed to be representative of the winter concentration in DSW. Discrete TCO_2 measurements at each station were linearly interpolated between sampling depths to 2-bar resolution to associate with the high-frequency CTD measurements. Similar to the model outputs, TCO_2 values were binned by potential density anomaly intervals of 0.02 kg/m^3 and were averaged to yield one TCO_2 value per bin (Table 4.2). The standard deviations of TCO_2 measurements within each bin are small (1 – 2 µmol/kg) and similar to the analytical uncertainty, giving confidence that these signatures are representative of the water in a particular bin. Water masses that were denser than those observed during summer (i.e., $\sigma^\theta > 27.92$ kg/m^3) were assigned TCO_2 values of the densest observation (i.e., mean TCO_2 between 27.90 kg/m^3 < σ^θ < 27.92 kg/m^3).

Inorganic carbon transport in DSW (CO_2^{DSW}; g C/month) was computed by the following equation

$$CO_2^{DSW} = Transport^{DSW} \times TCO_2^{DSW} \times \rho^{DSW} \times m_c \quad (3)$$

where $Transport^{DSW}$ is the monthly average volume transport (Sv; 10^6 m^3/s) between January 2011 and December 2013 from the Kusahara model, TCO_2^{DSW} (µmol/kg) and ρ^{DSW} (kg/m^3) are the observed mean TCO_2 concentration and density, respectively, within each

σ^{θ} bin, and m_c is the molar mass of carbon (g C/mol). The CO_2^{DSW} computations were scaled to monthly values (i.e., from units of seconds to month), then summed to yield annual estimates from both the Mertz and Ninnis Polynyas.

This approach to characterize the seasonal DSW fractions with TCO_2 concentrations observed during summertime is likely to underestimate the concentrations of TCO_2^{DSW}, and consequentially the amount of inorganic carbon that is exported from the Mertz and Ninnis Polynyas. Here, it is assumed that there is no seasonal variability in TCO_2^{DSW}. It is likely that TCO_2 concentrations in exported deep DSW fractions (σ^{θ} > 27.92 kg/m^3) that are present during wintertime were greater than those used estimated in this analysis. During the previous winter, respiration and remineralization of organic matter formed during the previous productive season increases TCO_2 in the winter water column. If it is assumed that 100% of the organic matter locally synthesized during the productive season was vertically exported below the depth of winter mixing in the previous season, was respired in DSW that is denser than what is observe in summer, and subsequently exported off the continental shelf prior to the summer observations, then the maximum underestimate of winter TCO_2 is equal to the amount of NCP.

4.4 Results

4.4.1 Hydrographic Properties

Water masses observed on the Adélie Land coast during the 2015 and 2017 voyages were consistent with those observed in previous summer studies (Lacarra et al., 2011; Shadwick et al., 2014, 2017; Figure 4.3, Table 4.1). The surface waters were relatively warm and fresh, characteristic of Antarctic Surface Water (AASW) properties in summer,

defined by the neutral density (γ^n) less than 28.00 kg/m^3. (Figures 4.3 and 4.4). Underway measurements taken along the cruise tracks are presented in Figure 4.4. Sea surface salinity was greater in the study region in 2015 (~33.7 to 34.5) as compared to 2017 (~32.6 to 33.9) suggesting a larger volume of sea ice melt and a resulting surface freshening prior to the 2017 voyage (Figure 4.4 a and b). In both years, relatively fresh waters were found adjacent to the seaward edge of the MGT. In 2017, salinity reached a maximum within the Ninnis Polynya and decreased latitudinally away from the coast overlying the Mertz Bank and Mertz Depression. Surface waters were typically cooler in the Adélie Depression in 2015 (~ -1.6 to 0.1 °C) and along the coast west of the MGT as compared to more widely varying SST during the 2017 voyage (~ -1.6 to 1.0 °C) east of the MGT, where increased surface temperatures were likely the result of summer warming (Figure 4.4 c and d).

Below the summer mixed layer, relatively warm mCDW and colder ISW occupied the intermediate depths (28.00 < γ^n < 28.27 kg/m^3). Intrusions of mCDW from offshore of the shelf break deliver a source of high salinity, low dissolved oxygen water to the region. As mCDW is isolated from exchange with the sea surface, it is also enriched in TCO_2 and inorganic nutrients due to the cumulative influence of organic matter remineralization over longer time scales (Figure 4.3). ISW is characterized by temperatures below the surface freezing point (θ < -1.925 °C), formed during the interactions of DSW with the MGT during the wintertime (Silvano et al., 2016).

CTD stations in January 2015 were repeated in January 2017 in the Mertz Polynya following the current and pre-calving positions of the MGT (Figure 4.5; see Figure 4.1 a, open circles). In both occupations, bottom waters were relatively cold and salty compared to surface waters. Surface waters in summer 2015 were relatively fresher (~32.8 vs 33.6)

and warmer (~0.5 °C vs -1.0 °C) than in summer 2017. The distribution of salinity in both years was nearly uniform with depth below 500 m, however the subsurface water column salinity was generally greater in 2017 than in 2015, converging to deep water salinity values of 34.67 and 34.61 respectively. Profiles of potential temperature are much more variable above 500 m but converge in both years to a bottom temperature of ~1.91 °C. Properties of TCO_2 and TA are discussed further below.

4.4.2 Surface fCO_2 and Air-Sea CO_2 Exchange

All surface seawater fCO_2 measurements across both voyages were undersaturated with respect to the atmospheric value (382 ± 1.2 µatm in January 2015 and 389 ± 0.6 µatm in January 2017), resulting in a net air-to-sea flux of CO_2 during the period of observations on both voyages (Figure 4.4 e and f). In both years, the distribution of fCO_2 exhibited a latitudinal gradient, with a larger degree of undersaturation found adjacent to the coast. Areas of cooler, fresher water in the Adélie Depression correspond to minimum values of fCO_2, in contrast to the cooler waters farther offshore in the Mertz Bank associated with maximum values of fCO_2. The range of fCO_2 values was smaller (~210 – 350 µatm) between the Adélie Depression and the MGT in 2015 as compared to fCO_2 values on the eastern side (~160 to 382 µatm) of the Adélie Land coast in 2017. In 2017, surface waters adjacent to the MGT and within the Ninnis Polynya exhibited the largest degree of undersaturation, with fCO_2 values as low as 150 µatm, consistent with reported high dissolved oxygen to argon ratio ($\Delta O_2/Ar$) found in these regions (Moreau et al., 2019).

The Adélie Land coast was a moderate sink for atmospheric CO_2 during the austral summers of 2015 and 2017 (Figure 4.4 e and f; Table 4.3). Although the direction of gas

exchange was consistently in the direction of sea surface uptake, the magnitude of CO_2 flux varied regionally and between years. Wind speeds were variable in both years, with daily mean wind speeds ranging between 2.1 and 5.8 m/s in 2015 and between 2.1 and 11.8 m/s in 2017. Highly undersaturated waters near the MGT recorded the largest ingassing flux in both years (~7 mmol C m^{-2} day^{-1} in 2015 and ~15 mmol C m^{-2} day^{-1} in 2017) consistent with previous studies occupied near the post-calving MGT (Shadwick et al., 2014, 2017). Smaller CO_2 uptakes were estimated in the Adélie Depression and near the edge of the continental shelf west of the MGT at 66°S (1 to 5 mmol C m^{-2} day^{-1}). Although surface waters in the Ninnis Polynya were highly undersaturated in fCO_2 ($-239 < \Delta fCO_2 < -100$ µatm), lower wind speeds resulted in a relatively small flux (~ 2 to 4 mmol C m^{-2} day^{-1}). The Adélie Land coast was a sink for atmospheric CO_2, with fluxes of approximately 6.6 mmol C m^{-2} day^{-1} on average over both cruise years.

4.4.3 CO_2 System Properties

The relationships of TCO_2 and TA with salinity are shown in Figure 4.6. The concentrations of TCO_2 and TA approximately ranged from 2,015 to 2,245 µmol/kg and from 2,240 to 2,350 µmol/kg, respectively, over a salinity range of 32.8 and 34.7 (Figure 4.6 a), similar to values reported in previous studies of the Mertz Polynya (Shadwick et al., 2014, 2017). At lower surface salinities ($S < 34.3$), TA and TCO_2 were relatively depleted from subsurface values ($S > 34.3$). The more conservative relationship between TA and salinity in the upper water column indicated that seasonal changes in surface TA were predominantly driven by changes in sea ice dynamics (e.g., sea ice melt), whereas the changes in surface TCO_2 were influenced by additional processes (e.g., photosynthesis, air-

sea CO_2 exchange; Figure 4.6 c). Lower sea surface salinities found near the calving face of the MGT in both voyages correspond to TCO_2 minima of approximately 2,100 µmol/kg during AU1402 and 2,015 µmol/kg during AU1602 and TA minima of approximately 2,290 µmol/kg during AU1402 and 2,240 µmol/kg during AU1602. Average mixed-layer concentrations of TCO_2 and TA were overall lower in 2017 (2,079 ± 36 µmol/kg; 2,279 ± 29 µmol/kg) as compared to 2015 (2,149 ± 30 µmol/kg; 2,308 ± 11 µmol/kg), but are within range of those previously reported in the Mertz Polynya from 2011 (2,107 ± 20 µmol/kg; 2,280 ± 18 µmol/kg) , 2012 (2,109 ± 20 µmol/kg; 2,313 ± 15 µmol/kg), and 2013 (2,159 ± 25 µmol/kg; 2,315 ± 10 µmol/kg; Shadwick et al., 2017).

TCO_2 and TA concentrations were normalized to a salinity of 34.5, the average salinity of both data sets (Figure 4.6 c). Salinity normalizing TCO_2 and TA accounts for the seasonal variations in salinity due to freshwater input and removal (e.g., sea ice formation and melt), as well as horizontal and vertical mixing, allowing for biogeochemical processes to be distinguished from salinity effects. The negative slope of the linear relationship between salinity-normalized TCO_2 ($nTCO_2$) and salinity-normalized TA (nTA) indicates the combined influence of air-sea CO_2 exchange and photosynthetic processes. The former process only impacts concentrations of TCO_2 (ingassing of atmospheric CO_2 increases TCO_2 concentrations) and exerts no influence on TA concentrations. The latter process, the production of organic matter, influences both TCO_2 and TA concentrations. Biological production and the fixation of CO_2 decreases TCO_2 concentrations and marginally increases in TA concentrations due to the assimilation of nitrate by phototrophs (Brewer & Goldman, 1976). As organic matter is remineralized, values of $nTCO_2$ increase and nTA decrease. The small increases in TA in surface and

major losses in the subsurface can be accounted for by computing the potential alkalinity (pTA) from nTA and salinity-normalized nitrate ($pTA = \frac{TA+1.36\times NO_3^-}{S} \times 34.5$; Wolf-Gladrow et al., 2007), flattening the pTA-nTCO_2 relationship (Figure 4.6 c). An increase in pTA relative to nTCO_2 at depth indicates calcium carbonate dissolution in deeper, older water masses on the Adélie Land coast, such as in mCDW, where concentrations of pTA and nTCO_2 increase in a ratio of 2:1 (Shadwick et al., 2014).

In some polar systems, sea ice formation and melt have been associated with the precipitation and/or dissolution of the calcium carbonate mineral ikaite and its impact on the CO_2-system chemistry of the underlying surface waters (e.g., Rysgaard et al., 2012). Ikaite precipitation in brine reduces the concentrations of TA and TCO_2 in a ratio of 2 to 1, leading to the preferential retention of TA and rejection of TCO_2 within the sea ice matrix. The net impact of remaining ikaite mineral dissolution in melting sea ice in the spring and summer is an enrichment of TA relative to TCO_2 in the surface waters. The conservative relationship between TA and salinity (Figure 4.6 a) and between pTA and nTCO_2 (Figure 4.6 c) suggests that the formation and dissolution of calcium carbonate mineral did not influence summertime mixed-layer TCO_2 concentrations during these studies.

Vertical profiles TCO_2 and TA concentrations from repeated stations along the MGT were similarly assessed for summer interannual variability between the two voyage years (Figure 4.5 c and d). Surface water concentrations of both TCO_2 and TA were lower in January 2017 than in January 2015, due to lower sea surface salinity and increased biological production. The impact of an increased subsurface water column salinity is seen more dramatically in TA (Figure 4.5 d), where subsurface water column TA concentrations

were greater in 2017 than in 2015. The subsurface concentrations of TCO_2 were more convergent at depth along the MGT. Profiles of TCO_2 show excellent agreement in concentration, particularly in the DSW water mass (depths greater than approximately 700 m) between the two years, suggesting the interannual variability in subsurface TCO_2 is small. Thus, to determine the amount of the inorganic carbon transported with DSW (section 4.4.5), the TCO_2 data sets from 2015 and 2017 are combined and are treated as one.

The vertical distribution of CO_2-system parameters highlights the magnitude of surface variability relative to depth (Figure 4.7). The vertical profiles of pH and Ω_{Ar} indicated an enrichment in the surface layer relative to depth, corresponding with the TCO_2 and TA depletions (Figures 4.7 c and g). The patterns of surface pH and surface aragonite saturation were coincident with patterns of surface TCO_2 and TA: pH and Ω_{Ar} maxima were consistent with TCO_2 and TA minima. Surface pH ranged approximately between 8.10 and 8.35, and gradually decreased with depth to 8.0 below 50 m and remained nearly constant below this depth. Surface Ω_{Ar} values were typically 1.5 or greater, indicating supersaturated conditions, with values above 2.0 found near the calving front of the MGT and reaching 2.5 in the Ninnis Polynya. However, in the deeper water masses below 900 m, the saturation state of aragonite was below 1 due to the influence of increasing TCO_2 concentrations. Although the introduction of sea ice melt would reduce pH and aragonite saturation state in the surface waters by dilution, the biological depletion of TCO_2 counteracted the ice melt dilution effect to increase the pH and Ω_{Ar} at the surface. This is consistent across the two survey years presented in this study as well as with previous estimates (Shadwick et al. 2013, 2017), indicating that the biological TCO_2 reduction exerts

a greater influence on the seasonal enhancement of pH and aragonite saturation than changes in salinity due to sea ice melt. Below approximately 150 m, all CO_2 system parameters converge in mCDW and DSW. TCO_2 concentrations from both data sets converged at a depth of approximately 150 m to values ranging between 2,225 and 2,245 µmo/kg (mean TCO_2 concentration below 150 m = 2,236 ± 5 µmol/kg). In the deepest waters within the Ninnis Polynya (depth > 1300 m), TCO_2 concentrations reached a maximum value of 2,244 µmol/kg.

4.4.4 Net Community Production

NCP was estimated on both voyages as the depth-integrated (surface to 100 m) difference between observed summer $nTCO_2$ and inferred winter $nTCO_2$ concentrations (Figure 4.7 e and Figure 4.8). Wintertime $nTCO_2$ was estimated from concentrations at 150 m depth, where values begin to converge with depth in deeper water masses ($nTCO_2^{winter}$ = 2,233 ± 3 µmol/kg, n = 35). Unlike the subsurface waters, mixed-layer $nTCO_2$ concentrations in the Mertz and Ninnis Polynyas were highly variable both regionally and between years, although some broad trends emerge (Table 4.3). The largest mixed-layer $nTCO_2$ deficits were found in the open surface waters adjacent to the MGT during both voyages. Along the calving edge of the MGT and the along the westward coastline in 2015, mixed-layer $nTCO_2$ deficits were greater in 2017 (107 to 114 µmol/kg) than in 2015 (74 to 86 µmol/kg) corresponding to rates of NCP of 60 to 78 mmol C m^{-2} day^{-1} in 2017 and NCP of 42 to 72 mmol C m^{-2} day^{-1} in 2015. This pattern of the largest $nTCO_2$ deficits near the MGT relative to the greater Adélie Land shelf region within a sampling year was consistently seen in previous years (Shadwick et al., 2017)) and agrees well with observed

spatial patterns of depth-integrated phytoplankton biomass and chlorophyll *a* concentration and with $\Delta O_2/Ar$ estimates (Moreau et al., 2019).. The magnitude of $nTCO_2$ deficit in the mixed layer (and NCP) along the calving edge of the MGT varied between years, highlighting the interannual variability in biological production in the region. The ranges of NCP along the previous western boundary of the MGT and north of the current MGT front were similar in both years, particularly farther offshore, with values between 26 to 48 mmol C m^{-2} day^{-1}. The ranges in NCP are in good agreement with previous studies, and these rates are considerably greater than NCP rates in the pre-calving conditions likely due in part to an increase in dissolved iron delivery from sea ice melt and/or stronger summer stratification improving light conditions since the MGT calving (Shadwick et al., 2017). The Ninnis Polynya similarly had high rates of NCP, ranging between 50 and 65 mmol C m^{-2} day^{-1}, with the exception of a few stations toward the coast. In waters overlying the Adélie Depression in 2015 and Mertz Depression in 2017, surface $nTCO_2$ deficits were smaller, ranging between 30 and 60 µmol/kg, corresponding to smaller NCP rates of 20 to 55 mmol C m^{-2} day^{-1}.

4.4.5 Inorganic Carbon Transport with DSW

There are regional and seasonal patterns in $Transport^{DSW}$ and $CO_2{}^{DSW}$ across the polynya boundaries (Figure 4.9; Table 4.4). DSW is exported off the shelf break along Adélie Land coast from three regions: the northern regions across the Adélie Sill and Adélie Bank (Mertz Polynya) and the Mertz Sill and Mertz Bank (Ninnis Polynya) and from the western side of the Mertz Polynya. The greatest DSW outflow from the Adélie Land coast occurred through the Adélie Sill from the northern Mertz Polynya with an

annual mean export of 473 ± 98 mSv (Standard deviations represent interannual variability.) peaking during the austral winter months (Figure 4.9 c). DSW export through the northern Mertz region begins to increase in May when sea ice production erodes summer stratification, followed by a peak in September due to a maximum in water column convection, and a slow decline though January into the austral summer. Correspondingly, the maximum CO_2^{DSW} (413 ± 86 Tg C/year) was exported from the northern region of the Mertz Polynya, with seasonal variation a function of seasonality in volume transport as well as the concentration of TCO_2 in the transported volume. Although there is quantitatively a higher concentration of inorganic carbon in the denser DSW fractions, the smaller rates of formation and subsequent transport of those denser fractions delivered less carbon to the deep ocean than the lighter DSW fractions with lower concentrations of TCO_2 but more volume transport.

The northern Ninnis Polynya has a weaker seasonal cycle and the lightest fraction of DSW is exported through the Mertz Sill. The model-derived transport estimates in the post-calving MGT scenario indicated that no waters denser than 27.90 kg/m^3 were exported from the region, and instead an annual mean of 186 ± 12 mSv of lighter DSW fractions was exported. Because of the weaker seasonal transport cycle, there is a smaller seasonal variability in CO_2^{DSW} from the northern Ninnis. On average, 13 ± 4 Tg C/month is exported from the northern Ninnis Polynya, corresponding to an export of 163 ± 10 Tg C/year.

The densest source of DSW (σ^θ > 28.20 kg/m) is exported from the western edge of the Mertz Polynya, west of the Adélie Depression and Adélie Sill, with an annual mean outflow of 299 ± 30 mSv and CO_2^{DSW} of 262 ± 26 Tg C/year (Figure 4.9 a). Kusahara et al. (2017) identify this DSW source as originating from the overflows of DSW production

in the Adélie Depression which are then ultimately transported off the shelf break farther west through the bathymetric sill found near the D'Urville Trough Sill between 136°E and 140°E, with peak export occurring at a two-month time lag (in November) relative to waters leaving through the Adélie Sill. Accounting for these three DSW transport pathways off the continental shelf along the Adélie Land coast, 838 ± 90 Tg C is exported annually.

The eastern edge of the Ninnis Polynya represents a major inflow pathway of characteristically lighter DSW, whereby a cumulative annual mean of 267 ± 106 mSv of DSW delivers 233 ± 93 Tg C/year into the region. The boundary between the eastern Mertz Polynya and western Ninnis Polynya are aligned such that DSW formed in the Ninnis Polynya flows into the eastern side of the Mertz, with a very small portion of the exchange flowing into the Ninnis Polynya from the Mertz Polynya. The net average annual transport (i.e., sum of all inflow and outflow pathways) of TCO_2 in DSW in the Mertz Polynya and Ninnis Polynya regions accounts for an annual mean export 378 ± 130 Tg C and 180 ± 108 Tg C, respectively, from the continental shelf to offshore.

4.5 Discussion

The Mertz Polynya system has been well studied relative to others in the East Antarctic (Rintoul, 1998; Shadwick et al., 2017; Williams & Bindoff, 2003; Williams et al., 2010). CO_2-system observations over the last decade have indicated a large interannual variability in summer surface waters, influenced predominantly by seasonal and regional sea ice dynamics and biological processes that impose correspondingly large variations in mixed-layer TCO_2 concentrations. While the seasonal deficit in mixed-layer TCO_2 from the shelf region on the Adélie Land coast was in general greater in 2017 compared to 2015,

the magnitudes from both years were within the range of seasonal TCO_2 deficits reported from three post calving summers (2011 – 2013; Shadwick et al., 2017). In January 2017, mixed-layer TCO_2 deficits along the front of the MGT calving face were roughly 70 µmol/kg greater than in 2015. While in both years the majority of this deficit was attributed to biological production, on average, a larger proportion of the TCO_2 deficit was attributed to an increased dilution from sea ice melt in 2017 (approximately 44%) than in 2015 (approximately 38%; Figure 4.10). The larger volumes of sea ice melt water during summer 2017 produced a shallower and more stable mixed layer (13 ± 1 m) as compared to summer 2015 (23 ± 9 m), consistent with widespread lower sea surface salinity in 2017 (Figure 4.4 b). These more recent observations continue to support the case of an enhancement in biological productivity and elevated surface pH and saturation state relative to pre-calving polynya configuration due to more favorable conditions for phytoplankton growth (i.e., shallower mixed layers, greater light availability), particularly in proximity to the MGT, that outweighs the opposing dilution effect from melting sea ice years after the glacial tongue calving (Moreau et al., 2019; Shadwick et al., 2017).

Prior to 2017, heavy sea ice conditions to the west of the Ninnis Glacier made the area inaccessible by ship. Grounded icebergs and fast ice provided a barrier to the westward advection of pack ice. These features were persistent over several decades (e.g., Frezzotti et al., 1998; Massom, 2003) but were disrupted due to the regime shift in sea ice production and polynya activity after the 2010 MGT calving (Tamura et al., 2012; Ohshima et al., 2016). New observations from within the Ninnis Polynya west of the Mertz Polynya reveal similarities in CO_2-system properties between the two regions. The Ninnis Polynya experienced high rates of NCP and was a sink of CO_2 from the atmosphere with a strong

undersaturation in fCO_2 during the austral summer. However, the air-to-sea CO_2 flux was relatively small due to weak summer winds. Surface waters within the Ninnis Polynya additionally had enhanced pH and saturation state as compared to Mertz Polynya and shelf waters offshore at the Mertz Depression. Because rates of NCP and the biological consumption of TCO_2 in the Ninnis Polynya were similar to those in the Mertz Polynya, the enhancements of pH and Ω can be attributed to a reduced influence of sea ice melt and a smaller dilution effect in CO_2-system parameters in the Ninnis Polynya. This is supported by an elevated surface salinity in the Ninnis Polynya relative to Mertz Polynya and Mertz Depression shelf waters in 2017.

The presence and formation of DSW in the Ninnis Polynya was confirmed during this study, as suggested by several modelling studies that focused on the entire Adélie Land coast (i.e., east of the MGT; Kusahara et al., 2010; 2011ab, 2017). Active formation of DSW within the Ninnis Depression could combine with the DSW volume produced in the Adélie Depression through cross-shelf circulation (e.g., Aoki et al., 2017; Snow et al., 2016), although many observational studies have shown the largest volumes of DSW are formed in the Adélie Depression. The mid-layer intrusions of mCDW in summer have been well observed on the continental shelf in Adélie Land in summer (Lacarra et al., 2011, Shadwick et al., 2014; Rintoul, 1998; Williams et al., 2010), which have the potential to, but do not always, extend toward the calving front of the MGT and farther inshore (Silvano et al., 2016). Signals of mCDW were not seen along the calving front of the MGT in 2015 and 2017, and were not found in the Ninnis Polynya in summer 2017. Instead, the summer water column is filled with lighter fractions of DSW. The bottom fraction of DSW found in the Ninnis Polynya was slightly fresher (~34.666) than found in the Mertz Polynya

(~34.673) in the same year, but the bottom fraction of DSW found in 2017 was saltier than in 2015 in the Mertz Polynya (~34.615; See Figure 4.5 a). The formation and export of DSW in Adélie Land is known to have a significant interannual variability as indicated by both modelling (Kusahara et al., 2011; 2017) and observational studies (Lacarra et al., 2013; Snow et al., 2018), linked to variations in local sea ice production as well as changes in circulation driven by wind and freshwater input. In the winter preceding our sampling in January 2017, there could have been a greater volume of sea ice produced, which would lead to a denser water column, increased bottom salinity, and more DSW export relative to 2015.

Unlike the surface CO_2-system properties, and the bottom layer salinity of DSW, observations from 2015 and 2017 show the subsurface (> 200 m) CO_2-system parameters were invariant between the two years, in particular with respect to TCO_2 concentrations. DSW is formed during wintertime as a product of brine rejection and surface cooling, in combination with mixing with inflowing mCDW. A majority of the TCO_2 on the Adélie Coast derives from the preconditioning of the water column due to the physical transformations of water masses within the polynya. The TCO_2 concentration in mCDW is seasonally and interannually invariant as the older, intermediate water mass has been out of contact with the atmosphere for long periods of time and has accumulated a substantial amount of respired organic matter. The small variations in mCDW TCO_2 concentrations (2,232 ± 3 µmol/kg) lead to small variations in DSW TCO_2 concentrations (2,240 ± 2 µmol/kg) that is further elevated in concentration from the local addition of brine. The observed mean TCO_2 concentration in DSW also compares well to the previously the reported concentration of 2,238 µmol/kg from within the Adélie Depression and Mertz

Polynya during summer 2008 before the MGT calving (Shadwick et al., 2014) confirming the importance of the mCDW, rather than local processes on the shelf, in setting this concentration.

A previous study by Shadwick et al. (2014) estimated that between 320 to 560 Tg CO_2 (equivalent to approximately 85 to 150 Tg C) is exported annually from the Mertz Polynya with DSW outflow, a smaller value than reported here. Similar to this analysis, the authors combine an observed summertime concentration of TCO_2 in DSW from the Mertz Polynya with model-derived volumetric DSW transport estimates from the Adélie Land coast obtained from a coupled sea ice-ocean model by Kusahara et al. (2011). In contrast to the present study, the authors bound their estimates by assuming an upper and lower bound for the critical density of DSW export of (27.88 kg/m^3 and 27.80 kg/m^3, respectively) and use annual average DSW export rates for each critical density threshold (0.21 Sv and 0.37 Sv, respectively). Additionally, the mixing between outflowing DSW and the entrainment of (relatively TCO_2-depleted) mCDW was explicitly accounted for. In our approach, including seasonal variations in DSW export yields significantly larger values, with approximately 838 ± 98 Tg C/year exported from the Adélie Land coast.

The transport of CO_2 in deep water from East Antarctica has been proposed by Takahashi and Chipman (2012), who use observations of TCO_2 and the partial pressure of CO_2 (pCO_2) from 1992 World Ocean Circulation Experiment (WOCE) to track the fate of CO_2 off the coast of Wilkes Land (168°E – 173°E), farther east of the Adélie Land coast. The analysis suggests a significant transport of CO_2 from the shelf waters into AABW due to the sinking of a dense plume of TCO_2-rich deep water originating from Ross Sea Bottom Water and the entrainment of TCO_2-rich Circumpolar Deep Water. A similar process

occurs on the Adélie Land coast, where DSW formation in the Mertz Polynya and Ninnis Polynya transports approximately 838 ± 98 Tg C per year out of the region, either directly (i.e., through the Adélie Sill and Mertz Sill) or indirectly (i.e., west through D'Urville Trough Sill) off the continental shelf break. Similarly, both dissolved and particulate forms of organic carbon will also be transported into the ocean interior through this process. The interaction between the physical export of the DSW, predominantly during winter, from the shallow continental shelf through the sills at the shelf break to the deep ocean, and the biogeochemical processes that enrich the outflowing water, lead to a net export of carbon from the Adélie Land coast that constitutes a continental shelf pump for carbon (Figure 4.11).

Although the majority of the exported inorganic carbon is sourced from the offshore mCDW signal, local processes on the shelf impact TCO_2 concentrations in DSW. If the organic matter formed during the productive season is exported below the mixed layer, subsequent remineralization processes will convert it CO_2. If it is assumed that the mean NCP from summer 2015 and 2017 (~50 mmol C m^{-2} day^{-1}) persisted through the duration of the bloom season (between November and February, 120 days) over the open water area on the Adélie Land coast (~33,664 km^2; Arrigo et al. 2015), and that 100% of the vertically exported organic matter is respired at depth and not buried in the underlying sediments, then roughly 2.4 Tg C per year is locally contributed to inorganic carbon export with DSW. The high levels of primary productivity in the polynyas result in the disequilibrium of fCO_2 between the surface waters and the atmosphere, driving a net air-to-sea flux of atmospheric CO_2. If the average CO_2 flux (~ 6.6 mmol C m^{-2} day^{-1}) is extended over the duration of the productive season, this would contribute less than 1 Tg C of CO_2 from the atmosphere. The

sum of these two components is within the variability of TCO_2 export and would leave relatively small, but not negligible, impact on net transport of TCO_2 off the continental shelf. However, because of the large interannual variability in mixed-layer TCO_2 concentrations, the local contribution of inorganic carbon to DSW will vary from year to year. In addition, previous work in this region suggests that outflowing DSW after the productive season is relatively depleted in TCO_2 through the biological modification over the continental shelf break (Shadwick et al., 2014), as outflowing water can entrain relatively CO_2-depleted AASW.

Given the small variations of TCO_2 concentration in DSW, the bulk of the variability in TCO_2 export is driven by the physical mechanisms of DSW formation and transport. Recent numerical modeling studies have shown that the changes to local shelf circulation that are regulated by wind stress and sea ice conditions can influence the volume and source of mCDW intrusion onto the continental shelf (e.g., Aoki et al., 2017; Snow et al., 2018). While an enhancement of mCDW onto the coast could bring a significant concentration of TCO_2 to the shelf, numerical analyses show that enhanced intrusions lead to an increase in a lighter fraction of DSW export in the spring and summer, as a larger volume of the less saline mCDW interacts with a smaller volume of salty water associated with brine rejection. Despite a larger volume of TCO_2 delivery to the shelf region, an increase in mCDW could decrease the amount of inorganic carbon exported with DSW if the denser DSW fractions do not form. Similarly, a reduction in sea ice production leads to a decrease in DSW export from Adélie Land, particularly in the densest, TCO_2-rich fractions.

This mode of carbon export with DSW from coastal polynyas has important implications for Southern Ocean carbon budget. The ability of the ocean to effectively remove CO_2 from the atmosphere is determined by the rate and efficiency by which carbon is transferred from the deep ocean and removed from the surface layer. The vertical transport of carbon to depth in the open ocean has been explored by many studies in terms of the biological pump (e.g., Ducklow et al., 2001) and solubility pump (e.g., Toggweiler et al., 2003). The biological pump describes the series of processes that transform TCO_2 into organic biomass in the euphotic zone and transport the material into the deep ocean. Below the euphotic zone, the organic material can be assimilated into higher trophic levels or respired into CO_2. Only a very small fraction (< 1%) of the particulate matter that sinks below the euphotic zone reaches the seafloor, where organic material is subsequently consumed or buried, and carbon is sequestered from exchange with the atmosphere. The presence of a permanent thermocline in open ocean systems provides a barrier that impedes the exchange of surface and deep water and facilitates the storage of CO_2 below the winter mixed layer on decadal to millennial timescales once CO_2 reaches depths on the order of 1,000s of meters. In high latitude systems, however, the permanent thermocline breaks down, and winter mixed layer depths can extend well below the euphotic zone. In contrast to systems that form DSW, Antarctic polynyas that do not supply bottom water to the deep ocean (e.g., the Amundsen Sea Polynya) lack the physical circulation mechanism to transport carbon into the ocean interior, such that organic and inorganic carbon may not be sequestered effectively (Lee et al., 2014). Deep winter mixing and on the continental shelf prevents efficient vertical carbon export and sedimentary burial by allowing deep water to exchange with the surface layer and atmosphere. In regions of deep water formation on

shallow continental shelves, such as in the Mertz Polynya and Ninnis Polynya, the lateral movement of DSW from the shallow continental shelf into the deep ocean during DSW export and AABW formation creates an alternative pathway for the delivery of shelf-derived carbon to the deep ocean. A similar process has been recorded in the Ross Sea (Bercovici et al., 2017). These results suggest that a continental shelf pump for CO_2 as described here appears to transport a significant amount carbon away from surface exchange, which could have important implications for carbon sequestration in the Southern Ocean.

4.6 Conclusion

Results from new observations in the Mertz Polynya and Ninnis Polynya in Adélie Land show the open surface waters continue to support high levels of biological productivity and sustain a sink for atmospheric CO_2 in the summertime. The deep Adélie Depression and Ninnis Depression found adjacent to the Mertz and Ninnis Polynyas allow for the characterization of TCO_2 in DSW formed during the previous winter to be established. The combination of TCO_2 in DSW with modelled DSW transport estimates indicated a large quantity of inorganic carbon is transported off the continental shelf into the deep ocean. In contrast to surface mixed layer concentrations, the concentration of TCO_2 in DSW was found to be similar in both summers, suggesting that the local contribution from summer processes including seasonal net community production and the associated sea surface uptake of atmospheric CO_2 makes a small imprint on the inorganic carbon signature in DSW. Instead, the variability in inorganic carbon export from the region is more strongly related to the variability in the physical preconditioning of the water

column from inflowing, TCO_2-rich mCDW and the quantity of brine rejected with sea ice production in the previous winter. Understanding the seasonality in TCO_2 export with DSW requires more observations outside of the summer season to accurately quantify the export of inorganic carbon with DSW during the peak formation months.

Table 4.1. Water mass definitions for the Mertz Polynya and Ninnis Polynya on the Adélie Land coast derived from Shadwick et al. (2014) and Kusahara et al. (2017).

Water Mass	γ^n **(kg/m^3)**	σ^θ **(kg/m^3)**	**θ (°C)**
Antarctic Surface Water (AASW)	$\gamma^n < 28.00$		
Modified Circumpolar Deep Water (mCDW)	$28.00 < \gamma^n < 28.27$		
Ice Shelf Water (ISW)	$28.00 < \gamma^n < 28.27$		$\theta < -1.925$
Dense Shelf Water (DSW)		$\sigma^\theta > 27.84$	$\theta < -0.5$

Table 4.2. Bin-averaged TCO_2 concentrations (μmol/kg) in DSW on the Adélie Land coast. The value of DSW bin concentration (± standard deviations) is the midpoint between two bins and the corresponding number of discrete bottle observations (No. of Obs.) in the combined dataset. Any volume of DSW denser than observed in the summer is assigned the concentration in the 27.93 kg/m^3 bin.

DSW bin (kg/m^3)	TCO_2 (μmol/kg)	No. of Obs.
27.85	2,238 ± 2	71
27.87	2,239 ± 2	45
27.89	2,240 ± 2	20
27.91	2,241 ± 2	44
27.93	2,243 ± 1	11

Table 4.3. Air-Sea CO_2 exchange and NCP (mmol C m^{-2} day^{-1}) with standard deviations on the Adélie Land coast. A negative CO_2 flux indicates sea surface uptake. A positive NCP indicates net autotrophy.

Region	**Air-Sea CO_2 Flux**	**NCP**
Adélie Depression	- 3.2 ± 2.6	47 ±18
MGT 2015	- 5.0 ± 2.4	54 ±15
MGT 2017	- 14.1 ±7.2	62 ±20
Ninnis Polynya	- 4.6 ±1.8	51 ± 14
Mertz Depression	- 5.9 ± 1.4	35 ± 13

All units mmol C m^{-2} day^{-1}.

Table 4.4. Annual cumulative DSW volume transport (mSv) and inorganic C transport (Tg C/year) with DSW from the Mertz and Ninnis Polynyas averaged between 2011 and 2013.

Region		**Volume Transport (mSv)**		**Inorganic C Transport (Tg C/year)**	
		Inflow	*Outflow*	*Inflow*	*Outflow*
West					
	Mertz	17 ± 7	299 ± 30	15 ± 6	262 ± 26
	Ninnis	27 ± 4	312 ± 230	24 ± 3	273 ± 201
North					
	Mertz	10 ± 10	473 ± 98	8 ± 9	413 ± 86
	Ninnis	6 ± 5	186 ± 12	5 ± 4	163 ± 10
East					
	Mertz	439 ± 254	126 ± 20	384 ± 222	110 ± 18
	Ninnis	267 ± 106	7 ± 1	233 ± 93	6 ± 1

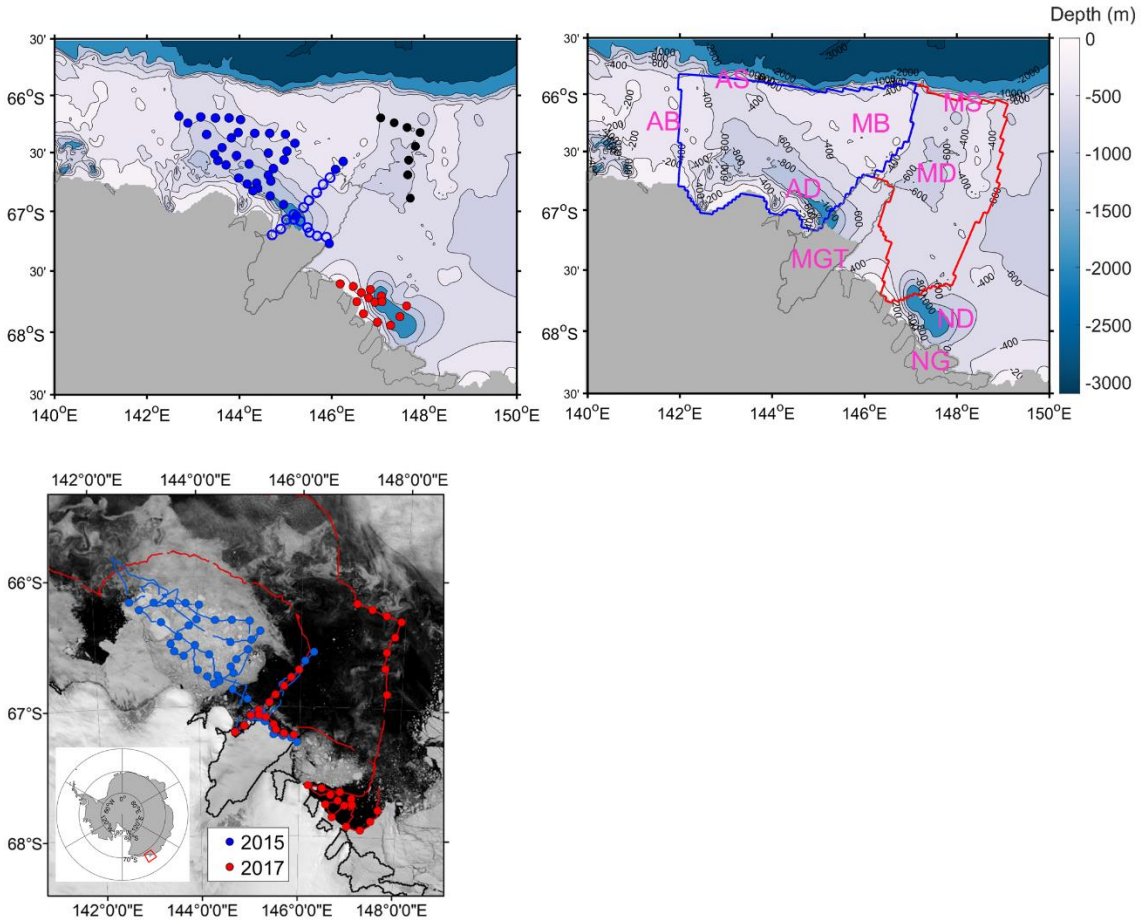

Figure 4.1. (a) CTD casts in the Mertz Polynya (blue), Ninnis Polynya (red), and Mertz Depression (black) from two summer voyages in January 2015 (AU1402) and January (2017) on a bathymetric map after Beaman et al. 2011. Repeat hydrocast stations along the Mertz Glacier Tongue on the two voyages are indicated with open blue circles. (b) bathymetric map delineating Kusahara et al. (2017) model boundaries for the Mertz Polynya (blue) and Ninnis Polynya (red) and geomorphic features: Adélie Bank (AB), Adélie Depression (AD), Adélie Sill (AS), Mertz Bank (MB), Mertz Depression (MD), Mertz Glacier Tongue (MGT), Mertz Sill (MS), Ninnis Depression (ND), and Ninnis Glacier (NG). (c) Satellite image of the Adélie Land coast between 141.4°E and 149°E taken on 22 January 2017. Underway (lines) and CTD station locations (circles) from the two summer voyages in January 2015 (blue) and January 2017 (red).

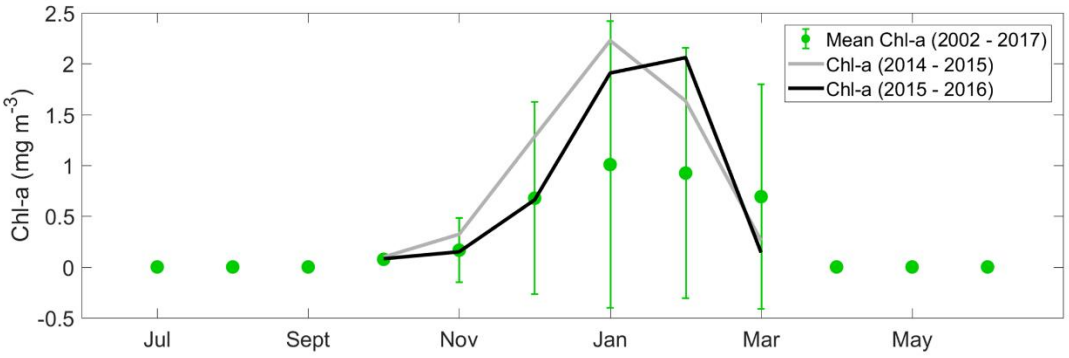

Figure 4.2. MODIS-Aqua derived monthly averaged surface chlorophyll *a* concentration (Chl-a; mg/m^3) on the Adélie Land coast between July 2002 and June 2018 (green) with error bars indicating the monthly standard deviations. The gray line indicates Chl-a concentration between July 2014 and June 2015, and the black line indicated Chl-a concentration between July 2016 and June 2017.

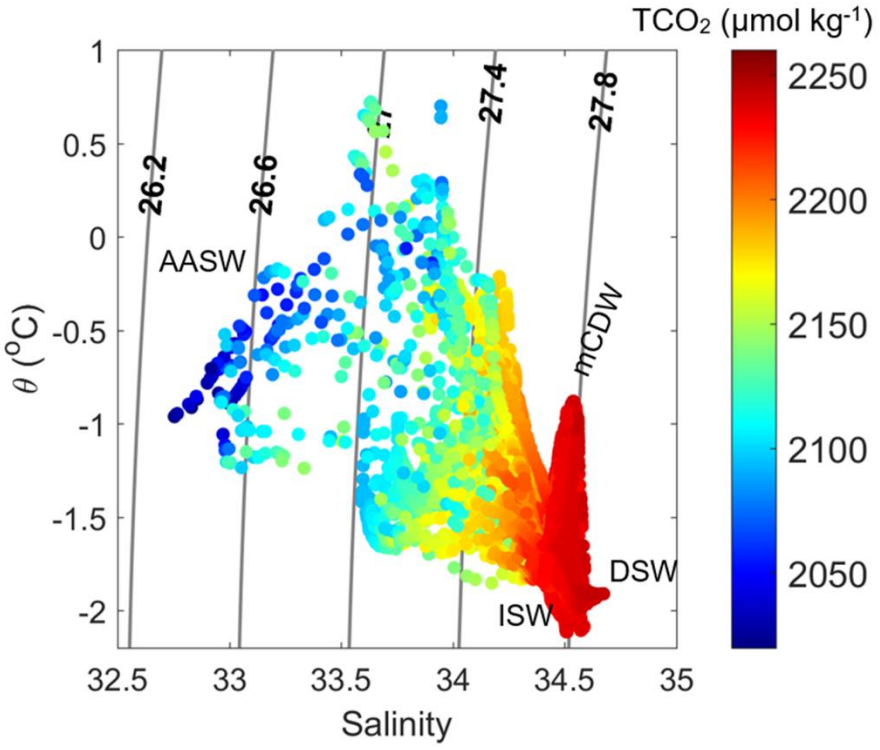

Figure 4.3. Potential Temperature (θ, °C) - Salinity diagram for discrete measurements on AU1402 and AU1602 with contours (gray lines) of potential density anomaly (kg/m^3) and color scaling for TCO_2 concentration (µmol/kg). Water masses are labeled as Antarctic Surface Water (AASW), modified Circumpolar Deep Water (mCDW), Ise Shelf Water (ISW), and Dense Shelf Water (DSW).

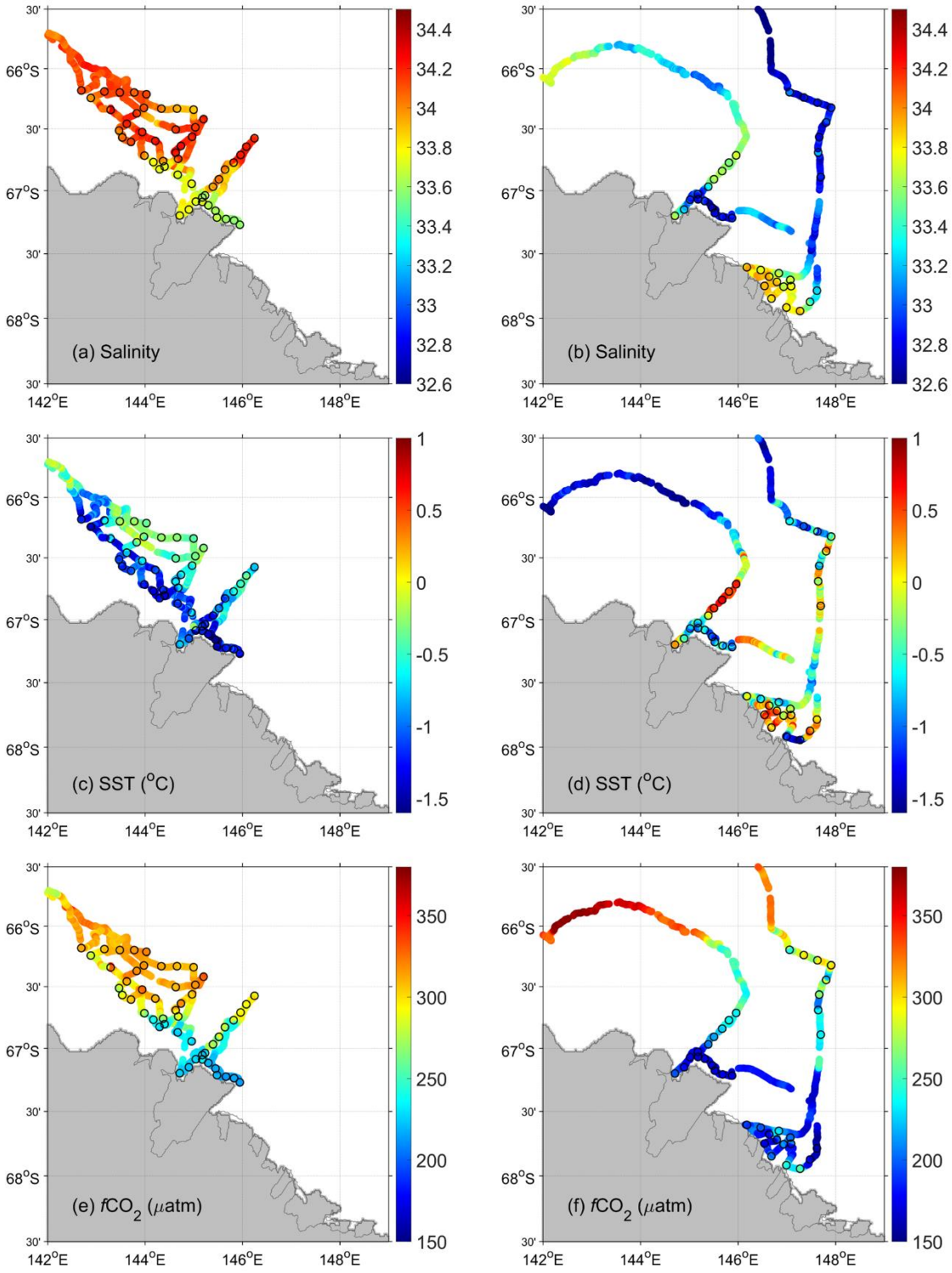

Figure 4.4. Underway measurements from AU1402 (left column) and AU1602 (right column) for (a, b) salinity, (c, d) sea surface temperature (SST; ºC), and (e, f) fCO_2 (µatm) on the Adélie Land coast. Mean atmospheric fCO_2 values were 382 µatm and 389 µatm in 2015 and 2017, respectively. Open black circles denote CTD station locations.

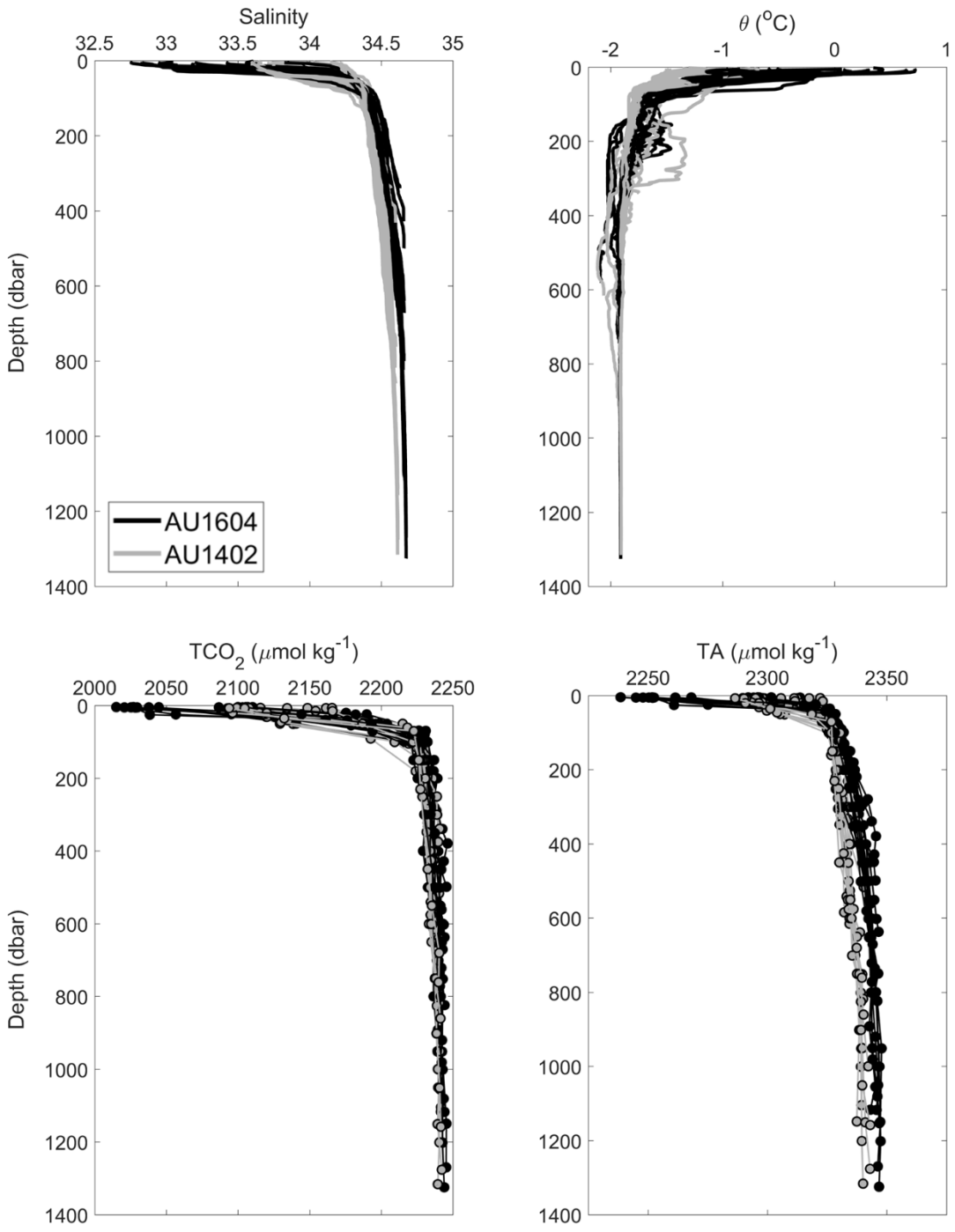

Figure 4.5. Vertical profiles of (a) salinity, (b) potential temperature, (c) TCO_2 (µmol/kg), and (d) TA (µmol/kg) from overlapped CTD stations in the Mertz Polynya along the MGT from the AU1602 (black) and AU1402 (gray) voyages. See Figure 4.1 a (open blue circles) for CTD station locations.

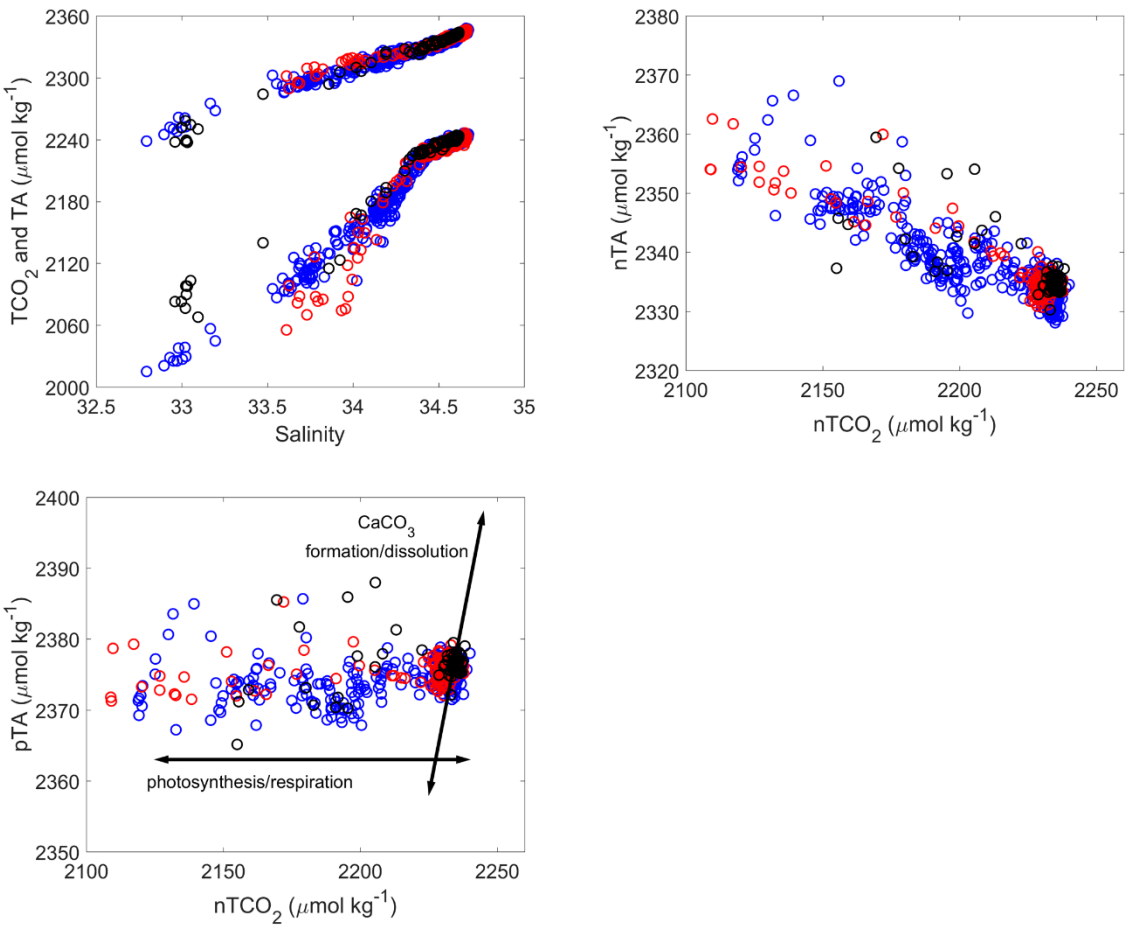

Figure 4.6. Relationships between (a) salinity and TCO_2 (µmol/kg) and salinity and TA (µmol/kg); (b) salinity-normalized TA (nTA; µmol/kg) and salinity-normalized TCO_2 ($nTCO_2$; µmol/kg); and (c) salinity-normalized potential alkalinity (pTA; µmol/kg) and $nTCO_2$ (µmol/kg).

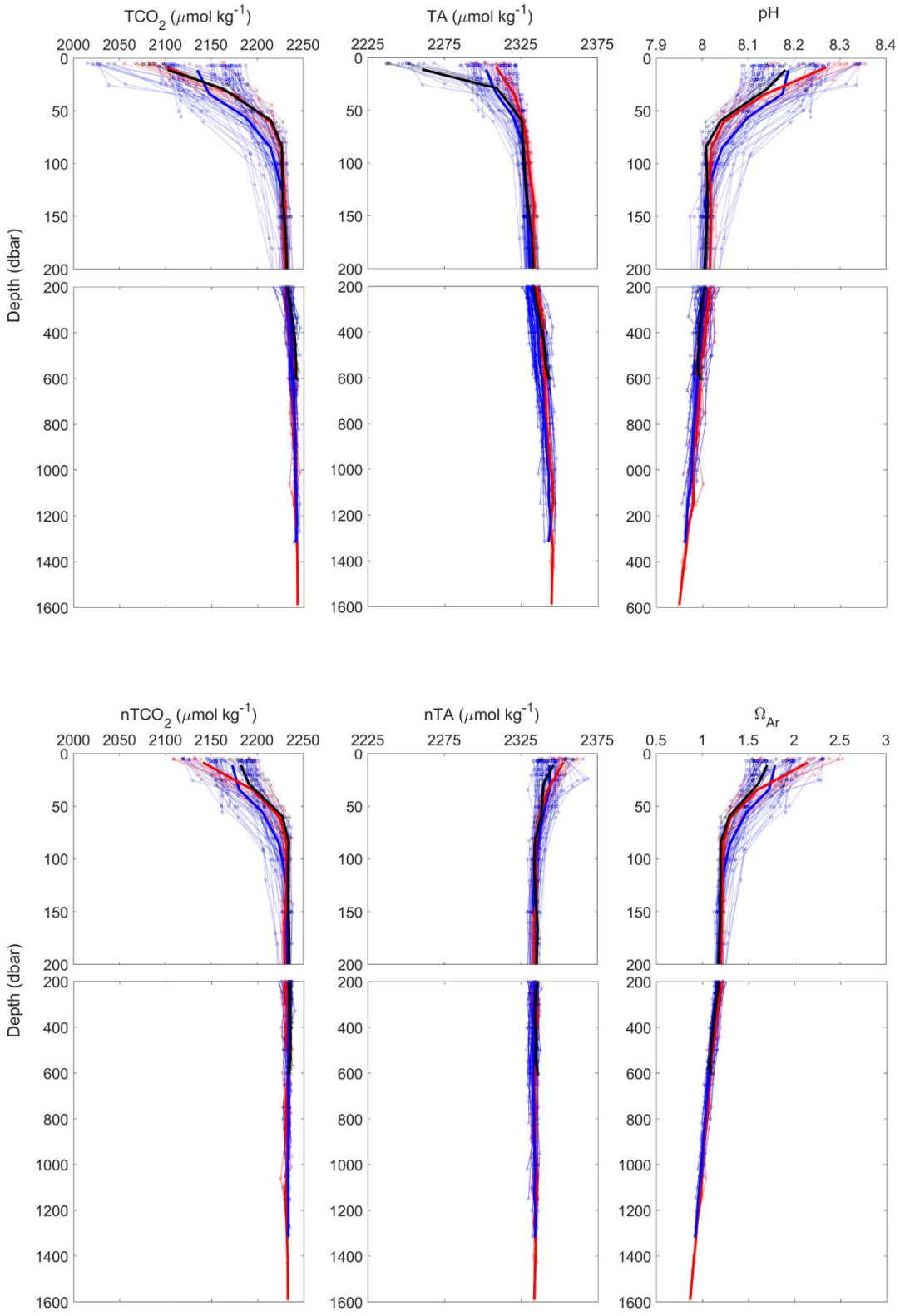

Figure 4.7. Vertical profiles of (a) TCO_2 (µmol/kg), (b) TA (µmol/kg), (c) pH, (e) $nTCO_2$ (µmol/kg), (f) nTA (µmol/kg) and (g) Ω_{Ar}. Color scheme follows Figure 4.1 a.

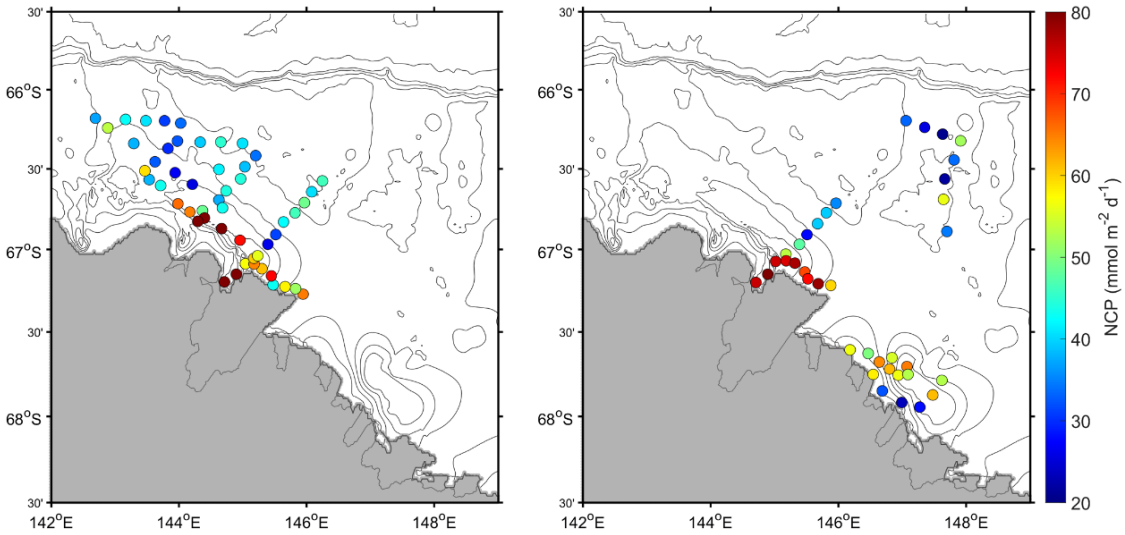

Figure 4.8. NCP (mmol C m^{-2} day^{-1}) during the (a) AU1402 and (b) AU1602 voyages.

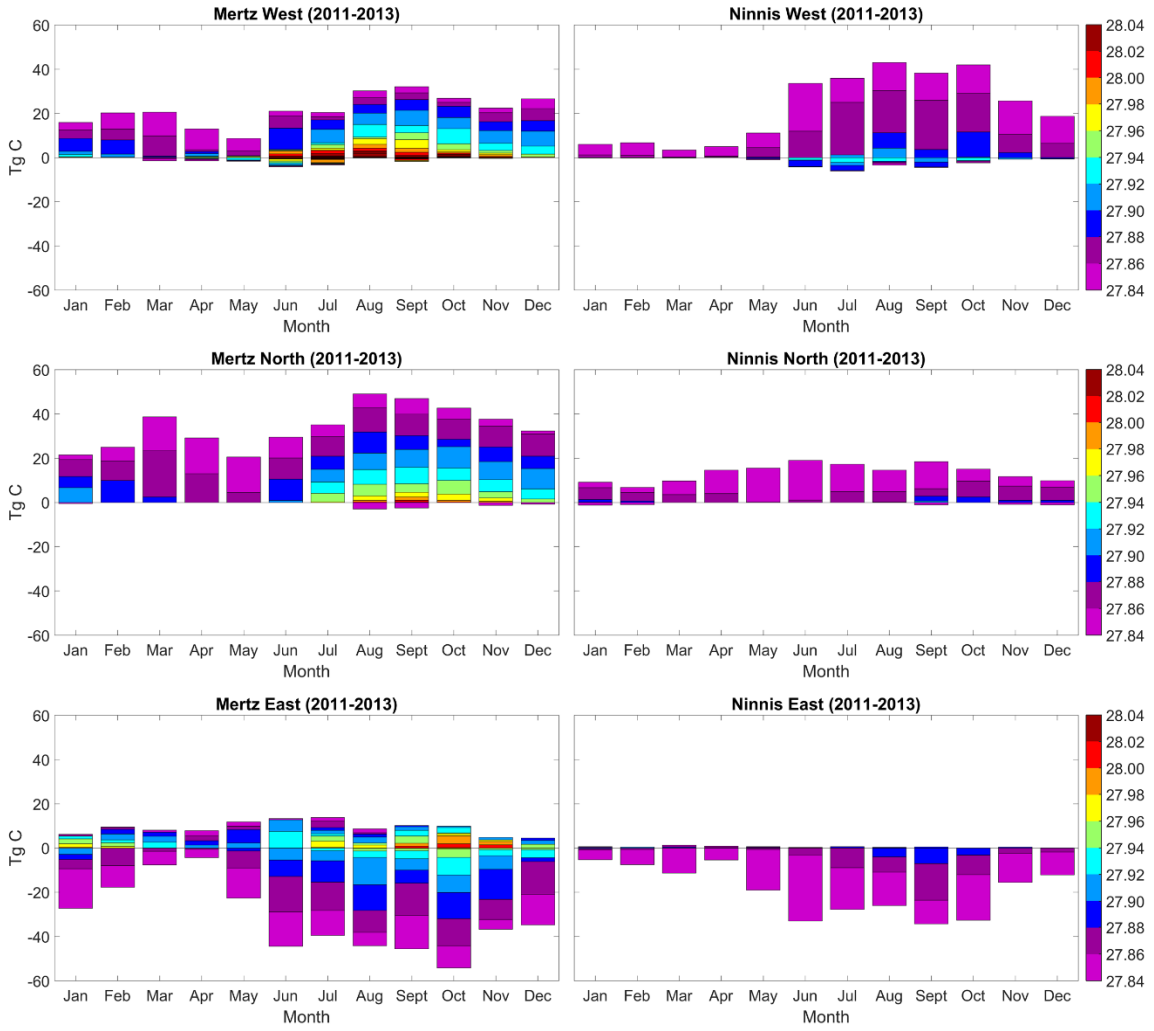

Figure 4.9. Monthly mean carbon transports (Tg C/month) with DSW from the (a, b) western, (c, d) northern, and (e, f) eastern boundaries of the Mertz Polynya (right column) and Ninnis Polynyas (left column) as binned by potential density anomaly in 0.02 kg/m^3 increments (color axis). Monthly DSW volume transports obtained from Kusahara et al. 2017 are averaged between the time period of January 2011 and December 2013. Denser DSW fractions are indicated in deep red. Positive values indicate outflows.

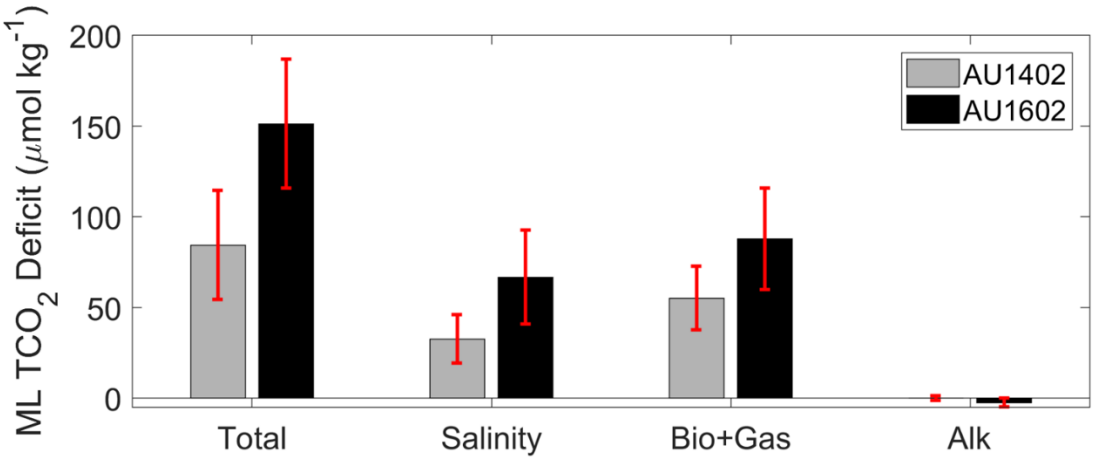

Figure 4.10. Drivers of mixed-layer TCO_2 (µmol/kg). Bars represent the total average deficit in TCO_2 and the average contributions due to changes in salinity, biological processes and air-sea CO_2 exchange (Bio+Gas), and carbonate mineral processes (Alk) for AU1402 (gray) and AU1602 (black). Red error bars denote one standard deviation.

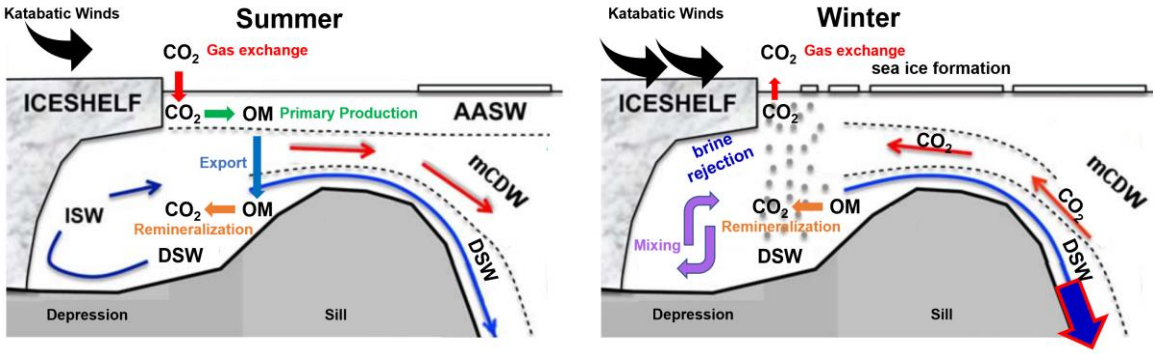

Figure 4.11. Schematic diagram of a continental shelf pump operating in the Mertz and Ninnis Polynyas. In summer (left), primary production in stratified AASW leads to organic matter (OM) production and uptake of atmospheric CO_2 through gas exchange. Some material sinks out of the surface mixed layer where it is remineralized. In winter (right), formation of sea ice impedes gas exchange, and brine rejection drives the sinking and subsequent export of CO_2-rich DSW off the shelf.

Chapter 5:

SUMMARY AND CONCLUSIONS

The research presented in this thesis investigates the processes that control the inorganic carbon budget in three coastal polynyas in the East Antarctic. Coastal polynya systems are widely diverse in their physical and biogeochemical variability with respect to ocean and sea ice conditions. The insights gained from two contrasting regions of focus in the East Antarctic, the Dalton Polynya on the Sabrina Coast (113°E – 121°E) and the Mertz Polynya and Ninnis Polynya on the Adélie Land coast (140°E – 150°E), provide an expansive view on the variability imposed upon CO_2-system processes. These findings contribute to the primary goal to better understand the physical and biogeochemical drivers of inorganic carbon dynamics in seasonally ice-covered Antarctic polynyas.

The summer carbonate chemistry and biogeochemical variability in the Dalton Polynya near the Totten and Moscow University Ice Shelves was investigated using newly available CO_2-system observations (Chapter 3). In open waters within the polynya, an observed deficit in mixed layer TCO_2 concentrations was attributed to a combination of seasonal sea ice melt and biological productivity, in contrast to sea ice covered regions near the Totten Ice Shelf, where TCO_2 deficits were small. Although rates of net community production indicated the open waters were net autotrophic, the Dalton Polynya acted a weak net source of CO_2 to the atmosphere as the biological community had not yet fully compensated for winter heterotrophy and deep mixing that increases TCO_2 and fCO_2 in the surface layer relative to equilibration with the atmosphere. Satellite remote sensing products suggest that the observations made in late December and early January preceded

the height of the productive season, inferred to occur in late February to early March. The results presented here suggesting the natural interannual variability in mixed-layer biogeochemistry is significant in the Dalton Polynya.

The Mertz Polynya and Ninnis Polynya located east of the Dalton Polynya are sources of DSW to the Australian-Antarctic Basin. The transport of inorganic carbon with DSW formation and export was quantified using a combination of summer TCO_2 observations and modelled water mass transport estimates (Chapter 4). The Adélie Land coast was a strong sink for atmospheric CO_2 due to biologically mediated CO_2 undersaturation and net autotropic conditions in surface waters. However, the estimates of net community production and air-sea CO_2 exchange indicate that the local contribution of CO_2 to shelf waters from summer processes is relatively small compared to the contribution from inflowing, CO_2-rich mCDW and brine rejection during sea ice formation. Given that the continental shelf is relatively narrow and shallow in the Mertz Polynya and Ninnis Polynya, the lateral movement of DSW off the continental shelf into northward-flowing AABW is an effective mechanism to deliver shelf- and offshore-derived CO_2 to the deep layers of the ocean.

The spatial and temporal variability observed in the three East Antarctic coastal polynyas studied in this thesis highlights the complexity of the inorganic carbon budget in coastal ocean environments. The Dalton Polynya is a relatively small, reoccurring coastal polynya sustained by offshore katabatic winds and the presence of the grounded Dalton Iceberg Tongue. In circumpolar analyses of the major Antarctic coastal polynyas, the Dalton Polynya consistently ranks low in terms of open water area (Nihashi & Ohshima, 2015), sea ice production (Tamura et al., 2016), and annual primary production and bloom

Chl *a* concentration (Arrigo & van Dijken, 2003). Although a few studies have highlighted a growing understanding of biogeochemical dynamics in larger coastal polynyas in the East Antarctic, such as Cape Darnley (68°E – 69°E; Roden et al., 2016), Prydz Bay (78°E; Roden et al., 2013), the Mertz Polynya (144°E – 145°E; Shadwick et al., 2014), there are little to no *in situ* data for the many smaller coastal polynyas that form on narrow continental shelf. The Dalton Polynya may thus serve as a more appropriate case study to speculate the behavior of other smaller coastal polynyas in terms of their summertime biogeochemistry. A similar magnitude in CO_2 system processes may occur in other polynyas with more comparable summer and winter water areas, length of the growing season, volume of sea ice produced annually, and in regions where DSW does not form. However, the full seasonal CO_2 drawdown was not captured in the Dalton Polynya with the observations presented in this study.

The enrichment of inorganic carbon in DSW as observed in the Mertz Polynya and Ninnis Polynya during summer highlights the instrumental role that these regions play in sequestering CO_2 to the deep ocean through AABW formation. This work builds and benefits from several previous biogeochemical surveys on the Adélie Land coast and supports a broader scientific effort to characterize the controlling drivers of physical and biogeochemical processes that impact the cycling and transport of inorganic carbon into the deep ocean. However, the results presented from the Mertz and Ninnis Polynyas additionally emphasize the need for more biogeochemical observations outside of the biologically productive summer season to better assess processes that impact the seasonal cycle of CO_2 on the Adélie Land coast and the ultimate export of inorganic carbon with DSW. The conditioning of shelf water masses by sea ice growth and brine rejection

typically begins in April, with a peak in bottom water densities in September, during times typically inaccessible by shipboard surveys (Williams et al., 2008). The Mertz and Ninnis Polynyas provide only a fraction of DSW that contributes to AABW and meridional overturning circulation (Kusahara et al., 2017), and the analytical techniques applied here can be extended to other major systems that produce DSW: the Ross Sea, the Weddell Sea, and Prydz Bay. Studies such as these have important implications for the coastal Antarctic contribution to the Southern Ocean carbon budget as a whole.

LITERATURE CITED

Aoki, S., Kobayashi, R., Rintoul, S. R., Tamura, T., & Kusahara, K. (2017). Changes in water properties and flow regime on the continental shelf off the Adélie/George V Land coast, East Antarctica, after glacier tongue calving. *Journal of Geophysical Research: Oceans*, *122*(8), 6277–6294. https://doi.org/10.1002/2017JC012925

Arrigo, K. R., DiTullio, G. R., Dunbar, R. B., Robinson, D. H., VanWoert, M., Worthen, D. L., & Lizotte, M. P. (2000). Phytoplankton taxonomic variability in nutrient utilization and primary production in the Ross Sea. *Journal of Geophysical Research: Oceans*, *105*(C4), 8827–8846. https://doi.org/10.1029/1998jc000289

Arrigo, K. R. & van Dijken, G. L. (2003). Phytoplankton dynamics within 37 Antarctic coastal polynya systems. *Journal of Geophysical Research*, *108*(C8), 3271. https://doi.org/10.1029/2002jc001739

Arrigo, K. R., van Dijken, G. L., & Long, M. (2008a). Coastal Southern Ocean: A strong anthropogenic CO_2 sink. *Geophysical Research Letters*, *35*(21), L21602. https://doi.org/10.1029/2008GL035624

Arrigo, K. R., van Dijken, G. L., & Bushinsky, S. (2008b). Primary production in the Southern Ocean, 1997-2006. *Journal of Geophysical Research: Oceans*, *113*(8), C08004. https://doi.org/10.1029/2007JC004551

Arrigo, K. R., van Dijken, G. L., & Strong, A. L. (2015). Environmental controls of marine productivity hot spots around Antarctica. *Journal of Geophysical Research: Oceans*, *120*(8), 5545–5565. https://doi.org/10.1002/2015JC010888

Arroyo, M. C., Shadwick, E. H., & Tilbrook, B. (2019). Summer carbonate chemistry in the Dalton Polynya, East Antarctica. *Journal of Geophysical Research: Oceans*, 2018JC014882. https://doi.org/10.1029/2018JC014882

Bates, N. R. (2006). Air-sea CO_2 fluxes and the continental shelf pump of carbon in the Chukchi Sea adjacent to the Arctic Ocean. *Journal of Geophysical Research*, *111*(C10), C10013. https://doi.org/10.1029/2005JC003083

Bates, N. R., Hansell, D. A., Carlson, C. A., & Gordon, L. I. (1998). Distribution of CO_2 species, estimates of net community production, and air-sea CO_2 exchange in the Ross Sea polynya. *Journal of Geophysical Research: Oceans*, *103*(C2), 2883–2896. https://doi.org/10.1029/97jc02473

Beaman, R. J., O'Brien, P. E., Post, A. L., & De Santis, L. (2011). A new high-resolution bathymetry model for the Terre Adélie and George V continental margin, East Antarctica. *Antarctic Science*, *23*(1), 95–103. https://doi.org/10.1017/s095410201000074x

Bercovici, S. K., Huber, B. A., DeJong, H. B., Dunbar, R. B., & Hansell, D. A. (2017). Dissolved organic carbon in the Ross Sea: Deep enrichment and export. *Limnology and Oceanography*, *62*(6), 2593–2603. https://doi.org/10.1002/lno.10592

Bindoff, N. L., Williams, G. D., & Allison, I. (2001). Sea-ice growth and water-mass modification in the Mertz Glacier polynya, East Antarctica, during winter. *Annals of Glaciology*, *33*, 399–406. https://doi.org/10.3189/172756401781818185

Bozec, Y., Thomas, H., Elkalay, K., & De Baar, H. J. W. (2005). The continental shelf pump for CO_2 in the North Sea - Evidence from summer observation. *Marine Chemistry*, *93*(2–4), 131–147. https://doi.org/10.1016/j.marchem.2004.07.006

Brewer, P. G., & Goldman, J. C. (1976). Alkalinity changes generated by phytoplankton growth1. *Limnology and Oceanography*, *21*(1), 108–117. https://doi.org/10.4319/lo.1976.21.1.0108

Broecker, W. S. (1982). Glacial to interglacial changes in ocean chemistry. *Progress in Oceanography*, *11*(2), 151–197. https://doi.org/10.1016/0079-6611(82)90007-6

Broecker, W. S., & Peng, T.-H. (1974). Gas exchange rates between air and sea. *Tellus*, *26*(1–2), 21–35. https://doi.org/10.3402/tellusa.v26i1-2.9733

Bromwich, D. H., & Kurtz, D. D. (1984). Katabatic wind forcing of the Terra Nova Bay polynya. *Journal of Geophysical Research*, *89*(C3), 3561–3572. https://doi.org/10.1029/JC089iC03p03561

Bromwich, D. H. (1989). An Extraordinary Katabatic Wind Regime at Terra Nova Bay, Antarctica. *Monthly Weather Review*, *117*(3), 688–695. https://doi.org/10.1175/15200493(1989)117<0688:aekwra>2.0.co;2

Carmack, E. C., & Foster, T. D. (1975). On the flow of water out of the Weddell Sea. *Deep-Sea Research and Oceanographic Abstracts*, *22*(11), 711–724. https://doi.org/10.1016/0011-7471(75)90077-7

Ciais, P., Sabine, C., Bala,G., Bopp, L., Brovkin, V., Canadell, J., et al. (2013). Chapter 6: Carbon and Other Biogeochemical Cycles. In Stocker, T.F., Qin, D., Plattner, G.-K., Tignor, M., Allen, S.K., Boschung,J., et al. (eds.) Climate Change 2013: The Physical Science Basis. Contribution of Working Group I to *the Fifth Assessment Report of the Intergovernmental Panel on Climate Change*. Cambridge University Press, Cambridge, United Kingdom and New York, NY, USA, 465–570. https://doi.org/10.1017/CBO9781107415324.015.

Caldeira, K., & Duffy, P. B. (2000). The role of the Southern Ocean in uptake and storage of anthropogenic carbon dioxide. *Science*, *287*(5453), 620–622. https://doi.org/10.1126/science.287.5453.620

Caldeira, K., & Wickett, M. E. (2003). Anthropogenic carbon and ocean pH. *Nature*, *425*(6956), 365. https://doi.org/10.1038/425365a

Carvalho, F., Kohut, J., Oliver, M. J., & Schofield, O. (2017). Defining the ecologically relevant mixed-layer depth for Antarctica's coastal seas. *Geophysical Research Letters*, *44*(1), 338– 345. https://doi.org/10.1002/2016GL071205

Cougnon, E. A., Galton-Fenzi, B. K., Meijers, A. J. S., & Legrésy, B. (2013). Modeling interannual dense shelf water export in the region of the Mertz Glacier Tongue (1992-2007). *Journal of Geophysical Research: Oceans*, *118*(10), 5858–5872. https://doi.org/10.1002/2013JC008790

Cougnon, E. A., Galton-Fenzi, B. K., Rintoul, S. R., Legrésy, B., Williams, G. D., Fraser, A. D., & Hunter, J. R. (2017). Regional Changes in Icescape Impact Shelf Circulation and Basal Melting. *Geophysical Research Letters*, *44*(22), 11,519-11,527. https://doi.org/10.1002/2017GL074943

DeJong, H. B., Dunbar, R. B., Mucciarone, D., & Koweek, D. A. (2015). Carbonate saturation state of surface waters in the Ross Sea and Southern Ocean: Controls and implications for the onset of aragonite undersaturation. *Biogeosciences*, *12*(23), 6881–6896. https://doi.org/10.5194/bg-12-6881-2015

DeJong, H. B., & Dunbar, R. B. (2017). Air-Sea CO_2 Exchange in the Ross Sea, Antarctica. *Journal of Geophysical Research: Oceans*, *122*(10), 8167–8181. https://doi.org/10.1002/2017JC012853

DeJong, H. B., Dunbar, R. B., Koweek, D. A., Mucciarone, D. A., Bercovici, S. K., & Hansell, D. A. (2017). Net community production and carbon export during the late summer in the Ross Sea, Antarctica. *Global Biogeochemical Cycles*, *31*(3), 473–491. https://doi.org/10.1002/2016GB005417

Dickson, A. G. (1981). An exact definition of total alkalinity and a procedure for the estimation of alkalinity and total inorganic carbon from titration data. *Deep Sea Research Part A, Oceanographic Research Papers*, *28*(6), 609–623. https://doi.org/10.1016/0198-0149(81)90121-7

Dickson, A. G., Afghan, J. D., & Anderson, G. C. (2003). Reference materials for oceanic CO_2 analysis: A method for the certification of total alkalinity. *Marine Chemistry*, *80(2)*, 185–197. https://doi.org/10.1016/S0304-4203(02)00133-0

Dickson, A. G., & Millero, F. J. (1987). A comparison of the equilibrium constants for the dissociation of carbonic acid in seawater media. *Deep Sea Research Part A, Oceanographic Research Papers*, *34*(10), 1733–1743. https://doi.org/10.1016/0198-0149(87)90021-5

Dickson, A.G., Sabine, C.L. and Christian, J.R. (Eds.) 2007. Guide to Best Practices for Ocean CO_2 Measurements. *PICES Special Publication 3*. North Pacific Marine Science Organization, Sydney, B.C., Canada, p. 191

Dieckmann, G. S., Nehrke, G., Papadimitriou, S., Göttlicher, J., Steininger, R., Kennedy, H., et al. (2008). Calcium carbonate as ikaite crystals in Antarctic sea ice. *Geophysical Research Letters*, *35*(8), L08501. https://doi.org/10.1029/2008GL033540

Dlugokencky, E. and Tans, P. (2010). Trends in atmospheric carbon dioxide, National Oceanic & Atmospheric Administration, Earth System Research Laboratory (NOAA/ESRL), available at: http://www.esrl.noaa.gov/gmd/ccgg/trends/global.html

Domack, W. E., & Anderson, J. B. (1983). Marine geology of the George V continental margin: combined results of Deep Freeze 1979 and the 1911-1914 Australasian expedition. In R. L. Oliver, P. R. James, & J. B. Jago (Eds.), *Antarctic Earth Science; Fourth International Symposium* (pp. 402–406). Cambridge: Cambridge University Press.

Ducklow, H., Steinberg, D., & Buesseler, K. (2001). Upper Ocean Carbon Export and the Biological Pump. *Oceanography*, *14*(4), 50–58. https://doi.org/10.5670/oceanog.2001.06

Edson, J. B., Fairall, C. W., Bariteau, L., Zappa, C. J., Cifuentes-Lorenzen, A., McGillis, W. R., et al. (2011). Direct covariance measurement of CO_2 gas transfer velocity during the 2008 Southern Ocean Gas Exchange Experiment: Wind speed dependency. *Journal of Geophysical Research: Oceans*, *116*(11), C00F10. https://doi.org/10.1029/2011JC007022

England, M. H. (1995). Using chlorofluorocarbons to assess ocean climate models. *Geophysical Research Letters*, *22*(22), 3051–3054. https://doi.org/10.1029/95GL02670

Evans, W., Mathis, J. T., Cross, J. N., Bates, N. R., Frey, K. E., Else, B. G. T., et al. (2015). Sea-air CO_2 exchange in the western Arctic coastal ocean. *Global Biogeochemical Cycles*, *29*(8), 1190–1209. https://doi.org/10.1002/2015GB005153

Eveleth, R., Cassar, N., Sherrell, R. M., Ducklow, H., Meredith, M. P., Venables, H. J., et al. (2017). Ice melt influence on summertime net community production along the Western Antarctic Peninsula. *Deep-Sea Research Part II: Topical Studies in Oceanography*, *139*, 89–102. https://doi.org/10.1016/j.dsr2.2016.07.016

Feely, R., Doney, S., & Cooley, S. (2009). Ocean Acidification: Present Conditions and Future Changes in a High-CO_2 World. *Oceanography*, *22*(4), 36–47. https://doi.org/10.5670/oceanog.2009.95

Feely, R. A., Sabine, C. L., Lee, K., Berelson, W., Kleypas, J., Fabry, V. J., & Millero, F. J. (2004). Impact of anthropogenic CO_2 on the $CaCO_3$ system in the oceans. *Science*, *305*(5682), 362–366. https://doi.org/10.1126/science.1097329

Foster, T. D., & Carmack, E. C. (1976). Frontal zone mixing and Antarctic Bottom water formation in the southern Weddell Sea. *Deep-Sea Research and Oceanographic Abstracts*, *23*(4), 301–317. https://doi.org/10.1016/0011-7471(76)90872-X

Frezzotti, M., Cimbelli, A., & Ferrigno, J. G. (1998). Ice-front change and iceberg behaviour along Oates and George V Coasts, Antarctica, 1912-96. *Annals of Glaciology*, *27*, 643–650. https://doi.org/10.3189/1998AoG27-1-643-650

Frölicher, T. L., Sarmiento, J. L., Paynter, D. J., Dunne, J. P., Krasting, J. P., & Winton, M. (2015). Dominance of the Southern Ocean in anthropogenic carbon and heat uptake in CMIP5 models. *Journal of Climate*, *28*(2), 862–886. https://doi.org/10.1175/JCLI-D-14-00117.1

Gerringa, L. J., Alderkamp, A. C., Laan, P., Thuróczy, C. E., De Baar, H. J., Mills, M. M., et al. (2012). Iron from melting glaciers fuels the phytoplankton blooms in Amundsen Sea (Southern Ocean): Iron biogeochemistry. *Deep-Sea Research Part II: Topical Studies in Oceanography*, *71–76*, 16–31. https://doi.org/10.1016/j.dsr2.2012.03.007

Gibson, J. A. E., & Trull, T. W. (1999). Annual cycle of fCO_2 under sea-ice and in open water. *Marine Chemistry*, *66*, 187–200. https://doi.org/10.1016/S0304-4203(99)00040-7

Gordon, A. L., & Tchernia, P. (1972). Waters of the continental margin off Adélie coast, Antarctica. In D. E. Hayes (Ed.), *Antarctic Oceanology 2: The Australian-New Zealand sector* (Vol. 19, pp. 59–69). American Geophysical Union. https://doi.org/https://doi.org/10.1029/AR019p0059

Grasshoff, K., Kremling, K., & Ehrhardt, M. (2007). *Methods of Seawater Analysis: Third Edition*. *Completely Revised and Extended Edition*. Weinheim, Germany: Wiley-VCH. https://doi.org/10.1002/9783527613984

Greenbaum, J. S., Blankenship, D. D., Young, D. A., Richter, T. G., Roberts, J. L., Aitken, A. R. A., et al. (2015). Ocean access to a cavity beneath Totten Glacier in East Antarctica. *Nature Geoscience*, *8*(4), 294–298. https://doi.org/10.1038/ngeo2388

Greene, C. A., Blankenship, D. D., Gwyther, D. E., Silvano, A., & Van Wijk, E. (2017). Wind causes Totten Ice Shelf melt and acceleration. *Science Advances*, *3*(11), e1701681. https://doi.org/10.1126/sciadv.1701681

Gruber, N., Gloor, M., Mikaloff Fletcher, S. E., Doney, S. C., Dutkiewicz, S., Follows, M. J., et al. (2009). Oceanic sources, sinks, and transport of atmospheric CO_2. *Global Biogeochemical Cycles*, *23*(1). https://doi.org/10.1029/2008GB003349

Gruber, N., Landschützer, P., & Lovenduski, N. S. (2019). The Variable Southern Ocean Carbon Sink. *Annual Review of Marine Science*, *11*(16). https://doi.org/10.1146/annurev-marine-121916

Herraiz-Borreguero, L., Lannuzel, D., van der Merwe, P., Treverrow, A., & Pedro, J. B. (2016). Large flux of iron from the Amery Ice Shelf marine ice to Prydz Bay, East Antarctica. *Journal of Geophysical Research: Oceans*, *121*(8), 6009–6020. https://doi.org/10.1002/2016JC011687

Ho, D. T., Law, C. S., Smith, M. J., Schlosser, P., Harvey, M., & Hill, P. (2006). Measurements of air-sea gas exchange at high wind speeds in the Southern Ocean: Implications for global parameterizations. *Geophysical Research Letters*, *33*(16), L16611. https://doi.org/10.1029/2006GL026817

Hood, E. M., Sabine, C. L., & Sloyan, B. M. (2010). *The GO-SHIP Repeat Hydrography Manual: A Collection of Expert Reports and Guidelines*. *IOCCP Report 14, ICPO Publication Series 134*. https://doi.org/10.21125/inted.2016.1955

IOC, IHO, and BODC. (2003) GEBCO Digital Atlas. Centenary ed., Intergovernmental Oceanographic Commission, International Hydrographic Organization and British Oceanographic Data Centre, CD-ROM. http:// www.gebco.net/data_and_products/gebco_digital_atlas/.

Jacobs, S. S., Amos, A. F., & Bruchhausen, P. M. (1970). Ross sea oceanography and antarctic bottom water formation. *Deep-Sea Research and Oceanographic Abstracts*, *17*(6), 935–962. https://doi.org/10.1016/0011-7471(70)90046-X

Johansson, O., & Wedborg, M. (1982). On the evaluation of potentiometric titrations of sea water with hydrochloric acid. *Oceanologica Acta*, *5*(2), 209–218. https://doi.org/10.1016/0198-0254(82)90093-0

Johnson, K. M., King, A. E., & Sieburth, J. M. (1985). Coulometric TCO_2 analyses for marine studies; an introduction. *Marine Chemistry*, *16*, 61–82. https://doi.org/10.1016/0304-4203(85)90028-3

Johnson, K. M., Williams, P. J., Brandstrom, L., & Sieburth, J. M. (1987). Coulometric total carbon analysis for marine studies: automation and calibration. *Marine Chemistry*, *21*, 117–133. https://doi.org/10.1016/0304-4203(87)90033-8

Johnson, K. M., Wills, K. D., Butler, D. B., Johnson, W. K., & Wong, C. S. (1993). Coulometric total carbon dioxide analysis for marine studies: maximizing the performance of an automated gas extraction system and coulometric detector. *Marine Chemistry*, *44*(2–4), 167–187. https://doi.org/10.1016/0304-4203(93)90201-X

Jones, E. M., Bakker, D. C. E., Venables, H. J., Whitehouse, M. J., Korb, R. E., & Watson, A. J. (2010). Rapid changes in surface water carbonate chemistry during Antarctic sea ice melt. *Tellus, Series B: Chemical and Physical Meteorology*, *62*(5), 621–635. https://doi.org/10.1111/j.1600-0889.2010.00496.x

Jones, E. M., Fenton, M., Meredith, M. P., Clargo, N. M., Ossebaar, S., Ducklow, H. W., et al. (2017). Ocean acidification and calcium carbonate saturation states in the coastal zone of the West Antarctic Peninsula. *Deep-Sea Research Part II: Topical Studies in Oceanography*, *139*, 181–194. https://doi.org/10.1016/j.dsr2.2017.01.007

Kalnay, E., Kanamitsu, M., Kistler, R., Collins, W., Deaven, D., Gandin, L., et al. (1996). The NCEP/NCAR 40-year reanalysis project. *Bulletin of the American Meteorological Society*, *77*(3), 437–471. https://doi.org/10.1175/1520-0477(1996)077<0437:TNYRP>2.0.CO;2

Kaufman, D. E., Friedrichs, M. A. M., Smith, W. O., Queste, B. Y., & Heywood, K. J. (2014). Biogeochemical variability in the southern Ross Sea as observed by a glider deployment. *Deep-Sea Research Part I: Oceanographic Research Papers*, *92*, 93–106. https://doi.org/10.1016/j.dsr.2014.06.011

Khatiwala, S., Primeau, F., & Hall, T. (2009). Reconstruction of the history of anthropogenic CO_2 concentrations in the ocean. *Nature*, *462*(7271), 346–9. https://doi.org/10.1038/nature08526

Khatiwala, S., Tanhua, T., Mikaloff Fletcher, S., Gerber, M., Doney, S. C., Graven, H. D., et al. (2013). Global ocean storage of anthropogenic carbon. *Biogeosciences*, *10*(4), 2169–2191. https://doi.org/10.5194/bg-10-2169-2013

Kusahara, K., Hasumi, H., Fraser, A. D., Aoki, S., Shimada, K., Williams, G. D., et al. (2017). Modeling ocean-cryosphere interactions off Adélie and George V Land,

East Antarctica. *Journal of Climate*, *30*(1), 163–188. https://doi.org/10.1175/JCLI-D-15-0808.1

Kusahara, K., Hasumi, H., & Tamura, T. (2010). Modeling sea ice production and dense shelf water formation in coastal polynyas around East Antarctica. *Journal of Geophysical Research: Oceans*, *115*(10), 10006. https://doi.org/10.1029/2010JC006133

Kusahara, K., Hasumi, H., & Williams, G. D. (2011a). Dense shelf water formation and brine-driven circulation in the Adélie and George V Land region. *Ocean Modelling*, *37*, 122–138. https://doi.org/10.1016/j.ocemod.2011.01.008

Kusahara, K., Hasumi, H., & Williams, G. D. (2011b). Impact of the Mertz Glacier Tongue calving on dense water formation and export. *Nature Communications*, *2*(1), 159. https://doi.org/10.1038/ncomms1156

Lacarra, M., Houssais, M.-N., Herbaut, C., Sultan, E., & Beauverger, M. (2014). Dense shelf water production in the Adélie Depression, East Antarctica, 2004-2012: Impact of the Mertz Glacier calving. *Journal of Geophysical Research: Oceans*, *119*(8), 5203–5220. https://doi.org/10.1002/2013JC009124

Lacarra, M., Houssais, M. N., Sultan, E., Rintoul, S. R., & Herbaut, C. (2011). Summer hydrography on the shelf off Terre Adélie/George V Land based on the ALBION and CEAMARC observations during the IPY. *Polar Science*, *5*(2), 88–103. https://doi.org/10.1016/j.polar.2011.04.008

Lannuzel, D., Schoemann, V., De Jong, J., Pasquer, B., Van Der Merwe, P., Masson, F., et al. (2010). Distribution of dissolved iron in Antarctic sea ice: Spatial, seasonal, and inter-annual variability. *Journal of Geophysical Research: Biogeosciences*, *115*(3), 3022. https://doi.org/10.1029/2009JG001031

Lannuzel, D., Schoemann, V., de Jong, J., Tison, J. L., & Chou, L. (2007). Distribution and biogeochemical behaviour of iron in the East Antarctic sea ice. *Marine Chemistry*, *106*(1–2 SPEC. ISS.), 18–32. https://doi.org/10.1016/j.marchem.2006.06.010

Le Quéré, C., Andrew, R. M., Friedlingstein, P., Sitch, S., Hauck, J., Pongratz, J., et al. (2018). Global Carbon Budget 2018. *Earth System Science Data*, *10*, 2141–2194. https://doi.org/10.5194/essd-10-2141-2018

Lee, S. H., Hwang, J., Ducklow, H. W., Hahm, D., Lee, S. H., Kim, D., et al. (2017). Evidence of minimal carbon sequestration in the productive Amundsen Sea polynya. *Geophysical Research Letters*, *44*(15), 7892–7899. https://doi.org/10.1002/2017GL074646

Legge, O. J., Bakker, D. C. E., Meredith, M. P., Venables, H. J., Brown, P. J., Jones, E. M., & Johnson, M. T. (2017). The seasonal cycle of carbonate system processes in Ryder Bay, West Antarctic Peninsula. *Deep-Sea Research Part II: Topical Studies in Oceanography*, *139*, 167–180. https://doi.org/10.1016/j.dsr2.2016.11.006

Lenton, A., Tilbrook, B., Law, R. M., Bakker, D., Doney, S. C., Gruber, N., et al. (2013). Sea–air CO_2 fluxes in the Southern Ocean for the period 1990-2009. *Biogeosciences*, *10*(6), 4037– 4054. https://doi.org/10.5194/bg-10-4037-2013

Li, X., Rignot, E., Morlighem, M., Mouginot, J., & Scheuchl, B. (2015). Grounding line retreat of Totten Glacier, East Antarctica, 1996 to 2013. *Geophysical Research Letters*. https://doi.org/10.1002/2015GL065701

Loose, B., Schlosser, P., Perovich, D., Ringelberg, D., Ho, D. T., Takahashi, T., et al. (2011). Gas diffusion through columnar laboratory sea ice: Implications for mixed-layer ventilation of CO_2 in the seasonal ice zone. *Tellus, Series B: Chemical and Physical Meteorology*, *63*(1), 23–39. https://doi.org/10.1111/j.1600-0889.2010.00506.x

Lüthi, D., Le Floch, M., Bereiter, B., Blunier, T., Barnola, J. M., Siegenthaler, U., et al. (2008). High-resolution carbon dioxide concentration record 650,000-800,000 years before present. *Nature*, *453*(7193), 379–382. https://doi.org/10.1038/nature06949

Marinov, I., Gnanadesikan, A., Toggweiler, J. R., & Sarmiento, J. L. (2006). The Southern Ocean biogeochemical divide. *Nature*, *441*(7096), 964–967. https://doi.org/10.1038/nature04883

Marshall, J., & Speer, K. (2012). Closure of the meridional overturning circulation through Southern Ocean upwelling. *Nature Geoscience*, *5*(3), 171–180. https://doi.org/10.1038/ngeo1391

Marsland, S. J., Bindoff, N. L., Williams, G. D., & Budd, W. F. (2004). Modeling water mass formation in the Mertz Glacier Polynya and Adélie Depression, East Antarctica. *Journal of Geophysical Research*, *109*(C11), C11003. https://doi.org/10.1029/2004JC002441

Marsland, S. J., Church, J. A., Bindoff, N. L., & Williams, G. D. (2007). Antarctic coastal polynya response to climate change. *Journal of Geophysical Research: Oceans*, *112*(7). https://doi.org/10.1029/2005JC003291

Massom, R. A. (2003). Recent iceberg calving events in the Ninnis Glacier region, East Antarctica. *Antarctic Science*, *15*(2), 303–313. https://doi.org/10.1017/S0954102003001299

Massom, R. A., Harris, P. T., Michael, K. J., & Potter, M. J. (1998). The distribution and formative processes of latent-heat polynyas in East Antarctica. *Annals of Glaciology*, *27*(1), 420–426. https://doi.org/10.3189/1998AoG27-1-420-426

McGillicuddy, D. J., Sedwick, P. N., Dinniman, M. S., Arrigo, K. R., Bibby, T. S., Greenan, B. J. W., et al. (2015). Iron supply and demand in an Antarctic shelf ecosystem. *Geophysical Research Letters*, *42*(19), 8088–8097. https://doi.org/10.1002/2015GL065727

McNeil, B. I., Sweeney, C., & Gibson, J. A. E. (2011). Short Note: Natural seasonal variability of aragonite saturation state within two Antarctic coastal ocean sites. *Antarctic Science*, *23*(04), 411–412. https://doi.org/10.1017/s0954102011000204

McNeil, B. I., Tilbrook, B., & Matear, R. J. (2001). Accumulation and uptake of anthropogenic CO_2 in the Southern Ocean, south of Australia between 1968 and 1996. *Journal of Geophysical Research: Ocean*, *106 (C12)*, 31431-31445. https://doi.org/10.1029/2000jc000331

Mehrbach, C., Culberson, C. H., Hawley, J. E., & Pytkowicx, R. M. (1973). Measurement of the apparent dissociation constants of carbonic acid in seawater at atmospheric pressure. *Limnology and Oceanography*, *18*(6), 897–907.https://doi.org/10.4319/lo.1973.18.6.0897

Mitchell, B. G., & Holm-Hansen, O. (1991). Observations of modeling of the Antarctic phytoplankton crop in relation to mixing depth. *Deep Sea Research Part A,*

Oceanographic Research Papers, *38*(8–9), 981–1007. https://doi.org/10.1016/0198-0149(91)90093-U

Mohajerani, Y., Velicogna, I., & Rignot, E. (2018). Mass Loss of Totten and Moscow University Glaciers, East Antarctica, Using Regionally Optimized GRACE Mascons. *Geophysical Research Letters*, 1–9. https://doi.org/10.1029/2018GL078173

Morales Maqueda, M. A., Willmott, A. J., & Biggs, N. R. T. (2004). Polynya dynamics: A review of observations and modeling. *Reviews of Geophysics*, *42*(1), RG1004. https://doi.org/10.1029/2002RG000116

Moreau, S., Lannuzel, D., Janssens, J., Arroyo., M. C., Corkill, C., Cougnon, E., et al. (2019). Sea-ice meltwater and circumpolar deep water drive contrasting productivity in three Antarctic polynyas., *Journal of Geophysical Research: Oceans*, https://doi.org/10.1029/2019JC015071

Morrison, A. K., Frölicher, T. L., & Sarmiento, J. L. (2015). Upwelling in the Southern Ocean. *Physics Today*. https://doi.org/10.1063/PT.3.2654

Mu, L., Stammerjohn, S. E., Lowry, K. E., & Yager, P. L. (2014). Spatial variability of surface pCO_2 and air-sea CO_2 flux in the Amundsen Sea Polynya, Antarctica. *Elementa: Science of the Anthropocene*, *2*, 000036. https://doi.org/10.12952/journal.elementa.000036

Murata, A., Kumamoto, Y.-i., & Sasaki, K.-i. (2019). Decadal-Scale Increases of Anthropogenic CO_2 in Antarctic Bottom Water in the Indian and Western Pacific Sectors of the Southern Ocean. *Geophysical Research Letters*, *46*(2), 833–841. https://doi.org/10.1029/2018GL080604

Nihashi, S., & Ohshima, K. I. (2015). Circumpolar mapping of antarctic coastal polynyas and landfast sea ice: Relationship and variability. *Journal of Climate*, *28*(9), 3650–3670. https://doi.org/10.1175/JCLI-D-14-00369.1

Ohshima, K. I., Fukamachi, Y., Williams, G. D., Nihashi, S., Roquet, F., Kitade, Y., et al. (2013). Antarctic Bottom Water production by intense sea-ice formation in the Cape Darnley polynya. *Nature Geoscience*, *6*(3), 235–240. https://doi.org/10.1038/ngeo1738

Ohshima, K. I., Nihashi, S., & Iwamoto, K. (2016). Global view of sea-ice production in polynyas and its linkage to dense/bottom water formation. *Geoscience Letters*, *3*(1), 13. https://doi.org/10.1186/s40562-016-0045-4

Orr, J. C., Fabry, V. J., Aumont, O., Bopp, L., Doney, S. C., Feely, R. A., et al. (2005). Anthropogenic ocean acidification over the twenty-first century and its impact on calcifying organisms. *Nature*, *437*(7059), 681–686. https://doi.org/10.1038/nature04095

Orsi, A. H., Johnson, G. C., & Bullister, J. L. (1999). Circulation, mixing, and production of Antarctic Bottom Water. *Progress in Oceanography*, *43*(1), 55–109. https://doi.org/10.1016/S0079-6611(99)00004-X

Orsi, A. H., Smethie, W. M., & Bullister, J. L. (2002). On the total input of Antarctic waters to the deep ocean: A preliminary estimate from chlorofluorocarbon measurements. *Journal of Geophysical Research*, *107*(C8), 3122. https://doi.org/10.1029/2001jc000976

Peloquin, J. A., & Smith, Jr., W. O. (2007). Phytoplankton blooms in the Ross Sea, Antarctica: Interannual variability in magnitude, temporal patterns, and composition. *Journal of Geophysical Research: Oceans*, *112*(8), C08013. https://doi.org/10.1029/2006JC003816

Pierrot, D., Neill, C., Sullivan, K., Castle, R., Wanninkhof, R., Lüger, H., et al. (2009). Recommendations for autonomous underway pCO_2 measuring systems and data-reduction routines. *Deep-Sea Research Part II: Topical Studies in Oceanography*, *56*(8–10), 512–522. https://doi.org/10.1016/j.dsr2.2008.12.005

Rignot, E., Jacobs, S., Mouginot, J., & Scheuchl, B. (2013). Ice-shelf melting around Antarctica. *Science*, *341*(6143), 266–70. https://doi.org/10.1126/science.1235798

Riley, J. P., & Tongudai, M. (1967). The major cation/chlorinity ratios in sea water. *Chemical Geology*, *2*(C), 263–269. https://doi.org/10.1016/0009-2541(67)90026-5

Rintoul, S. R. (1998). On the origin and influence of Adélie land bottom water. In *Ocean, Ice, and Atmosphere: interactions at the Antarctic continental margin* (Vol. 75, pp. 151–171). American Geophysical Union. https://doi.org/10.1029/ar075p0151

Rintoul, S. R., Silvano, A., Pena-Molino, B., van Wijk, E., Rosenberg, M., Greenbaum, J. S., & Blankenship, D. D. (2016). Ocean heat drives rapid basal melt of the Totten Ice Shelf. *Science Advances*, *2*(12), e1601610. https://doi.org/10.1126/sciadv.1601610

Roden, N. P., Shadwick, E. H., Tilbrook, B., & Trull, T. W. (2013). Annual cycle of carbonate chemistry and decadal change in coastal Prydz Bay, East Antarctica. *Marine Chemistry*, *155*, 135–147. https://doi.org/10.1016/j.marchem.2013.06.006

Roden, N. P., Tilbrook, B., Trull, T. W., Virtue, P., & Williams, G. D. (2016). Carbon cycling dynamics in the seasonal sea-ice zone of East Antarctica. *Journal of Geophysical Research: Oceans*, *121*(12), 8749–8769. https://doi.org/10.1002/2016JC012008

Rosenberg M., & Rinoul, S. R. (2016) Aurora Australis Marine Science Cruise AU1402, Totten and Mertz CTDs and moorings – oceanographic field measurements and analysis. Hobart, Australia.

Rosenberg, M., & Rintoul, S. R. (2017). Aurora Australis Marine Science Cruise AU1602, Dalton, Mertz, and Ninnis CTDs - Oceanographic Field Measurements and Analysis. Hobart, Australia.

Rysgaard, S., Glud, R. N., Lennert, K., Cooper, M., Halden, N., Leakey, R. J. G., et al. (2012). Ikaite crystals in melting sea ice - Implications for pCO_2 and pH levels in Arctic surface waters. *Cryosphere*, *6*(4), 901–908. https://doi.org/10.5194/tc-6-901-2012

Sabine, C. L., Feely, R. A., Gruber, N., Key, R. M., Lee, K., Bullister, J. L., et al. (2004). The oceanic sink for anthropogenic CO_2. *Science*, *305*(5682), 367–71. https://doi.org/10.1126/science.1097403

Sambrotto, R. N., Matsuda, A., Vaillancourt, R., Brown, M., Langdon, C., Jacobs, S. S., & Measures, C. (2003). Summer plankton production and nutrient consumption patterns in the Mertz Glacier Region of East Antarctica. *Deep-Sea Research Part II: Topical Studies in Oceanography*, *50*(8–9), 1393–1414. https://doi.org/10.1016/S0967-0645(03)00076-6

Sarmiento, J. L., Gruber, N., Brzezinski, M. A., & Dunne, J. P. (2004). High-latitude controls of thermocline nutrients and low latitude biological productivity. *Nature*, *427*(6969), 56–60. https://doi.org/10.1038/nature02127

Sedwick, P. N., & DiTullio, G. R. (1997). Regulation of algal blooms in Antarctic shelf waters by the release of iron from melting sea ice. *Geophysical Research Letters*, *24*(20), 2515–2518. https://doi.org/10.1029/97GL02596

Shadwick, E. H., Rintoul, S. R., Tilbrook, B., Williams, G. D., Young, N., Fraser, A. D., et al. (2013). Glacier tongue calving reduced dense water formation and enhanced carbon uptake. *Geophysical Research Letters*, *40*(5), 904–909. https://doi.org/10.1002/grl.50178

Shadwick, E. H., Tilbrook, B., & Currie, K. I. (2017). Late-summer biogeochemistry in the Mertz Polynya: East Antarctica. *Journal of Geophysical Research: Oceans*, *122*(9), 7380– 7394. https://doi.org/10.1002/2017JC013015

Shadwick, E. H., Tilbrook, B., & Williams, G. D. (2014). Carbonate chemistry in the Mertz Polynya (East Antarctica): Biological and physical modification of dense water outflows and the export of anthropogenic CO_2. *Journal of Geophysical Research: Oceans*, *119*(1), 1–14. https://doi.org/10.1002/2013JC009286

Sigman, D. M., & Boyle, E. A. (2000). Glacial/interglacial variations in atmospheric carbon dioxide. *Nature*, *407*(6806), 859–869. https://doi.org/10.1038/3503800

Silvano, A., Rintoul, S., & Herraiz-Borreguero, L. (2016). Ocean-Ice Shelf Interaction in East Antarctica. *Oceanography*, *29*(4), 130–143. https://doi.org/10.5670/oceanog.2016.105

Silvano, A., Rintoul, S. R., Peña-Molino, B., & Williams, G. D. (2017). Distribution of water masses and meltwater on the continental shelf near the Totten and Moscow University ice shelves. *Journal of Geophysical Research: Oceans*, *122*(3), 2050–2068. https://doi.org/10.1002/2016JC012115

Silvano, A., Rintoul, S. R., Peña-Molino, B., Hobbs, W. R., Van Wijk, E., Aoki, S., et al. (2018). Freshening by glacial meltwater enhances melting of ice shelves and reduces formation of Antarctic Bottom Water. *Science Advances*, *4*(4), eaap9467. https://doi.org/10.1126/sciadv.aap9467

Smith, Jr., W. O., & Gordon, L. I. (1997). Hyperproductivity of the Ross Sea (Antarctica) polynya during austral spring. *Geophysical Research Letters*, *24*(3), 233–236. https://doi.org/10.1029/96GL03926

Smith, Jr., W. O., & Jones, R. M. (2015). Vertical mixing, critical depths, and phytoplankton growth in the Ross Sea. *ICES Journal of Marine Science*, *72*(6), 1952–1960. https://doi.org/10.1093/icesjms/fsu234

Smith, Jr., W. O., Marra, J., Hiscock, M. R., & Barber, R. T. (2000). The seasonal cycle of phytoplankton biomass and primary productivity in the Ross Sea, Antarctica. *Deep-Sea Research Part II: Topical Studies in Oceanography*, *47*(15–16), 3119–3140. https://doi.org/10.1016/S0967-0645(00)00061-8

Smith, Jr., W. O., Shields, A. R., Peloquin, J. A., Catalano, G., Tozzi, S., Dinniman, M. S., & Asper, V. A. (2006). Interannual variations in nutrients, net community production, and biogeochemical cycles in the Ross Sea. *Deep-Sea Research Part II: Topical Studies in Oceanography*, *53*(8–10), 815–833. https://doi.org/10.1016/j.dsr2.2006.02.014

Snow, K., Rintoul, S. R., Sloyan, B. M., & Hogg, A. M. C. (2018). Change in Dense Shelf Water and Adélie Land Bottom Water Precipitated by Iceberg Calving. *Geophysical Research Letters*, *45*(5), 2380–2387. https://doi.org/10.1002/2017GL076195

Snow, K., Sloyan, B. M., Rintoul, S. R., Hogg, A. M., & Downes, S. M. (2016). Controls on circulation, cross-shelf exchange, and dense water formation in an Antarctic polynya. *Geophysical Research Letters*, *43*(13), 7089–7096. https://doi.org/10.1002/2016GL069479

Sweeney, C., Hansell, D. A., Carlson, C. A., Codispoti, L. A., Gordon, L. I., Marra, J., et al. (2000). Biogeochemical regimes, net community production and carbon export in the Ross Sea, Antarctica. *Deep-Sea Research Part II: Topical Studies in Oceanography*, *47*(15–16), 3369–3394. https://doi.org/10.1016/S0967-0645(00)00072-2

Sweeney, C. (2003). The annual cycle of surface water CO_2 And O_2 in the Ross Sea: A model for gas exchange on the continental shelves of Antarctica. In

Biogeochemistry of the Ross Sea (Vol. 78, pp. 295–312). American Geophysical Union. https://doi.org/10.1029/078ars19

Sweeney, C., Gloor, E., Jacobson, A. R., Key, R. M., McKinley, G., Sarmiento, J. L., & Wanninkhof, R. (2007). Constraining global air-sea gas exchange for CO_2 with recent bomb ^{14} C measurements. *Global Biogeochemical Cycles*, *21*(2), GB2015, https://doi.org/10.1029/2006GB002784

Takahashi, T., & Chipman, D. (2012). CO_2 Transport in Deep Waters Off Wilkes Land. *Oceanography*, *25*(3), 24–25. https://doi.org/10.5670/oceanog.2012.70

Takahashi, T., Sutherland, S. C., Wanninkhof, R., Sweeney, C., Feely, R. A., Chipman, D. W., et al. (2009). Climatological mean and decadal change in surface ocean pCO_2, and net sea-air CO_2 flux over the global oceans. *Deep-Sea Research Part II: Topical Studies in Oceanography*, *56*(8–10), 554–577. https://doi.org/10.1016/j.dsr2.2008.12.009

Tamura, T., Ohshima, K. I., Fraser, A. D., & Williams, G. D. (2016). Sea ice production variability in Antarctic coastal polynyas. *Journal of Geophysical Research: Oceans*, *121*(5), 2967–2979. https://doi.org/10.1002/2015JC011537

Tamura, T., Williams, G. D., Fraser, A. D., & Ohshima, K. I. (2012). Potential regime shift in decreased sea ice production after the Mertz Glacier calving. *Nature Communications*, *3*(1), 826. https://doi.org/10.1038/ncomms1820

Thomas, H., Bozec, Y., Elkalay, K., & de Baar, H. J. W. (2004). Enhanced open ocean storage of CO_2 from shelf sea pumping. *Science*, *304*(5673), 1005–1008. https://doi.org/10.1126/science.1103193

Timmermann, R., Le Brocq, A., Deen, T., Domack, E., Dutrieux, P., Galton-Fenzi, B., et al. (2010). A consistent data set of Antarctic ice sheet topography, cavity geometry, and global bathymetry. *Earth System Science Data*, *2*(2), 261–273. https://doi.org/10.5194/essd-2-261-2010

Toggweiler, J. R., Gnanadesikan, A., Carson, S., Murnane, R., & Sarmiento, J. L. (2003). Representation of the carbon cycle in box models and GCMs: 1. Solubility pump. *Global Biogeochemical Cycles*, *17*(1). https://doi.org/10.1029/2001GB001401

Tortell, P. D., Guéguen, C., Long, M. C., Payne, C. D., Lee, P., & DiTullio, G. R. (2011). Spatial variability and temporal dynamics of surface water pCO_2, ΔO_2/Ar and

dimethylsulfide in the Ross Sea, Antarctica. *Deep-Sea Research Part I: Oceanographic Research Papers*, *58*(3), 241–259. https://doi.org/10.1016/j.dsr.2010.12.006

Tsunogai, S., Watanabe, S., & Sato, T. (1999). Is there a "continental shelf pump" for the absorption of atmospheric CO_2? *Tellus B: Chemical and Physical Meteorology*, *51*(3), 701–712. https://doi.org/10.3402/tellusb.v51i3.16468

van Heuven, S., Pierrot, D., Rae, J. W. B., Lewis, E., & Wallace, D. W. R. (2011). MATLAB Program Developed for CO_2 System Calculations. ORNL/CDIAC-105b. *ORNL/CDIAC-105b. Carbon Dioxide Information Analysis Center, Oak Ridge National Laboratory, U.S. Department of Energy, Oak Ridge, Tennessee*. https://doi.org/10.3334/CDIAC/otg.CO2SYS_MATLAB_v1.1

Wanninkhof, R. (1992). Relationship between wind speed and gas exchange over the ocean. *Journal of Geophysical Research*, *97*(C5), 7373. https://doi.org/10.1029/92JC00188

Wanninkhof, R. (2014). Relationship between wind speed and gas exchange over the ocean revisited. *Limnology and Oceanography: Methods*, *12*(JUN), 351–362. https://doi.org/10.4319/lom.2014.12.351

Wanninkhof, R., Sullivan, K. F., & Top, Z. (2004). Air-sea gas transfer in the Southern Ocean. *Journal of Geophysical Research C: Oceans*, *109*(8), https://doi.org/10.1029/2003JC001767

Weiss, R. F. (1974). Carbon dioxide in water and seawater: the solubility of a non-ideal gas. *Marine Chemistry*, *2*(3), 203–215. https://doi.org/10.1016/0304-4203(74)90015-2

Whitworth, T., Orsi, A. H., Kim, S.-J., Nowlin, W. D., & Locarnini, R. A. (1998). Water Masses and Mixing Near the Antarctic Slope Front. In *Ocean, Ice, and Atmosphere: interactions at the Antarctic continental margin* (pp. 1–27). American Geophysical Union. https://doi.org/10.1029/ar075p0001

Williams, G. D., Aoki, S., Jacobs, S. S., Rintoul, S. R., Tamura, T., & Bindoff, N. L. (2010). Antarctic bottom water from the Adélie and George v Land Coast, East Antarctica (140-149°E). *Journal of Geophysical Research: Oceans*, *115*(4), C04027. https://doi.org/10.1029/2009JC005812

Williams, G. D., & Bindoff, N. L. (2003). Wintertime oceanography of the Adélie Depression. *Deep Sea Research Part II: Topical Studies in Oceanography*, *50*(8), 1373–1392. https://doi.org/10.1016/S0967-0645(03)00074-2

Williams, G. D., Bindoff, N. L., Marsland, S. J., & Rintoul, S. R. (2008). Formation and export of dense shelf water from the Adélie depression, East Antarctica. *Journal of Geophysical Research: Oceans*, *113*(4), C04039. https://doi.org/10.1029/2007JC004346

Williams, G. D., Meijers, A. J. S., Poole, A., Mathiot, P., Tamura, T., & Klocker, A. (2011). Late winter oceanography off the Sabrina and BANZARE coast (117-128°E), East Antarctica. *Deep-Sea Research Part II: Topical Studies in Oceanography*, *58*(9–10), 1194–1210. https://doi.org/10.1016/j.dsr2.2010.10.035

Wolf-Gladrow, D. A., Zeebe, R. E., Klaas, C., Körtzinger, A., & Dickson, A. G. (2007). Total alkalinity: The explicit conservative expression and its application to biogeochemical processes. *Marine Chemistry*, *106*, 287–300. https://doi.org/10.1016/j.marchem.2007.01.006

Yager, P. L., Wallace, D. W. R., Johnson, K. M., Smith, W. O., Minnett, P. J., & Deming, J. W. (1995). The Northeast Water Polynya as an atmospheric CO_2 sink: a seasonal rectification hypothesis. *Journal of Geophysical Research*, *100*(C3), 4389–4398. https://doi.org/10.1029/94JC01962

Yager, P., Sherrell, R., Stammerjohn, S., Ducklow, H., Schofield, O., Ingall, E., et al. (2016). A carbon budget for the Amundsen Sea Polynya, Antarctica: Estimating net community production and export in a highly productive polar ecosystem. *Elementa: Science of the Anthropocene*, *4*(0), 000140. https://doi.org/10.12952/journal.el

Zeebe, R. E., & Wolf-Gladrow, D. (2001). *CO_2 in seawater: Equilibrium, Kinetics, Isotopes*. Elsevier Oceanography Series. https://doi.org/10.1016/S0924-7963(02)00179-3

Zhao, C. L., & Tans, P. P. (2006). Estimating uncertainty of the WMO mole fraction scale for carbon dioxide in air. *Journal of Geophysical Research Atmospheres*, *111*(8). https://doi.org/10.1029/2005JD006003